

Utah State University

DigitalCommons@USU

All Graduate Theses and Dissertations

Graduate Studies

5-2015

Computational Modeling to Study Disease Development: Applications to Breast Cancer and an in vitro Model of Macular Degeneration

Qanita Bani Baker
Utah State University

Follow this and additional works at: <https://digitalcommons.usu.edu/etd>



Part of the [Computer Sciences Commons](#)

Recommended Citation

Bani Baker, Qanita, "Computational Modeling to Study Disease Development: Applications to Breast Cancer and an in vitro Model of Macular Degeneration" (2015). *All Graduate Theses and Dissertations*. 4409.

<https://digitalcommons.usu.edu/etd/4409>

This Dissertation is brought to you for free and open access by the Graduate Studies at DigitalCommons@USU. It has been accepted for inclusion in All Graduate Theses and Dissertations by an authorized administrator of DigitalCommons@USU. For more information, please contact digitalcommons@usu.edu.



COMPUTATIONAL MODELING TO STUDY DISEASE DEVELOPMENT:
APPLICATIONS TO BREAST CANCER AND AN *IN VITRO* MODEL OF
MACULAR DEGENERATION

by

Qanita Bani Baker

A dissertation submitted in partial fulfillment
of the requirements for the degree

of

DOCTOR OF PHILOSOPHY

in

Computer Science

Approved:

Dr. Nicholas S. Flann
Major Professor

Dr. Gregory J. Podgorski
Committee Member

Dr. Xiaojun Qi
Committee Member

Dr. Stephen Clyde
Committee Member

Dr. Elizabeth Vargis
Committee Member

Dr. Mark R. McLellan
Vice President for Research and
Dean of the School of Graduate Studies

UTAH STATE UNIVERSITY
Logan, Utah

2015

Copyright © Qanita Bani Baker 2015

All Rights Reserved

ABSTRACT

Computational Modeling to Study Disease Development: Applications to Breast Cancer
and an *In Vitro* Model of Macular Degeneration

by

Qanita Bani Baker, Doctor of Philosophy

Utah State University, 2015

Major Professor: Dr. Nicholas S. Flann
Department: Computer Science

The progression of many diseases, such as breast cancer and age-related macular degeneration, is not fully understood. These diseases are mechanistically complex, nonlinear, and are driven by complex interacting processes that occur at different scales of time and space. When paired with traditional biological investigations, computational models can play a significant role in understanding disease progression, because computational models formalize and quantify mechanisms between interacting components and can test hypotheses about pathogenesis orders of magnitude faster than biological investigations. The results of these computational studies can then be used by biologists to inform their *in vivo* studies, and meaningful insights can be gained into disease, i.e., how to control its progression and how to treat it.

The ability of agent-based models to encompass multiple spatiotemporal scales of biological process makes this modeling framework well suited to explore biological systems and disease development. In this dissertation, we extend a multicellular hybrid agent-based modeling approach and use it to study the development of breast cancer and to better understand an *in vitro* model for age-related macular degeneration (AMD). To achieve this,

we needed to identify methods, algorithms and techniques that increase the effectiveness of agent-based models applied to disease development.

The transition in breast cancer from ductal carcinoma *in situ* to invasive ductal carcinoma was studied in the framework of two-dimensional breast duct structures. This model includes ductal, stromal and tumor cell types acting along with multiple biochemical and biomechanical interactions. The results of the model were qualitatively validated using micrographs of progressing ductal carcinoma and biochemical and biophysical properties reported in the literature. We also developed and applied an *in silico* model to an *in vitro* model of age-related macular degeneration. This *in vitro* model uses retinal cells grown in culture in territories of different controlled size to explore how the distribution of cells effects the production of vascular-endothelial growth factor (VEGF). VEGF overproduction plays a central role in AMD. The agent-based model was used to study the underlying mechanism of VEGF production, and predict the VEGF with varying configurations of cells. The model was quantitatively validated from experimental *in vitro* data. We developed an error-minimizing searching approach that uses available information about VEGF metabolism at the cell population level to predict currently unknown parameters of VEGF metabolisms at the cell level, essentially bridging the gap in scales between the multicellular and cellular levels of organization.

(121 pages)

PUBLIC ABSTRACT

Computational Modeling to Study Disease Development: Applications to Breast Cancer
and an *In Vitro* Model of Macular Degeneration

Qanita Bani Baker

There have been several techniques developed in recent years to develop computer models of a variety of disease behaviors. Agent-based modeling is a discrete-based modeling approach used agents to represent individual cells that mechanically interact and secrete, consume or react to soluble products. It has become a powerful modeling approach, widely used by computational researchers. In this research, we utilized agent-based modeling to study and explore disease development, particularly in two applications, breast cancer and bioengineering experiments. We further proposed an error-minimization search approach and used it to estimate cellular parameters from multicellular *in vitro* data.

In this dissertation, in the first study, we developed a 2D agent-based model that attempted to emulate the *in vivo* structure of breast cancer. The model was applied to describe the progression from DCIS into DCI. This model confirms that the interaction between tumor cells and the surrounding stroma in the duct plays a critical role in tumor growth and metastasis. This interaction depends on many mechanical and chemical factors that work with each other to produce tumor invasion of the surrounding tissue. In the second study, an *in silico* model was developed and applied to understanding the underlying mechanism of vascular-endothelial growth factor (VEGF) auto-regulation in REP and emulate the *in vitro* experiments as part of bioengineering research. This model may provide a system with robust predictive modeling and visualization that could enable discovery of the molecular mechanisms involved in age-related macular degeneration (AMD) progression and provide

routers to the development of effective treatments. In the third and final study, a searching approach was applied to estimate cellular parameters from spatiotemporal data produced from bioengineered multicellular *in vitro* experiments. We applied a search method to an integrated cellular and multicellular model of retinal pigment epithelial cells to estimate the auto-regulation parameters of VEGF.

To my wonderful husband and best friend, Aisa, for his support, love, and encouragement.

To my little sons, for their patience.

To my parents, and parents in-law, for their support.

ACKNOWLEDGMENTS

This work would not have been completed without the help and support of many individuals. I would like to thank everyone who has helped me along the way.

First and foremost, I offer my sincerest gratitude to my advisor, Dr. Nicholas S. Flann, who supported me throughout my research in this dissertation with his patience, knowledge, and guidance. Working with him has been an amazing experience. I hope I can follow his example in the future, when I am advising students of my own.

I am extremely grateful to my research committee members. First and foremost, I would like to thank Dr. Gregory J. Podgorski for his suggestions, support, and guidance. I am very grateful for his invaluable suggestions and contribution.

I would like also to thank Dr. Elizabeth Vargis for sharing her work and supporting me with her valuable knowledge.

I also would like to thank Dr. Stephen Clyde and Dr. Xiaojun Qi for being excellent teachers, their valuable knowledge, and serving on my committee.

I would like to thank Dr. Soonjo Kwon for sharing his knowledge, and support.

I am very grateful to Dr. Al Forsyth for his support and helpful suggestions for this dissertation writing.

Qanita Bani Baker

CONTENTS

	Page
ABSTRACT	iii
PUBLIC ABSTRACT	v
ACKNOWLEDGMENTS	viii
LIST OF TABLES	xi
LIST OF FIGURES	xii
ACRONYMS	xvi
CHAPTER	
1 INTRODUCTION	1
1.1 Modeling Approaches and Techniques in Computational Systems Biology	2
1.2 Objectives	6
1.3 Projects Outlines	7
1.4 Research Methodology and Strategies	9
1.5 Research Impacts	11
2 AN AGENT-BASED MODELING APPROACH TO EXPLORE INTERACTIONS OF STROMA AND TUMOR CELLS: THE PROGRESSION OF IN DUCTAL CAR- CINOMA <i>IN SITU</i> TO INVASIVE DUCTAL CARCINOMA	13
2.1 Abstract	13
2.2 Introduction	14
2.3 Background	15
2.4 Methods	20
2.5 Results	31
2.6 Conclusions	39
2.7 Appendix	41
3 DEVELOPING AN <i>IN SILICO</i> MODEL TO STUDY THE EFFECT OF RETINAL PIGMENT EPITHELIAL CELL PATCH SIZE ON VEGF PRODUCTION	43
3.1 Abstract	43
3.2 Introduction	44
3.3 Materials and Methods	46
3.4 Results	51
3.5 Discussion	56

4 BRIDGING THE MULTISCALE GAP: IDENTIFYING CELLULAR PARAMETERS FROM MULTICELLULAR DATA	59
4.1 Abstract	59
4.2 Introduction	60
4.3 Multicellular Experiment and Model	61
4.4 Method	64
4.5 Results	67
4.6 Conclusions	71
5 CONCLUSIONS	74
REFERENCES	76
APPENDICES	97
CURRICULUM VITAE	101

LIST OF TABLES

Table	Page
2.1 List of parameters symbol description	41
2.2 List of Equations number per cell type	41
2.3 List of soluble factor per cell type	42
2.4 <i>In Vitro</i> Parameters for DCIS Model	42
3.1 Initial Number of Cells in Each Patch based on [1]	50
3.2 Model's parameter descriptions	51
4.1 Known and unknown parameter descriptions	64

LIST OF FIGURES

Figure	Page
1.1 Multiscale models of the human body targeting complex processes that span diverse time and length scales of biological organization [2].	2
1.2 A diagrammatic representation of several biological scales and their associated modeling techniques and experimental approaches as in [3].	5
2.1 a- The developing of normal breast. b- The transition from normal mammary ducts to an invasive tumor in breast cancer. From Butcher et al. 2009 [4]	15
2.2 Particle Shoving: $R_t(\sigma_i)$ is the radius of a particle of state $t(\sigma_i)$, α_t is the shoving factor for this state t and d is the distance between the objects. When two particles i and j are closer than $\alpha_t(R_{t_i} - R_{t_j})$ then a force is applied to push them apart. For an impregnable boundary, the force is only applied to the particle.	22
2.3 Extracellular Matrix formation as crosslinks between ECM particles (spheres in the figure).	24
2.4 (a) ECM stiffening viewed over time(earlier to later is left to right). Blue particles are secreting stiffening enzyme (LOX) that increases amount of ECM (spheres) and cross links between ECM particles, causing the ECM to stiffen; (b) ECM degradation. Red particles are secreting MMPs that degrade the surrounding fibers.	25
2.5 The initial condition of the DCIS to IDC simulation. The duct is a tubular arrangement of epithelial cells, surrounded by basement membrane and myoepithelial cells. The duct is embedded within stroma that includes: ECM, fibroblasts and blood vessels cells. There is a single tumor cell on the internal wall of the duct.	26
2.6 The diagram represents the overview of inhibition and activation reactions and the coupling among biomechanical and biochemical model components. The blue rectangles represent cell/ECM types, the pink circles represent the soluble factors, the orange circle represents the biomechanical stress(pressure), and the green circle represents the nutrient. The arrows show whether the influence is either inhibitory or activating. The red arrows represent the transitions between cells types that is regulated by a factor. For example, the red arrow from fibroblast to myofibroblast signifies that this cell type transition is regulated by TGF- β	27

2.7	The stages from a normal duct into an invasive tumor during simulation. (A) The initial condition for DCIS at iteration 2. (B) The growing tumor triggers the activation of TGF- β that promotes differentiation of fibroblasts into myofibroblasts at iteration 100. (C) Newly differentiated myofibroblasts secrete LOX that begins stiffening the ECM with additional cross-linking and accretion. The ductal wall integrity at the location of tumor initiation has been compromised, but tumor cells are still contained within the duct at iteration 130. (D) The tumor cells have filled the duct, broken through the ductal wall and begun invasion of the surrounding stroma at iteration 180. (E) The duct is so weakened that multiple breaches have occurred and tumor cells have invaded throughout the stroma at iteration 215.	31
2.8	Simulated microdissection sites around the duct where biochemical concentrations and biomechanical forces are quantified. L1 is the point of tumor initiation.	32
2.9	Spatial distributions of pressure and MMP in different simulation iterations (iteration 2, iteration 100, iteration 130,180, and iteration 215, respectively) along with the corresponding morphology. Red indicates a high value, blue a low value.	34
2.10	Pressure and MMP levels as a function of model iteration in the different locations in the duct given in Figure 2.8.	35
2.11	Spatial distribution of TGF- β and LOX as the simulation progresses. . . .	36
2.12	TGF- β and LOX concentrations as a function of iteration in different locations in the duct.	37
2.13	The number of TCs, myofibroblasts, and TCs outside the duct as a function of iteration.	38
2.14	The architectural relationship of the basement membrane, myoepithelial cells, and epithelial cells of ducts in a normal human mammary gland. The left one is micrograph image where the arrow identifies the basement membrane (brown), the arrowhead designates a ME cell (red) [5]. The right one is simulation image where the bold arrow identifies the basement membrane (black) and the thin arrow designates myoepithelial cell (yellow).	39
2.15	Disruption of the myoepithelial cells layer and breach of the basement membrane are prerequisites for invasion. The myoepithelial cell layer and basement membrane in one duct is locally disrupted and the epithelial cells are in direct contact with the stroma (an arrow) [5].	40

3.1	Micropatterning method used in [1]. Substrate functionalization and cell seeding are accomplished by molding a PDMS stamp from an etched silicon master as in steps (a, and b). Then, the stamp is inked using a fibronectin solution, allowed to dry and then placed in contact with a polystyrene or glass culture dish as in steps(c-f). After that, the surface is blocked with Pluornic prior to seeding RPE cells onto the fibronectin-patterned substrate as in steps (g, and h).	45
3.2	The result as shown in the experiments performed by Vargis et al. in [1] (a) Patches of stained RPE cells at 72 h for each patch size. [1]. (b) Time course of VEGF expression per cell measured at 4, 24, 30, 48, and 72 h as in [1]. (c) Time course of VEGF expression per cell measured before the addition of the VEGF agonist(at 4 h) and after (24, 30, 48, 54, 72 h) [1]. .	48
3.3	Patch arrangement in the simulation. (A)Patch 100 μm , 12 patches in each side. (B) Patch 200 μm , 6 patches in each side. (C) Patch 300 μm , 4 patches in each side. (D) Patch 400 μm , 3 patches in each side.	50
3.4	Comparing VEGF concentration per cell <i>in vitro</i> and in simulation. (a) The left graph represents the data obtained <i>in vitro</i> from [1]. (b) The right graph represents the data obtained from the simulation.	52
3.5	Comparing the time course of VEGF expression per cell measured at 4, 24, 30, 48, and 72 h, different patch sizes (100 μm , 200 μm , 300 μm , and 400 μm), <i>in vitro</i> and in simulation. (a) The left graph represents the data obtained <i>in vitro</i> from [1]. (b) The right graph represents the data obtained from the simulation.	53
3.6	<i>In vitro</i> and simulated effects of the VEGF agonist addition on VEGF expression. The agonist was added after 20 h of culture. (a) Data obtained <i>in vitro</i> . (b) Results of the simulation.	54
3.7	Simultaneous evolution of the VEGF distribution profile in 2400 micrometers area for different patches size.	55
3.8	(a) Closeup of initial condition of a 400 μm patch (b) Experiment with 400 μm , 3 patches in each side. (c) Closeup of the VEGF distribution after 72 h, (d) VEGF distribution over whole domain after 72 h.	57
3.9	Patch arrangement in the simulation. (A)Patch 100 μm , 12 patch in each side. (B) Patch 200 μm , 6 patches in each side. (C) Patch 300 μm , 4 patches in each side. (D) Patch 400 μm , 3 patches in each side.	58
3.10	VEGF expression per cell measured at 4, 24, 30, 48, and 72 h from the simulation in inverse distributions of the cells as shown in Figure 3.9. . . .	58

4.1	(a) Patches of stained RPE cells at 72 h for each patch size [1]. (b) Time course of VEGF expression per cell measured at 4, 24, 30, 48, and 72 h (data for each time from the <i>in vitro</i> [1]).	64
4.2	(a) Closeup of initial condition of a 400 μm patch (b) Experiment with 400 μm , 3 patches in each side. (c) Closeup of the VEGF distribution after 72 h, (d) VEGF distribution over whole domain after 72 h.	65
4.3	An overview for the error-minimization multicellular search-based approach. In (A), RPE cells are cultured using micropatterning techniques. In (B), the parameters are initialized in the XML protocol file. In (C), a simulation is performed and the results are calculated. In (D), the error is calculated based on the difference in VEGF concentration per cell between the experimental results and simulation outputs as in Equation 4.3. Based on the change in error, new parameter values are selected for another simulation run (E and F). This process(B-F) will be repeated until an exit condition is met where the error improvement is below a threshold value or the search time runs out.	66
4.4	Error based on different K values with iteration number It	68
4.5	The heat map of error between K and VEGF binding coefficient/rate (β) determined from the first round sweep.	70
4.6	The heat map of error between K and VEGF binding coefficient/rate (β) determined from the second round sweep.	70
4.7	The heat map of error between K and VEGF binding coefficient/rate (β) from the third round sweep.	71
4.8	The VEGF autoregulatory function of RPE cells showing how the secretion rate of VEGF is down regulated as a function of the VEGF in the microenvironment.	72
4.9	(a) Time course of VEGF expression per cell measured at 4, 24, 30, 48, and 72 h (data from the <i>in vitro</i> work [1]. (b) Time course of VEGF expression per cell measured at 4, 24, 30, 48, and 72 h (data from the <i>in silico</i> model after optimization).	73

ACRONYMS

- ABM** Agent-Based Model. One of a class of computational models for simulating the actions and interactions of autonomous agents (both individual or collective entities such as organizations or groups) with a view to assessing their effects on the system as a whole..
- AMD** Age-related Macular Degeneration. A deterioration or breakdown of the eye's macula. The macula is a small area in the retina that is the light-sensitive tissue lining the back of the eye. The macula is the part of the retina that is responsible for central vision, allowing one to see fine details clearly.
- CA** Cellular Automata. A class of spatially and temporally discrete mathematical systems that are characterised by local interaction and synchronous dynamical evolution.
- DCIS** Ductal Carcinoma *in Situ*. The presence of tumor cells inside a milk duct in the breast. DCIS is a noninvasive condition. DCIS can progress to become invasive cancer, but estimates of the likelihood of this vary widely.
- ECM** Extracellular Matrix. A collection of extracellular molecules secreted by cells that provide structural and biochemical support to the surrounding cells. It forms a meshwork of proteins and carbohydrates that binds cells together or divides one tissue from another.
- ECs** Epithelial Cells. Cells that line the inner and outer surfaces of the body by forming cellular layers (EPITHELIUM) or masses.
- IDC** Invasive Ductal Carcinoma. The cancer cells that began forming in the milk ducts and have spread beyond the ducts into other parts of the breast tissue. Invasive cancer cells can also spread to other parts of the body. It is also sometimes called infiltrative ductal carcinoma.
- LOX** Lysyl Oxidase. A copper-dependent amine oxidase enzyme that initiates the crosslinking of collagens and elastin. It plays a critical role in the biogenesis of connective tissue matrices by crosslinking the extracellular matrix proteins, collagen and elastin.
- MEs** Myoepithelial Cells. Smooth, musclelike cells of ectodermal origin, found between the epithelium and basement membrane in the surface of some acini of the salivary glands, which is believed to be responsible for facilitating the secretion of fluids from the gland.
- MMPs** Matrix Metalloproteinase. Also called matrixins. A large family of calcium-dependent zinc-containing endopeptidases, that are responsible for the tissue remodeling and degradation of the extracellular matrix. They play major roles in morphogenesis, wound healing, tissue repair and remodelling in response to injury.

RPE Retinal Pigmented Epithelium or Retinal Pigmented Epithelial (when used in the context of "cell"). The pigment cell layer that nourishes the retinal cells. It is located just outside the retina and is attached to the choroid, a layer filled with blood vessels that nourish the retina.

TCs Tumor Cells. An abnormal growth of tissue resulting from uncontrolled, progressive multiplication of cells and serving no physiological function.

TGF- β Transforming Growth Factor Beta. A secreted protein that controls many cellular functions, including cell growth, cell proliferation, cell differentiation and apoptosis.

VEGF Vascular Endothelial Growth Factor. A signal protein produced by cells that stimulates vasculogenesis and angiogenesis

CHAPTER 1

INTRODUCTION

Biological systems are intrinsically complex. They operate on multiple functional scales that span across multiple temporal and spatial domains at scales from the atomic level (10^{-10} m) to the whole living organism (1 m), and from nanoseconds (10^{-9} s) to years (10^8 s) (Figure 1.1). A successful understanding of biological function emerges if all relevant information at several levels of organization is integrated, as discussed in [6–8]. For example, in the context of heart function and pathology, Noble [9] illustrated how the success of drug therapy depends not only on understanding the functions at the protein level, but also on knowing how a protein interacts with its surrounding cellular machinery to generate functions at a higher level. There is no doubt that an understanding of the inter-scale and intra-scale interactions is critical to the study of human diseases and potential treatments.

The need to model complex temporal and spatiotemporal processes at many scales has led to the emergence of numerous computational modeling techniques including systems of differential equations, cellular automata simulators, and agent-based models [10]. Multi-scale computational models provide unique capabilities to capture the connectivity between diverse scales of biological function [11,12] and they can also bridge the gap in understanding between *in vitro* experiments and *in vivo* models [13–15]. The advent of powerful computing systems, combined with quantitative data from high-throughput experimental platforms, has expanded multi-scale modeling more comprehensively investigate biological phenomena [16].

The main challenge in multi-scale modeling is maintaining the balance between the computational complexity of the model and its fidelity [17]. The level of model resolution is tightly coupled to computational complexity, where the computational load increases as a function of the model details [18]. Computational modeling that aims to explore such

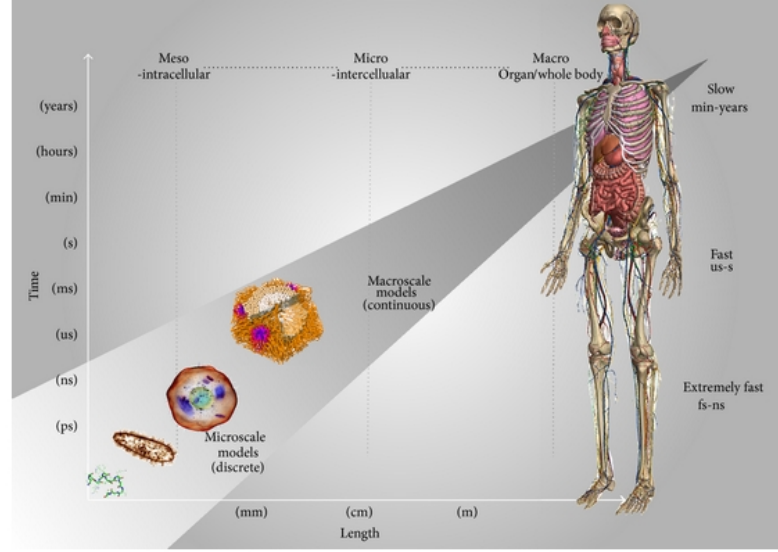


Figure 1.1. Multiscale models of the human body targeting complex processes that span diverse time and length scales of biological organization [2].

multi-scale systems has to incorporate several techniques because of the diverse time and space scales involved. In section 1.1 we provide an overview of different approaches and techniques used to handle these tasks. Then, in Section 1.2, we summarized the main objectives for the research performed in this dissertation. In Section 1.3, we present the projects that were included in this research. In Section 1.4, the research methodology and strategies are explained. Finally, we demonstrate the impacts of the research in Section 1.5.

1.1 Modeling Approaches and Techniques in Computational Systems Biology

1.1.1 Top-down, Middle-Out, or Bottom-up Approaches

There are three approaches to multiscale modeling: top-down, middle-out or bottom-up [19]. The bottom-up approach begins with modeling the system components in isolation and then integrating them to study the emergent properties and predict the behavior of the entire system. The basic principle of the bottom-up approach is to mathematically or

graphically model relationships between the system's components, starting from the lowest level of the multi-scale structure, such as genes and proteins, setting model parameters based on available experimental values, then verifying the model by comparing its behaviors with real system behaviors [20, 21]. The bottom-up approach has a computational problem, which comes from the difficulty and complexity of the integration process across multiple scales. Also, the limitations of bottom-up understanding, as well as a lack of knowledge of many cellular- and tissue-level responses to stimuli that could be used to validate models, present additional long-term, fundamental challenges [22].

Top-down approaches start by considering biological properties and behaviors in the whole system. These behaviors are then used to develop a model that can describe the high-level properties used discover and characterize biological mechanisms at lower levels. Basically, the top-down approach involves defining ways in which the systemic function of interest varies with time or/and conditions, then inferring hypothetical lower-level structures responsible for this function. For instance, in [23], the researchers presented a top-down approach to modeling the single-chain antibody folding pathway [24, 25]. After the scope of the model was established, model development started with the construction of the most basic mathematical model. Incrementally, they appended desired biological details to the developing model and evaluated their effects on model performance until the desired level of detail had been achieved. The top-down approach is applicable to systems of all sizes and with all amounts of available biological information [26].

The third modeling strategy is the middle-out approach, which begins with an intermediate scale such as a cell, then is gradually expanded to include both smaller and larger scales. The middle-out approach is designed to overcome the intrinsic limitations of the above approaches, and it is typically constructed and tested at the levels where we have the most detailed information [27, 28]. For example Noble [9] used a middle-out approach in modeling the heart that it benefited from the wealth of accessible experimental data available at the cellular level and the data-rich modeling of the 3D geometry of the whole heart. In this dissertation, developed for ductal carcinoma in situ is a bottom-up approach

and the model developed for studying VEGF metabolism is a middle-out model.

1.1.2 Continuum, Discrete, or Hybrid Techniques

Modeling can take: discrete, continuum, or hybrid approaches. Continuum models use partial differential equations that are capable of capturing larger-scale systems and provide insight into the relationship among the components of the system. They can be used for modeling several levels of biological systems. Although a continuum model is relatively quicker and easy to implement, it does not capture the discrete nature of systems consisting of individual cells and becomes limited when it is used to model a complex process involving multiple variables [29, 30].

On the other hand, in discrete models, individual cells are explicitly represented in space and time. In these models, individual cell behaviors and interactions with other cells and with the environment can be simulated, enabling emergent system behaviors and properties. Discrete models are usually limited to relatively small numbers of cells due to a large computational demand, and as a result a typical discrete model is usually designed with low domain size [31, 32]. Two major, related discrete modeling strategies currently exist: Cellular Automata (CA) and Agent-Based Model (ABM). A typical CA is a collection of cells on a grid of specified shape. CA has a finite set of cell states, a regular discrete lattice, a finite set of neighboring cells, and rules for the transition of cell states, such as division, migration, apoptosis, and differentiation [29, 29, 33]. In contrast, an ABM asynchronously represents phenomena as dynamic systems of rule-based interactions among agents and their environment, following a set of rules. It is a rule-based, discrete-time, and discrete-event computational modeling methodology that employs computational objects called agents, as in [34–37]. ABM and CA are similar in that the behaviors of agents or cells are controlled by the rules in their environment or neighborhood, both belong to the bottom-up approach, and global emergent properties and behaviors are generated from local interactions. However, CA models impose a simpler quantization space which is unrealistic and limits fidelity, thus CA is weaker in its spatial representation [10]. Recently, agent-based models have become a powerful framework, widely used by computational biological and cancer researchers, since

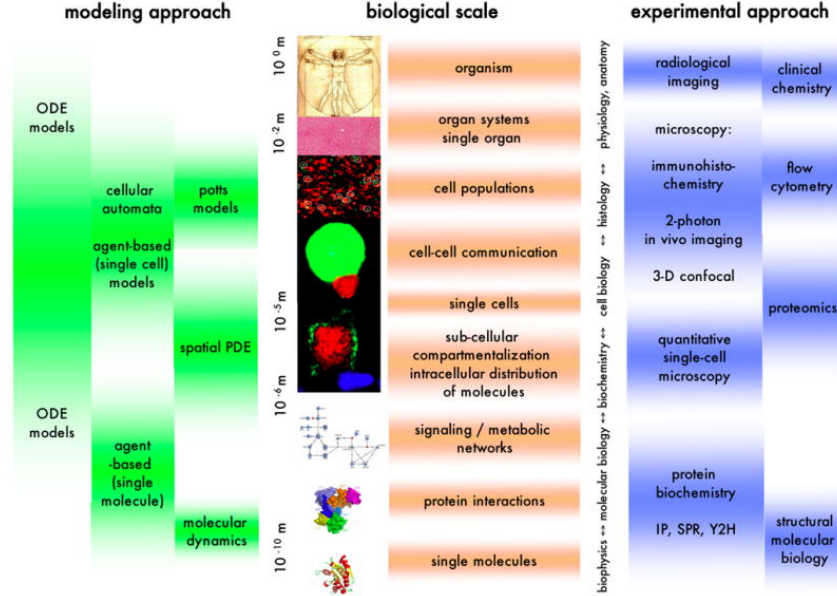


Figure 1.2. A diagrammatic representation of several biological scales and their associated modeling techniques and experimental approaches as in [3].

they have potential to encompass several scales of biological organization and the locations of the agents.

A promising alternative modeling technique is the hybrid models which combine discrete and continuum approaches, and take the strengths of each approach. Recently, hybrid models have attracted considerable attention due to their success in many biological application [38–41]. The models developed in this dissertation are hybrid models that consider particles - the discrete component - and soluble products, such as diffusion proteins, and nutrient - the continuous part of the model.

A choice among modeling approaches should depend on the biological questions that are being addressed. Establishing which model framework to use and what level of detail to include still remain open questions. Many researchers provide strategies and tactics that can help in choosing a suitable approach based on the problem characteristics. Meier-Schellersheim et al. [3] provided an overview of how different scales of experimental research can be combined with the appropriate computational modeling techniques to

carry out multi-scale modeling of cell-to-organ systems as summarized in Figure 1.2. In this dissertation, we develop a hybrid, agent-based framework to model the transition in breast cancer from ductal carcinoma *in situ* to invasive ductal carcinoma (Project 1), and study the effect of retinal pigment epithelial cell patch size on VEGF expression (Project 2). Finally, we fit the developed model in Project 2 to available *in vitro* experimental data, so as to estimate the model's parameters (Project 3).

1.2 Objectives

The core goal of this research is to utilize a multicellular hybrid agent-based modeling approach in studying disease development and progression. The major question on which this research focuses is: how can a hybrid agent-based modeling approach be utilized to study and explore disease development, particularly in two applications, breast cancer and bioengineering experiments related to AMD? To achieve this, we need to identify methods, algorithms and techniques that increase the effectiveness of these models. We have realized this overall goal by completing three specific aims:

The first aim of the dissertation is to introduce a multicellular agent-based model of ductal carcinoma *in situ* growth and invasion that includes ductal, stromal and tumor cell types acting along with multiple biochemical and biomechanical interactions. This model replicates the disease state associated with breast cancer from initiation to invasion. This work provides a robust predictive modeling and visualization system to enable discovery of molecular mechanisms involved in tumorigenesis and metastasis, testing of candidate therapeutics, and more rapid identification of therapeutics against malignancy.

The second aim of this dissertation is to apply an agent-based framework to provide an *in silico* model that can be used to understand a central aspect of an *in vitro* model for age-related macular degeneration (AMD): the effect of retinal pigment epithelial cell patch sizes on growth factor expression. This framework provides a model for emulating disease states associated with the deterioration of retinal tissue during AMD.

The third and final aim of this dissertation is to develop an alternative approach to bridge the multi-scale gap by identifying cellular biochemical and biophysical parameters

from multicellular data. A search method is developed and applied to estimate cellular parameters related to VEGF metabolism from spatiotemporal data available from a bio-engineered multicellular *in vitro* model of AMD development. The method successfully identifies values for VEGF properties that can be used in the model produced in Project 2 to reproduce the spatiotemporal derived from *in vitro* experimental data.

1.3 Projects Outlines

1.3.1 Project 1: Interactions of Stroma and Tumor Cells in Carcinoma *in Situ* to Invasion: An Agent-Based Modeling Approach

Breast cancer is one of the main causes of cancer-related deaths in women. *In situ* ductal carcinoma of the breast is the most common precursor to invasive ductal carcinoma (IDC). Ductal carcinoma *in situ* (DCIS) develops over two to twelve years [42] and is not a life-threatening cancer, but is clinically important because it can be detected and treated before the duct is breached allowing the tumor to invade neighboring tissues. Left untreated, 14%-15% of DCIS progress to invasive cancer [43].

In this project, we developed a multicellular agent-based model of ductal carcinoma growth and invasion that includes ductal, stromal and tumor cell types, transforming growth factor beta (TGF- β), matrix metalloproteinase (MMP), lysyl oxidase (LOX), and extracellular matrix (ECM) protein assemblies, including the basement membrane. Unlike models that consider only biochemical inputs, the model developed in this work explicitly determined tensional and compressive forces within the developing tissue along with the distributions of and cellular responses to biochemical agents. The model demonstrated that MMP secretion sufficiently weakens the ductal basement membrane and epithelial tight junctions to undermine ductal integrity and that compressive and tensile stress within the growing tissue contributes to metastasis.

1.3.2 Project 2: Developing An *in Silico* Model to Study The Effect of Retinal Pigment Epithelial Cell Patch Sizes on VEGF Production

Age-related macular degeneration (AMD) is a leading cause of irreversible blindness world-wide [44,45]. Degeneration of retinal pigment epithelial (RPE) cells severely damages the visual function of retina photoreceptors. Age-related alterations of the RPE include changes in pigmentation and the reduction of cell density of RPE [46]. There are two forms of AMD: dry (atrophic) and wet (exudative). In exudative AMD, new blood vessels from the underlying choriocapillaris grow toward the RPE. These processes often lead to irreversible loss of the central visual field [47]. Anti-VEGF therapy is used to treat exudative AMD because of the central role that VEGF plays in neovascularization. *In vitro* studies provide powerful tools for examining the links between growth factor expression, tissue reorganization and the progression of the disease, and replicate the effect of atrophic and leaky RPE cells on VEGF expression. However, the stimuli leading to enhanced VEGF secreted from RPE cells and the subsequent neovascularization processes in the choroid are still not fully understood [48, 49].

Vargis et al. [1] used the bioengineered micropatterning techniques to create a regular arrangement of circular colonies, called patches, populated with RPE cells surrounded by a empty substrate. Creation of this micropatterns involves many sequential steps. The non-populated regions imitate necrotic regions in the retina that result from repeated exposure to reactive oxidative species, triggering death of the retinal pigment epithelium followed by death of the overlying photoreceptors and neovascularization, which is leading exudative AMD [50, 51].

The goal of this study was to develop a computational model to replicate the *in vitro* cellular model [1], and then to use the computational model to study how different configurations of cells influenced on VEGF expression. Quantitative analysis of RPE patch morphology and VEGF expression was performed. VEGF levels in each patch were studied as a function of cell number and patch area through time. VEGF expression from various sized patches was quantified following VEGF agonist administration in order to study

the hypothesis that VEGF expression is linked to VEGF auto-regulation in the microenvironment [52, 53] through targeting VEGF [54]. This work complements the experimental studies performed *in vitro* and provides a framework that can be used to study the influence of cell patterning on the secretion of VEGF by RPE tissue. The model has potential to point toward a path to mimicking the effects of tissue damage or atrophy that occurs in the retina during AMD. This model was applied to study additional mechanism and predict.

1.3.3 Project 3: Bridging the Multiscale Gap: Identifying Cellular Parameters from Multicellular Data

One of the main challenges in the computational modeling of biological systems is identifying values of model parameters. This problem is particularly acute with multiscale models. In this project, we developed an approach that estimates cellular parameters from spatiotemporal data produced from *in vitro* studies.

We developed a search technique to discover the values of biochemical parameters related to VEGF metabolism. The method began with data available from a multicellular model of retinal pigment epithelial cells. Understanding VEGF regulation is critical in treating AMD and many other diseases. Thousands of simulations were performed as the search method explored the parameter space. For each potential solution, multiple simulations were needed over each experimental case (different patch sizes) and because of the need for repeats due to model stochasticity. The method successfully identifies realistic values for VEGF autoregulatory parameters that reproduce the spatiotemporal *in vitro* experimental data.

1.4 Research Methodology and Strategies

The using modeling framework is an extension of iDynoMiCS [55], which is a hybrid agent-based modeling framework and originally developed to simulate biofilm development. Two major components of the framework are particles and soluble products, integrated within a reaction diffusion system. Particles, the discrete part of the model, represent individual cells that mechanically interact, secrete, consume or react to soluble products.

Soluble products represent extracellular diffusible biomolecules that make up the continuous component of the system whose distributions are determined by a diffusion solver that resolves all the local changes in concentration induced by the particle secretion and uptake and long-range diffusion.

In Project 1, the DCIS model was executed from an normal duct configuration at model initialization and run to simulate the development of the ductal tumor from initiation to ductal breach and invasion. This model is complex and includes a large number of parameters, including some parameters that cannot yet be measured. First, the known parameters were set from the literature, then the other parameters were estimated and refined by evaluating the ability of the model to recapitulate observed tumor progression. The model was limited to a relatively small numbers of cells due to the large computational demand, and as a result the model was defined over a small domain size as shown in Figure 2.5. Several assumptions were taken into consideration in the design of the model. For example, it was assumed that the ductal tissue has a limited number of fibroblasts that do not grow.

In Project 2, the RPE model was executed from the initial experimental conditions and simulated the *in vitro* model of VEGF metabolism from 1-72 hours. The known parameters were set from the experimental data in [1]. Unknown parameters (VEGF secretion rate of each RPE cell, VEGF binding affinity, and autoregulation strength were randomly initialized; then they were refined based on the results of the optimization process in Project 3. The ultimate goal of any modeling effort is to provide actionable predictions. Ideally, important experiments that could not be performed *in vitro* could instead be done using the *in silico* approach. For instance, a more realistic model of retinal degeneration is a configuration in which there are cell-free areas in the midst of a largely cell-covered surface of the culture dish. This was modeled using circular patches where the cells are applied to the outside areas and the patches were left empty. This arrangement is the inverse used in the engineered *in vitro* cellular model and it provides a more realistic configuration.

In Project 3, the main objective is to develop a general-purpose techniques for determining the free parameters, error functions, realistic ranges, experimental measurements, search space constraints, and refinement operators. In order to minimize the error and identify likely values for the free-parameters in the model developed in Project 2, thousands of simulations are required. A single execution of the model can take hours, and hundreds of simulations must be run to identify the sensitive parameters, to adjust their ranges and to study model behavior. These computational challenges were taken in consideration, and we used several fast machines(The memory for each machine is 16GB RAM, and the processor is Intel(R) Core(TM) i7-3770K CPU, 3.50GHz (eight CPUs))to run the experiments 24 hours a day.

1.5 Research Impacts

The work in Project 1 could provide a system with robust predictive modeling and visualization to enable discovery of molecular mechanisms involved in tumorigenesis and metastasis, testing of candidate therapeutics, and more rapid identification of therapeutics against malignancy. In addition, the emphasis on the interaction between biochemical and biomechanical properties in cancer progression may open the door to new treatments that exploit these mechanisms. We believe this model will have higher impacts in the future when this model is integrated with histological clinical and experimental data, such as that being collected in the TCGA project [56,57].

The work in Project 2 complements experimental studies performed *in vitro* and provides an *in silico* framework with reliable predictive modeling and visualization to examine the effects of the spatial organization of retinal pigment epithelial (RPE) cells grown in patches of several sizes on VEGF production. It could aid in the development of agents that target VEGF and inhibit angiogenesis, and may be useful in evaluating biomarkers of anti-angiogenic therapies in age-related macular degeneration. This work models the bioengineered multicellular configurations that provide strong experimental controls and customizations to target specific cellular mechanisms.

The multicellular search-based approach introduced in Project 3 is applied to identify

the parameter values of a cellular regulatory mechanism using spatiotemporal multicellular data. This approach was applied to predict the dynamic concentrations of VEGF and other VEGF parameters that are difficult to quantify experimentally. In addition, the results may aid understanding of how uncertainty in the values of particular parameters influence model outputs.

CHAPTER 2

AN AGENT-BASED MODELING APPROACH TO EXPLORE INTERACTIONS OF STROMA AND TUMOR CELLS: THE PROGRESSION OF IN DUCTAL CARCINOMA *IN SITU* TO INVASIVE DUCTAL CARCINOMA

2.1 Abstract

Invasive ductal carcinoma marks a significant drop in patient survival and is one of the leading causes of death in women. The timing and severity of ductal breach is primarily driven by biochemical and biomechanical mechanisms that interact to weaken duct integrity and induce stress in the duct wall. Understanding the cellular responses to these biomechanical and biochemical stimuli may lead to new therapeutic approaches to breast cancer. We introduce a multicellular agent-based model of ductal carcinoma growth and invasion that considers ductal, stromal and tumor cell types, transforming growth factor beta (TGF- β), matrix metalloproteinases (MMPs), lysyl oxidase (LOX), extracellular matrix (ECM) protein assemblies, including the basement membrane, and that explicitly determines tensional and compressive forces within the developing tissue along with the distributions of and cellular responses to biochemical agents. The model predicts that MMP secretion sufficiently weakens the ductal basement membrane and epithelial tight junctions to undermine ductal integrity and that compressive and tensile stress within the growing tissue contributes to metastasis.

⁰The coauthors for this chapter are: Qanita Bani Baker, Ahmadreza Ghaffarizadeh, Soonjo Kwon, Gregory J. Podgorski and Nicholas S. Flann

2.2 Introduction

Breast cancer is one of the main causes of cancer-related deaths in women. Ductal carcinoma *in situ* (DCIS) of the breast is the most common precursor to invasive ductal carcinoma (IDC). Ductal carcinoma *in situ* develops over two to twelve years [42] and is not a life-threatening cancer, but is clinically important because it can be detected and treated before the duct is breached. Clinical studies show that 14%-53% of misdiagnosed DCIS, if left untreated, will progress to invasive cancer [43].

Breast ducts are composed of radial layers of cells and extracellular matrix. Moving from the lumen outwards, these layers are epithelial cells (ECs), basement membrane, and myoepithelial cells (MEs) surrounded by stroma consisting of ECM, fibroblasts, myofibroblasts, and blood vessels (see Figure 2.1a). Figure 2.1 shows the steps in the transition from normal ducts to an invasive carcinoma [4]. DCIS occurs when abnormal epithelial cells begin growing within the duct. These are tumor cells (TCs) and they exert outward biomechanical stress on the ductal system of epithelial cells, myoepithelial cells and the supporting basement membrane and also secrete proteinases which weaken the ductal wall and trigger biomechanical changes in the surrounding stroma.

While the progression from DCIS to IDC is understood in outline, many open questions on DCIS biology remain. How do the mechanical properties of breast tissue contribute to disease progression, compromise treatment or alter metastasis risk? How does inter ductal pressure influence tumor progression, metastasis, and responses to cancer therapy? How are the material properties of breast tissues established and maintained? How do cells adapt to biochemical and biophysical changes that occur during *in situ* tumor growth? Answers to these questions have important implications for clinical practice.

The simulation system developed here may aid in answering these questions. The objective of this paper is to explore the interplay between the buildup and relief of forces within the duct as a tumor grows and as both the cells and ECM change their biophysical properties in response to these forces. The model also considers how biochemical events, such as activation of growth factors and production of enzymes that change the mechanical

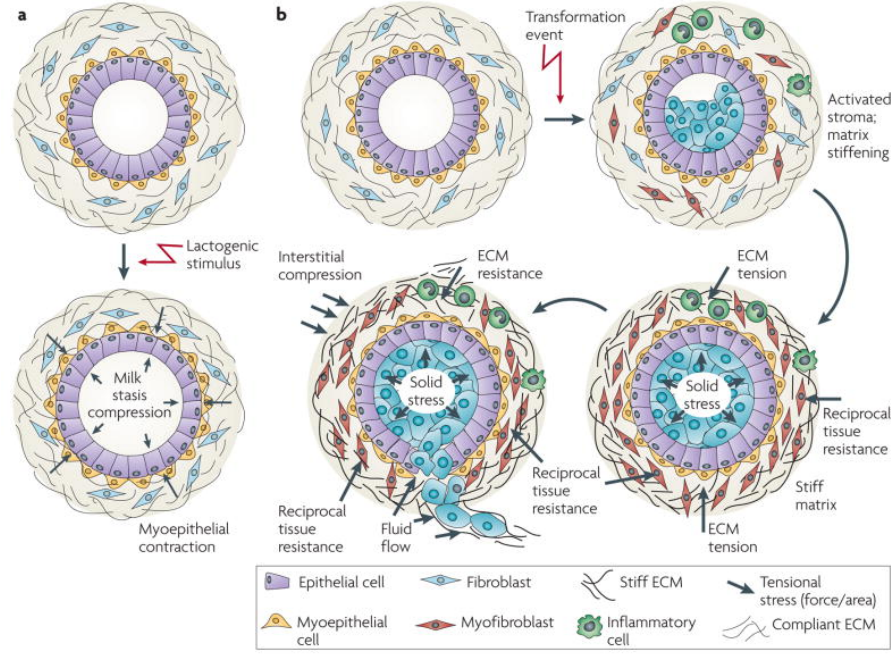


Figure 2.1. a- The developing of normal breast. b- The transition from normal mammary ducts to an invasive tumor in breast cancer. From Butcher et al. 2009 [4]

properties of the ECM, shape the unfolding biomechanical dynamics of the duct during tumor growth. The emphasis on the interaction between biochemical and biomechanical properties in cancer progression may open the door to new treatments that exploit these mechanisms.

2.3 Background

2.3.1 Previous Models of Ductal Carcinoma *in situ*

Many of computational approaches and modeling paradigms have been developed to understand and predict the dynamics of DCIS and its transition to IDS. Current computational cancer modeling approaches fall into three main categories: discrete, continuum, or hybrid approaches [37]. Continuum models usually use partial differential equations that are capable of capturing larger-scale systems and provide insight into the relationship among the components of the system. Continuum models can be used for modeling several levels

of biological systems. While a continuum model is relatively quick and easy to implement, it does not capture the discrete nature of systems consisting of individual cells and becomes limited when it is used to model a complex process involving multiple variables [29,30].

On the other hand, in discrete models, individual cells are explicitly represented in space and time. In these models, individual cell behaviors and interactions with other cells and with the environment can be simulated enabling emergent system behaviors and properties. Discrete models are usually limited to relatively small numbers of cells due to a large computational demand, and as a result a typical discrete model is usually designed with low domain size [31,32]. Two major, related discrete modeling strategies currently exist: Cellular Automata (CA) and Agent-Based Models (ABMs). A typical CA model considers a collection of cells on a grid of specified shape. CA models usually include a finite set of cell states, a regular discrete lattice, a finite set of neighboring cells, and rules for the transition of cell states, such as division, migration, apoptosis, and differentiation as explained [29,33]. In contrast, ABM models represent phenomena as dynamic systems of rule-based interactions among agents and their environment, using discrete-time, and discrete-event modeling methodology [34–37]. ABM and CA modeling approaches are similar in that the behaviors of agents or cells are controlled by their environment or neighborhood, and both are bottom-up modeling approaches, and global system emergent properties and behaviors are generated from local interactions. However, CA models impose a simple quantization space that is unrealistic and limits fidelity, thus the CA modeling approach is weaker in its representation of space [10]. ABMs have recently been more widely used by computational biological and cancer researchers, because of their potential to encompass several scales of biological organization and their robust ability to consider the spatial arrangement of agents.

Even more promising alternative modeling techniques are hybrid models which combine discrete and continuum approaches and take advantage of each approach. Recently, hybrid models have attracted considerable attention due to their success in many biological applications [38–41]. The work reported here applies an agent-based modeling framework

to perform a study into how biomechanical and biochemical processes interact within ductal and stromal cells to trigger DCIS to IDS transition.

Franks et al. [58] described the initial stages of DCIS, where a nutrient-limited growth model was introduced that used Stokes flow to describe the behavior of the tumor cells. They applied numerical and asymptotic methods to examine the shape of the tumor boundary and the extent of tumor cell adhesion to the duct wall in early DCIS. They extended this work in [59] to develop a continuum mathematical model that was used to examine the effects of proteolytic enzyme production on tumor growth and invasion. This model predicts that mechanical stress on the duct wall is the dominant mechanism in the transition of invasive carcinoma.

Sontag and Axelrod [60] combined a population-scale model with machine learning techniques and statistical analyses to describe the progression from DCIS to IDC. Here four signalling pathways were investigated that describe relationships between different grades of DCIS and IDC found in the same patient.

Rejniak and Dillon [61] employed a cell-based technique to make predictions for DCIS morphologies based on differential growth and cell polarity. Their model utilized the immersed boundary method that treats cells as elastic bodies and models the cytoplasm and extracellular matrix as viscous incompressible fluids. They found that the formation of the four specific DCIS morphologies (micropapillary, cribriform, tufting, and solid) result from changes in cell orientation and growth rates.

Figueredo et al. [62] compared agent-based modeling approaches to approaches that use ordinary differential equations. They considered three case studies using models of immune interactions within early-stage DCIS. They demonstrated that the stochastic elements that are essential components of agent-based models increase fidelity and provide unique insights beyond those of models based on differential equations. Norton et al. [63] developed a 2D model using a lattice-free agent model and conducted an investigation of the relationship among polarised cell adhesion, intraductal pressure, and subsequent DCIS morphology. Kim et al. [64] applied an agent-based model to study interactions among DCIS cells and

stromal cells via TGF- β and EGF soluble factors; their work included the effects of basement membrane expansion. Macklin et al. [65] developed an agent-based cell model and applied it to the process of necrosis in tumor morphology. In this work the first patient-specific calibration method was introduced to help constrain the model based on clinically-accessible histopathology data. Their work illustrated how computational modeling can provide new insights into the biophysical underpinnings of cancer. D’Antonio et al. [66] introduced an agent-based model to simulate the interactions between cells and the basement membrane. They modeled the basement membrane as a linked series of Hookean springs, each with time-varying length, thickness, and spring constant. In this model, each BM spring node exchanges adhesive and repulsive forces with the cell agents. Also, they modeled elastic BM-ECM interactions with analogous ECM springs. They found that varying the balance of BM and ECM elasticity can trigger heterogeneous distribution of BM thickness that can lead to ductal breaching.

2.3.2 Key Biological Components involved in Ductal Carcinoma *in situ* progress

The accumulation of genetic and epigenetic alterations in the ductal epithelium cells accompanied by alterations in the matrix leads to unchecked proliferation and enhanced proliferation of luminal epithelial cells within the ductal tree [67]. With prolonged growth, luminal mammary epithelial cells eventually expand to fill the breast ducts.

Importantly, the abnormal luminal mammary epithelial cells secrete soluble factors including MMPs that diffuse into the stromal matrix. MMPs are a family of zinc- and calcium-dependent proteinases that degrade the collagen of the ECM and stimulate the expression of fibronectin through the activation of transforming growth factor-beta (TGF- β). The TGF- β is released as an inactive latent complex. Latent TGF- β can be activated by metalloproteases MMP-9 and MMP-2, which are often expressed by malignant cells [68], [69].

TGF- β activate resident fibroblasts to differentiate into myofibroblasts which are responsible for the changes in the composition, post-translational modifications and topology of ECM proteins, causing the ECM to stiffen over time. The number of myoepithelial

cells surrounding the abnormal luminal mammary epithelial cells mass decreases and the basement membrane thins, probably owing to increased (MMP) activity, decreased protein deposition, and compromised epithelial tight junctions [70], [71].

In the non-malignant state structural and metabolic proteins are present in the ECM. A subset of ECM proteins are overexpressed in the surrounding stromal matrix during tumorigenesis. ECM remodeling is driven by:

1. The increased levels of (LOX)-dependent ECM cross-linking [72], [73]. LOX is an amine oxidase which catalyzes the conversion of lysine and hydroxylysine residues in collagen molecules to their semi-aldehydes. This is the first step in forming of covalent intra- and intermolecular collagen crosslinks, and the creation of collagen fibrils and fibers to stabilize the mechanical integrity of collagen. Thus, LOX plays an important role *in vivo* in the stabilization of newly synthesized collagen and the stiffening of ECM [74], [75], [76].
2. Abnormal MMPs expression and function [77], including overexpression of MMP2 in the transformed ECs [78] and MMP3, MMP11, MMP12, and MMP13 in the tumor stroma. The synthesis and degradation of the ECM of the stromal matrix also depends on a balance between another class of MMPs and their tissue inhibitors (TIMPs).
3. Post-translational modifications of ECM proteins including altered deposition of proteoglycans [79], [80].

In this study, to model DCIS progression to IDC, we introduced a multicellular agent-based model of ductal carcinoma growth and invasion in a way that incorporates ductal, stromal and tumor cell types, transforming growth factor beta(TGF- β), matrix metalloproteinase (MMP), lysyl oxidase (LOX), and extracellular matrix (ECM) protein assemblies, including the basement membrane. This model can visualize and predict how perturbation of the local biochemical and biomechanical state influence DCIS evolution.

2.4 Methods

2.4.1 Domain-Independent Agent Based Model

Our modeling framework is an extension of iDynoMiCS [55], a modeling framework that was originally developed to simulate biofilm development. Two major components of our model are particles and soluble products integrated within a reaction diffusion system. Particles, the discrete part of the model, represent individual cells that mechanically interact and secrete, consume or react to soluble products. Soluble products represent extracellular diffusible biomolecules that make up the continuous component of the system. The distribution of the biomolecules is determined by a diffusion solver that resolves all the local changes in concentration induced by cell physiology and diffusion.

Particles

A particle is an incompressible sphere with a mass and set of regulatory components that depends on its type. The particle is positioned in space and occupies the volume of a single cell. Particles grow and mechanically interact with each other through packing constraints, pressure relief, adhesion, chemotaxis and other mechanisms. Signalling among particles is implemented through diffusion. Particles can be specified to represent distinct cell types through assignment of unique reaction-diffusion equations and biomechanical properties such as adhesion. Switching between cell states is possible and is triggered by the properties of the particle’s internal state and external environment.

Particle Dynamics

A configuration of particles represents the spatiotemporal state of the biological system. To update the configuration, the net force acting on each particle is first determined, then the particles are moved based on a force vector that is determined dynamically as the model runs. The mechanical forces acting on a particle (σ_i) are computed by vector addition of force contributions of each mechanism in play during the simulation, $F_m(\sigma_i, \sigma_j)$ where i, j are indexes to each near-by particle and m is the specific mechanism. Since the particles

are over damped, inertial effects are ignored and particle velocity is proportional to force. A weak stochastic force η is added to each particle to model underlying fluctuations in cell movement using a Gaussian distribution with a variance of 0.1; this stochastic movement is essential for reaching cellular configurations of near-minimum energy.

The change in position of an arbitrary particle σ_i , denoted as $\Delta p(\sigma_i)$ is defined as:

$$\Delta p(\sigma_i) = (\sum_{m \in M} \sum_j F_m(\sigma_i, \sigma_j) + \sum_{l \in M} F_l(\sigma_i) + \eta) \Delta t \quad (2.1)$$

Once forces are generated, a relaxation algorithm is executed to determine the quasi-steady state that minimizes the forces acting on the system. The process continues until the magnitude of particle movement drops below some threshold. The complete particle configuration is asynchronously updated by randomly selecting each particle then applying a small displacement based on equation 2.1 to avoid artifacts.

Growth and Mass Decay

Growth reactions lead to changes in the biomass of a particle. As the biomass increases so does the spherical particle volume and radius. When the radius equals or exceeds a maximum type-specific particle size parameter called the split radius R_{sp} , the particle is divided in two along a random cleavage plane. Any overlap with neighboring cells is ignored during placement and resolved during force relaxation.

Particle size can reduce through biochemical reactions that consume biomass or lead to decay, particle apoptosis, or necrosis. When the radius equals or falls below the minimum particle size parameter called the death radius (R_d), the particle is removed from the domain.

Pairwise Particle Interaction

Packing constraints cause particles to exert opposing forces (positive) on each other to minimize spatial overlapping caused by growth or cell movement. The process is illustrated in Figure 2.2. In this work, the opposing force magnitude is directly proportional to the overlap distance between each particle. So

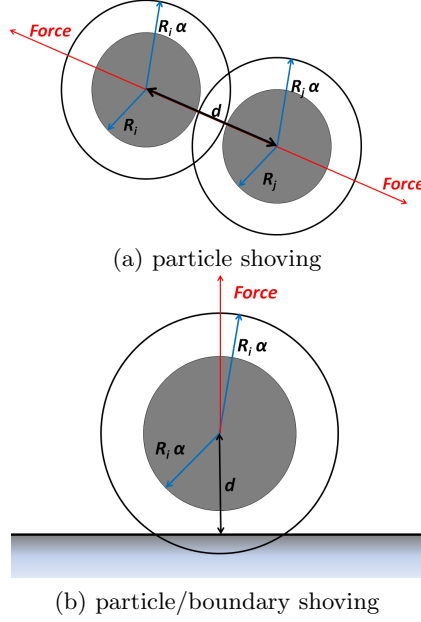


Figure 2.2. Particle Shoving: $R_t(\sigma_i)$ is the radius of a particle of state $t(\sigma_i)$, α_t is the shoving factor for this state t and d is the distance between the objects. When two particles i and j are closer than $\alpha_t(R_{t_i} - R_{t_j})$ then a force is applied to push them apart. For an impregnable boundary, the force is only applied to the particle.

$$F_{ov}(\sigma_i, \sigma_j) = (\alpha_t |R_{t_i} + R_{t_j}| - d(\sigma_i, \sigma_j)), \quad (2.2)$$

$$d(\sigma_i, \sigma_j) < \alpha_t |R_{t_i} + R_{t_j}|$$

where R_{t_i} is the designated radius of particle i based on its type $t(\sigma_i)$. α_t is termed the shoving factor and it determines the average packing density of particles of size R_{t_i} and R_{t_j} . Additionally, nearby particles experience attractive forces due to adhesion and surrounding ECM. This is represented as potential function applied when $d(\sigma_i, \sigma_j)$ is greater than or equal $\alpha_t |R_{t_i} + R_{t_j}|$. Initially attractive forces increase from zero then fall off to zero as the particle separate. The potential function in this case is a generalized Morse function [81].

Pairwise particle interactions can be associated or disassociated. Associated interactions model tight junction among cells of the ductal epithelium, the basement membrane, and the extracellular matrix crosslinks. Here the particle's neighbors are initialized and do not change as particles move, creating a tight mesh that models the basement membrane,

between epithelial cells, and in crosslinked stiff ECM. In contrast, disassociated particles recompute their neighbors at each relaxation iteration before aggregate force calculation. In this way, the attractive forces among disassociated particles drops off as they are separated through movement, enabling displacement and separation by other particles as in the case of growth, invasion, or ductal breach.

Mechanical Stress Fields

The particle forces mechanism described above is insufficient for capturing and resolving all the movements in our simulation when ECM stiffens in response to the formation of new cross-links due to LOX or weakens due to MMP. While particle shoving is a local level interaction sufficient to model simple particle growth and division, a global mechanism is needed to compute the movements imposed both by tightly linked particles and by particle shrinkage that occurs in the modeling framework. Mechanical stress fields, increased by cell linking and growth, and decreased by cell shrinkage or death, are used to apply movement vectors to particles move them toward the locations as the stress is relaxed. This pressure, termed “biomass pressure,” is expressed as the following elliptic differential equation [82], [83]:

$$-\nabla \cdot \left(\frac{k}{\mu} \nabla P \right) = \sum_{i=1}^n \frac{1}{\rho_i} \frac{dM_i}{dt} \quad (2.3)$$

where P is the pressure generated from the growth or loss of biomass, $\frac{dM_i}{dt}$ is the local biomass production or loss rate, ρ is the density, and the summation is iterated over all n biomass types present in the model. This second order elliptic partial differential equation specifies that the gradient of pressure transport is proportional to rate of volume production or decay at each grid point. This equation is solved in our simulation by a semi-multigrid equation solver to relax the pressure to a quasi stable state. Computing the pressure gradient and applying the movement vectors is performed before applying the shoving.

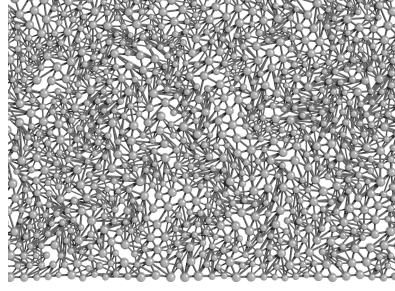


Figure 2.3. Extracellular Matrix formation as crosslinks between ECM particles (spheres in the figure).

Extracellular Cellular Matrix

We model the ECM using a hybrid of discrete and continuous models. The discrete component is as an organization of particles interacting with each other as described above. The density, adhesion strength and particle interactions of this group specifies the emergent properties of the formed matrix; particles do not represent the matrix directly, but rather the cross-links between fibers (see Figure 2.3). The density of the links and their pair-wise interaction responses indirectly determine the stiffness of the tissue-scale ECM.

The continuum component of ECM, introduced by Alpkvist et al. [82], models the local secretion and accretion of ECM proteins as a local diffusion process. ECM is secreted from one particle to accrete on a neighboring particle to form fibrous crosslinks (bonds between particles).

ECM degradation occurs when MMPs reduce the stiffness of the ECM, weakening bonds between particles and ultimately causing the particle's disappearance. This process is modeled by reducing the mass of ECM particles proportional to the amount of MMP in the microenvironment, and removing ECM and the associated crosslinks if their mass falls below a threshold [84]. An example of this process is illustrated in Figure 2.4 along with the reciprocal process of ECM stiffening caused by secretion of LOX.

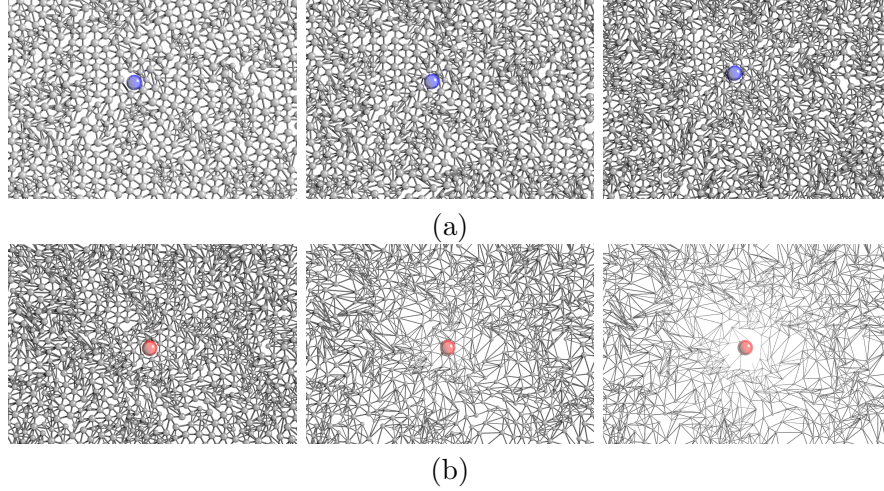


Figure 2.4. (a) ECM stiffening viewed over time (earlier to later is left to right). Blue particles are secreting stiffening enzyme (LOX) that increases amount of ECM (spheres) and cross links between ECM particles, causing the ECM to stiffen; (b) ECM degradation. Red particles are secreting MMPs that degrade the surrounding fibers.

2.4.2 Ductal Carcinoma Model

This model incorporates the primary processes in ECM remodeling during the progression of DCIS to IDC described in Section 2.3. Figure 2.5 represents breast duct microarchitecture in cross-section in the initial state of the model. The duct is a tubular arrangement of epithelial cells (pink particles), surrounded by myoepithelial cells (yellow particles) and the basement membrane (small black linked particle forming a tight mesh). The initialing tumor cell (TC) is the single blue particle positioned on the internal duct surface. Surrounding and supporting the duct is the stroma consisting of: ECM (the small light gray particles) that contains fibroblasts (big gray particles) and myofibroblasts (cyan particles). The stroma also contains blood vessels (red particles) that supply the duct with nutrients, oxygen, and growth factors through the basement membrane.

In addition to different cell types, the model includes three diffusible biochemical factors that determine cellular and ECM properties important for DCIS progression. Figure 2.6 illustrates an overview of the model components and their interactions. The model considers two broad spatial domains: the region within the duct that contains epithelial cells and

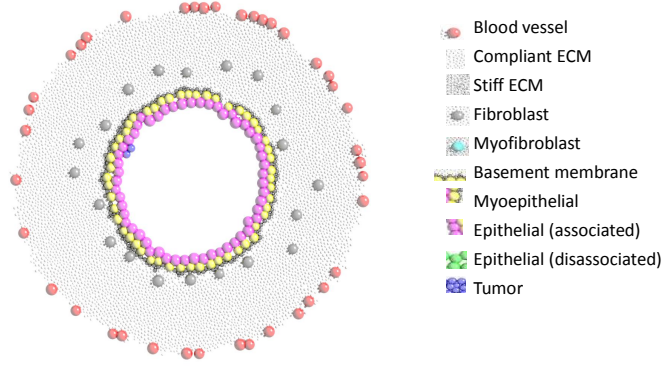


Figure 2.5. The initial condition of the DCIS to IDC simulation. The duct is a tubular arrangement of epithelial cells, surrounded by basement membrane and myoepithelial cells. The duct is embedded within stroma that includes: ECM, fibroblasts and blood vessels cells. There is a single tumor cell on the internal wall of the duct.

tumor cells and the stroma that contain the ECM and all other cell types. Tumor cells produce MMPs (many forms of MMP aggregated by the model as a single class) that act on the basement membrane and that can diffuse into the stroma.

In the basal state prior to DCIS, the rate of TGF- β production, a central regulator of normal cell proliferation, is controlled, and ECM stiffening and degradation are in balance. When ductal tumor cells begin to proliferate, they cause activation of latent TGF- β trigger by the increased MMPs production by the tumor cells [68,85]. The increased activity of TGF- β in the stroma stimulates differentiation of fibroblasts into myofibroblasts (Figure 2.6). Fibroblasts and myofibroblasts produce local ECM components at a constant rate. Additionally, myofibroblasts secrete LOX that stiffens the ECM [86] .

In the model, MMPs degrade the ECM and MMPs are over produced by malignant epithelial cells. MMPs secretion is up-regulated by mechanical stress experienced locally by each cell due to the ECM stiffening and tumor growth. The secreted MMP transforms the basement membrane from a tight association with epithelial cells to being dissociated from

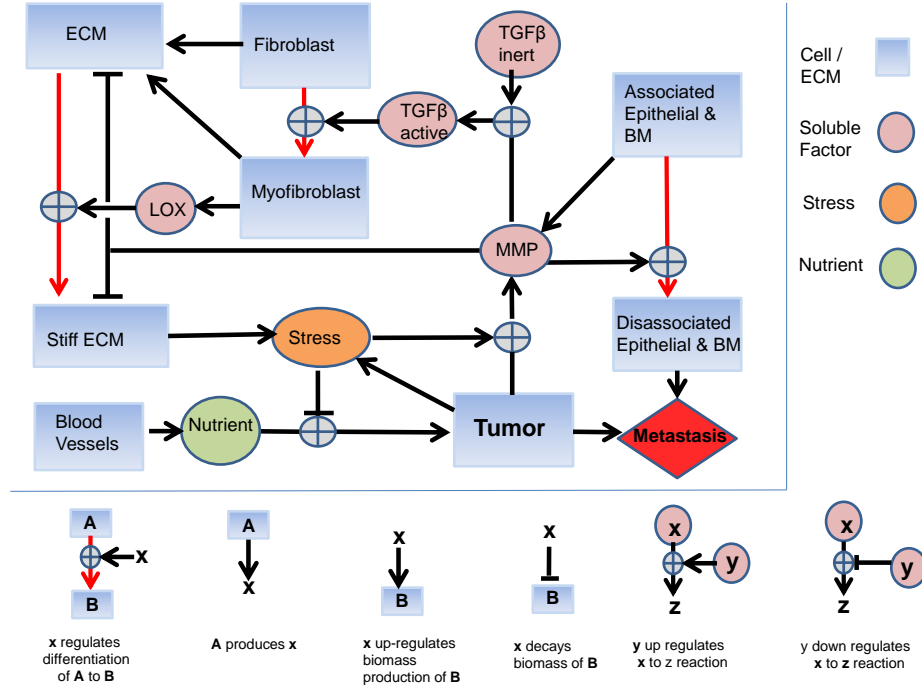


Figure 2.6. The diagram represents the overview of inhibition and activation reactions and the coupling among biomechanical and biochemical model components. The blue rectangles represent cell/ECM types, the pink circles represent the soluble factors, the orange circle represents the biomechanical stress (pressure), and the green circle represents the nutrient. The arrows show whether the influence is either inhibitory or activating. The red arrows represent the transitions between cell types that is regulated by a factor. For example, the red arrow from fibroblast to myofibroblast signifies that this cell type transition is regulated by $\text{TGF-}\beta$.

epithelial cells. MMPs weaken cross links between the ECM and ECs particles and causes transformation from associated ECs to disassociated ECs. LOX initiates the covalent cross-linking of collagen and the elastin, increasing the tensile strength (stiffness) of the ECM modeled the addition of particle links. The model, we assumed that the LOX is secreted only by myofibroblasts after their differentiation from fibroblasts [87].

In the following model equations, all soluble factors are denoted S_i , cell and ECM mass is denoted M_i , D_i represents diffusion rate, and μ_i represents maximum specific rate, where i denotes for cell or particle type. See Table 2.1 for a summary of model parameters.

Nutrient (oxygen) Secretion

The model considers that nutrients are secreted by capillary endothelial cells of capillaries (M_{bc}) and consumed by tumor cells (M_{tc}) based on the following equation:

$$\frac{\partial S_n}{\partial t} = D_{S_n} \nabla^2 S_n + \mu_{S_n} M_{bc} - \mu_{S_{cn}} M_{tc} \quad (2.4)$$

In this equation, D_{S_n} is the nutrients diffusion coefficient, μ_{S_n} is the maximum specific rate of nutrients secretion (units of 1/hour), $\mu_{S_{cn}}$ is the maximum specific rate of the nutrient consumption (units of 1/hour), and M_{tc} is the mass of tumor cells.

Tumor Growth

The tumor growth is activated by nutrients supplied by blood vessels, and down-regulated by mechanical pressure effects according to Equation 2.5.

$$\frac{\partial M_{tc}}{\partial t} = \mu_{tc} \frac{S_n}{S_n + K_n} \frac{K_{tc}}{P + K_{tc}} M_{tc} \quad (2.5)$$

Here, μ_{tc} is the maximum specific rate of tumor growth (units of 1/hour), and M_{tc} is the mass of tumor cells. Note that pressure down-regulates growth (shown in Figure 2.6).

MMP Secretion

The model includes the influence of increasing mechanical stress (represented by pressure P) on the up-regulation of MMP secretion as shown in equation 2.6.

$$\frac{\partial S_m}{\partial t} = D_{S_m} \nabla^2 S_m + \mu_{S_m} \frac{P}{K_m + P} M_{tc} \quad (2.6)$$

Here, D_{S_m} is MMP diffusion coefficient, P is the pressure that affects the cell, μ_{S_m} is the maximum rate of MMP secretion (units of 1/hour,) and M_{tc} is the mass of the tumor cell.

TGF- β Secretion

TGF- β is a protein that controls cellular proliferation, and differentiation. The TGF- β exists in a latent, ECM-bound form that is converted to an active, diffusible form of TGF- β according to Equation 2.7 .

$$\frac{\partial S_{tg}}{\partial t} = D_{S_{tg}} \nabla^2 S_{tg} + \mu_{Stg} \frac{S_m}{K_{tg} + S_m} M_e \quad (2.7)$$

Here $D_{S_{tg}}$ is the active form TGF- β diffusion coefficient, μ_{Stg} is the maximum rate of the TGF- β release (units of 1/hour), and M_e is the mass of ECM. TGF- β is converted from a latent to an active form when the MMPs concentration exceeds a threshold [68].

LOX Secretion

LOX is an amine oxidase that plays a critical role in the biogenesis of connective tissue matrices by cross-linking, collagen and elastin in the ECM. The LOX is secreted in the stroma by myofibroblasts based on Equation 2.8.

$$\frac{\partial S_l}{\partial t} = D_{S_l} \nabla^2 S_l + \mu_{Sl} M_{mc} \quad (2.8)$$

In this equation, D_{S_l} is the LOX diffusion coefficient, μ_{Sl} is the maximum rate of the LOX secretion (units of 1/hour), and M_{mc} is the mass of myofibroblasts.

ECM Protein Secretion

The model considers that ECM proteins are synthesized by fibroblasts and myofibroblasts according to the following equation:

$$\frac{\partial S_e}{\partial t} = D_{S_e} \nabla^2 S_e + \mu_{Sem} M_{mc} + \mu_{Seff} M_{fc} \quad (2.9)$$

Here, D_{S_e} is the ECM protein diffusion coefficient, μ_{Sem} is the maximum secretion rate of ECM protein secretion by myofibroblasts (in units of 1/hour). μ_{Seff} is the maximum secretion rate of ECM protein secretion by fibroblasts (units of 1/hour). M_{mc} is the mass

of myofibroblasts, and M_{fc} is the mass of fibroblasts. We assumed that ECM proteins are secreted at constant rate by both myofibroblasts and fibroblasts and that ECM protein secretion rate by myofibroblasts is greater than by fibroblasts.

ECM Degradation and Accretion

The ECM is degraded by MMPs based on equation 2.10 .

$$\frac{\partial M_e}{\partial t} = -\mu_{Me} \frac{S_m}{K_m + S_m} M_e + \mu_{Se} S_e \quad (2.10)$$

In this equation, μ_{Me} is the maximum ECM degradation, M_e is the mass of ECM, S_m is the MMP concentration, and μ_{Se} is the accretion rate at which the soluble ECM proteins are incorporated into the insoluble ECM.

Mechanical Stress

As the right-hand side of Equation 2.3 shows, the changes in the rate of volume increase alter the pressure fields. In the progression of DCIS to IDC, tumor growth, ECM decay, and production and remodeling are the main sources of volume changes. If the right part of Equation 2.3 is rewritten using these terms, new equation can be written that is tailored for this model:

$$-\nabla \cdot (\lambda \nabla P) = \frac{1}{\rho_{tc}} \frac{\partial M_{tc}}{\partial t} + \frac{1}{\rho_e} \frac{\partial M_e}{\partial t} \quad (2.11)$$

where ρ_{tc} and ρ_e are the spatial density distributions of tumor cells and the ECM, respectively. This equation reflect the activity of the feedback loops seen in Figure 2.6. Cross-linking and cells growth increase pressure while cell shrinkage or death decrease pressure.

Table 2.2 summarizes the reactions in each type of cell and ECM used in the model.

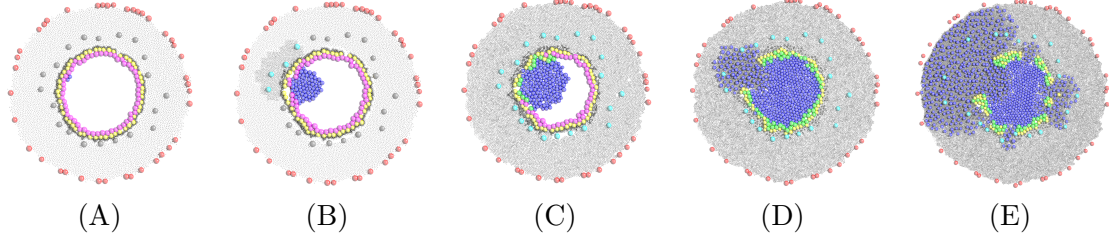


Figure 2.7. The stages from a normal duct into an invasive tumor during simulation. (A) The initial condition for DCIS at iteration 2. (B) The growing tumor triggers the activation of $\text{TGF-}\beta$ that promotes differentiation of fibroblasts into myofibroblasts at iteration 100. (C) Newly differentiated myofibroblasts secrete LOX that begins stiffening the ECM with additional cross-linking and accretion. The ductal wall integrity at the location of tumor initiation has been compromised, but tumor cells are still contained within the duct at iteration 130. (D) The tumor cells have filled the duct, broken through the ductal wall and begun invasion of the surrounding stroma at iteration 180. (E) The duct is so weakened that multiple breaches have occurred and tumor cells have invaded throughout the stroma at iteration 215.

2.5 Results

In this study, we execute the model of the progression of DCIS to IDC, starting from the initial condition of single cancerous cell in a mammary duct as shown in Figure 2.5. Once known parameters were set from the literature (see Table 2.4), the few remaining parameters were estimated and refined by evaluating the ability of the model to recapitulate tumor progression.

Five studies were performed:

1. The fidelity of the tissue-scale behavior of the simulation was evaluated by comparing the sequence of events that emerge in running the model with the sequence of events that unfold in the progression of DCIS to IDC.
2. Interactions that weaken ductal integrity were studied to understand how tumor growth-driven biomechanical stress leads to MMP secretion and subsequent epithelial tight-junction and basement membrane degradation.

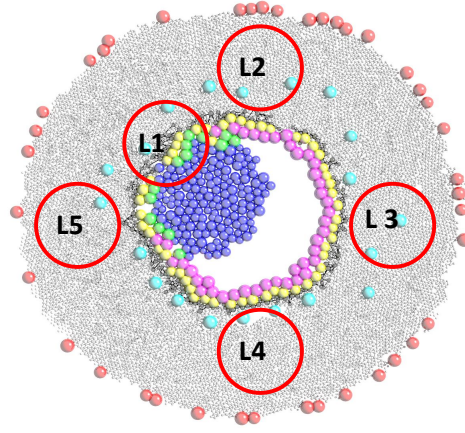


Figure 2.8. Simulated microdissection sites around the duct where biochemical concentrations and biomechanical forces are quantified. L1 is the point of tumor initiation.

3. The effects of stromal stiffening due to $\text{TGF-}\beta$ activation, fibroblast differentiation, LOX secretion and ECM cross linking were explored.
4. The growth of tumor and stromal cells were studied to understand their effect on breach of the duct basement membrane.
5. Micrographs of ductal tissue during progression from DCIS to IDC were compared to the model output.

2.5.1 Emergence of DCIS Progression to IDC Developmental Stages / Emergence Stages of DCIS Progression to IDC

The simulator is initialized at a state of health breast duct microarchitecture, as shown in Figure 2.5. The initial location of the tumor cell is specified randomly. We identify five stages of progression to IDC that occur at iteration 2, 100, 130, 180, and 215 (see Figure 2.7). These are: (A) TCs start growing, consuming nutrients and producing higher amounts of MMP due in response to biomechanical stress, converts $\text{TGF-}\beta$ into active

TGF- β , as shown in Figure 2.7 (A). (B) The active TGF- β within the ECM promotes the differentiation of fibroblasts into myofibroblasts, shown in Figure 2.7 (B). (C) The myofibroblasts begin secreting LOX that in turn induces collagen cross-linking and stiffens ECM, shown as small dark gray particles in Figure 2.7. (D) A feedback loop between the stroma and ECs is formed, where tumor growth combined with the stiffening-ECM heightens the compressive and tensile forces on the duct. The increasing pressure promotes ECs and TCs to secrete yet more MMP to bring the tissue back to homeostasis. The increased MMPs degrade more ECM and weaken the junctions between epithelial cells and basement membrane particles, as shown in Figure 2.7 (D). (E) As a result, the TCs breach the basement membrane and initiate invasion of the surrounding stroma (Figure 2.7 (E)).

2.5.2 Biomechanical Stress and MMP Effects on Ductal Integrity

We monitored the spatial distribution of biomechanical stress (referred to as tissue pressure) and MMP concentration, illustrated in Figure 2.9 A through E. In the early stage of tumor growth, a small amount of MMP is secreted by TCs, while tumor growth produces a local region of pressure centered on the site of tumor initiation. The pressure prompts the TCs to increase their MMPs secretion. The increased MMP weakens the junctions between EC particles and the basement membrane, and degrades the ECM. In addition, the pressure inside the duct builds, causing the TCs to push against the basement membrane. The increased pressure inside the duct, and the weakened junctions between epithelial cells and the basement membrane causes tumor cells to breach the basement membrane and escape within stroma.

The model indicates a significant pressure relief within the duct as multiple breach points occur and tumor cells disperse through the surrounding stromal tissue, as illustrated in Figure 2.9 stage E. This intra-ductal pressure relief is countered by a significant increase in pressure in the surrounding stroma that can lead to increased MMP secretion and subsequent ECM weakening, further promoting invasion.

The pressure and MMP concentration is illustrated in Figure 2.10 at the locations around the duct shown in Figure 2.8. Figure 2.10 illustrates how the evolution of pressure

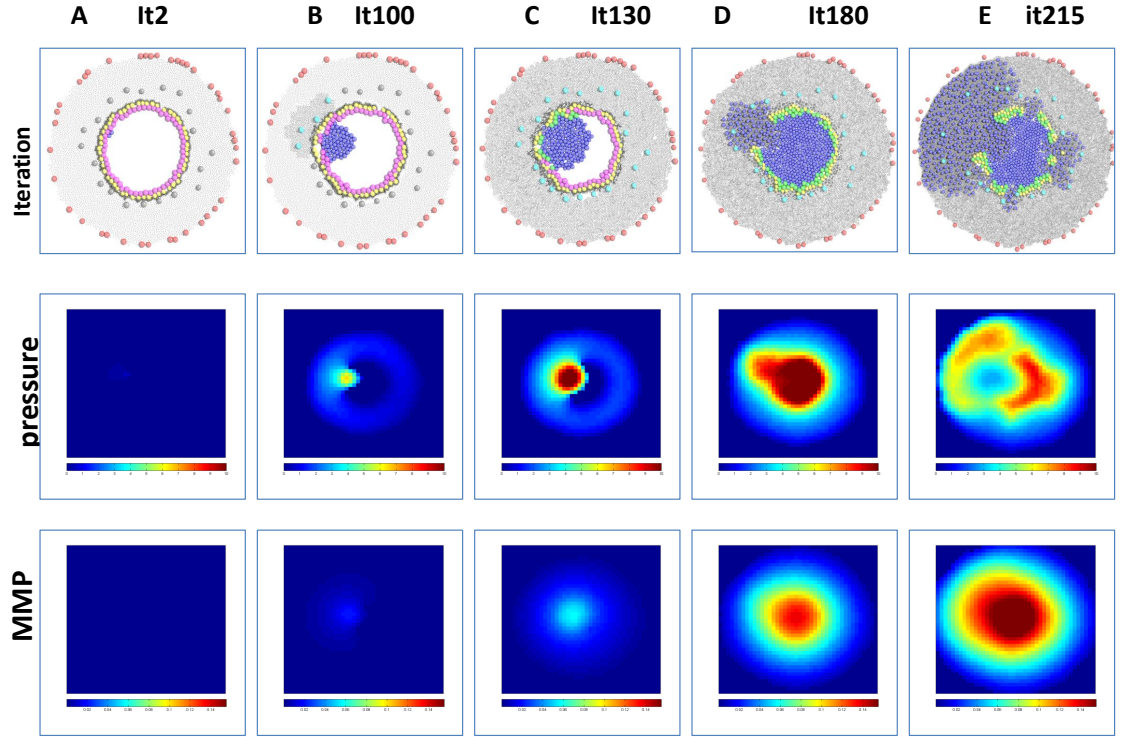


Figure 2.9. Spatial distributions of pressure and MMP in different simulation iterations (iteration 2, iteration 100, iteration 130,180, and iteration 215, respectively) along with the corresponding morphology. Red indicates a high value, blue a low value.

and MMP concentration in the surrounding stroma varies by location. We noted that the region near the growing tumor has the highest pressure and MMP concentration where the breach occurs. We observed that the pressure increases at L1 until about iteration 130, when pressure decreases within the duct after release of stress into the stroma due to the breach of duct basement membrane. In contrast, at L2, a stromal location near the breach point, and at L3, a stromal location opposite the break point, the pressure rapidly increases following the breach. The simulation indicates that pressure at breach points is highest, the pressure is relaxed after breach of the basement membrane, and the breach point occurs near the site of the initial tumor cells.

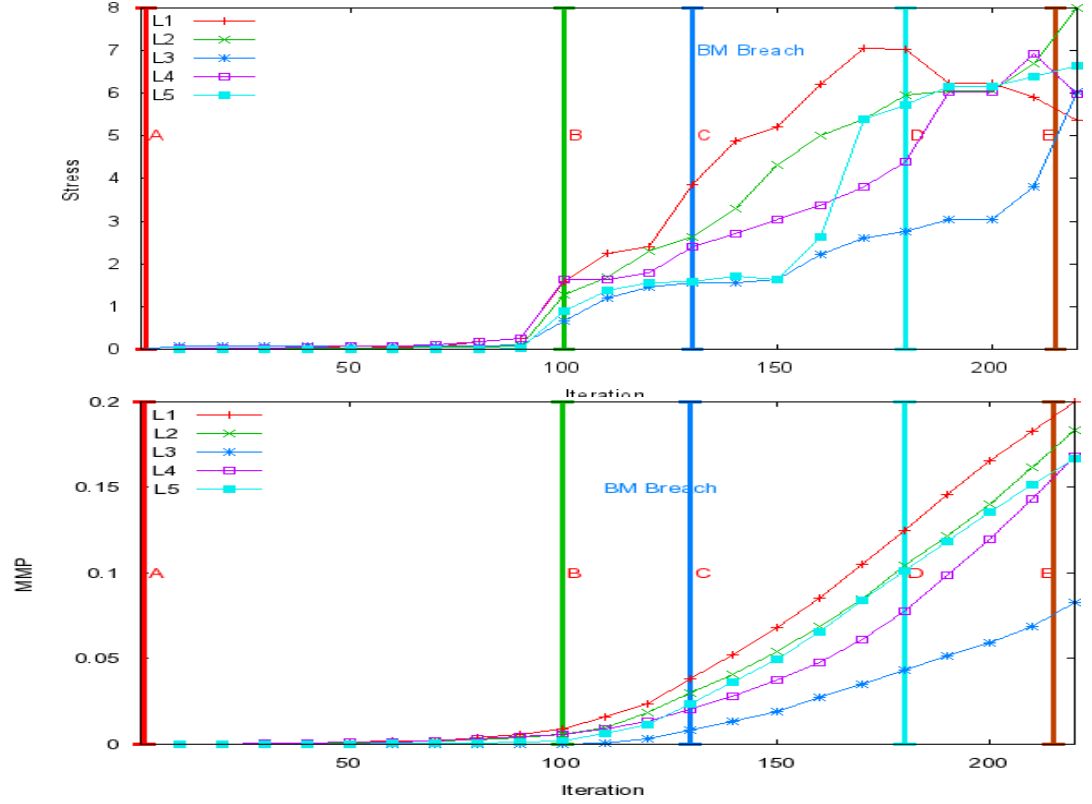


Figure 2.10. Pressure and MMP levels as a function of model iteration in the different locations in the duct given in Figure 2.8.

2.5.3 TGF- β and LOX Effects on Stromal Stiffening

We investigated the biomechanical and biochemical mechanisms that lead to stiffening of the ECM. Figure 2.11 shows the spatial distribution of active TGF- β , which triggers fibroblast-to-myfibroblast differentiation, and the concentration of LOX, which stiffens the ECM. In an early stage, at iteration 2, a high level of active TGF- β appears at the tumor initiation site. This is due to increased MMP secretion. At this early stage, the TGF- β concentration in the ECM is still low and insufficient to prompt fibroblast differentiation. The LOX concentration is also very low since there no myofibroblasts, the source of LOX, in the stroma. By iteration 100, these has been sufficient tumor growth to secret a high amount of MMP. This triggers the conversion of latent TGF- β into active TGF- β . This

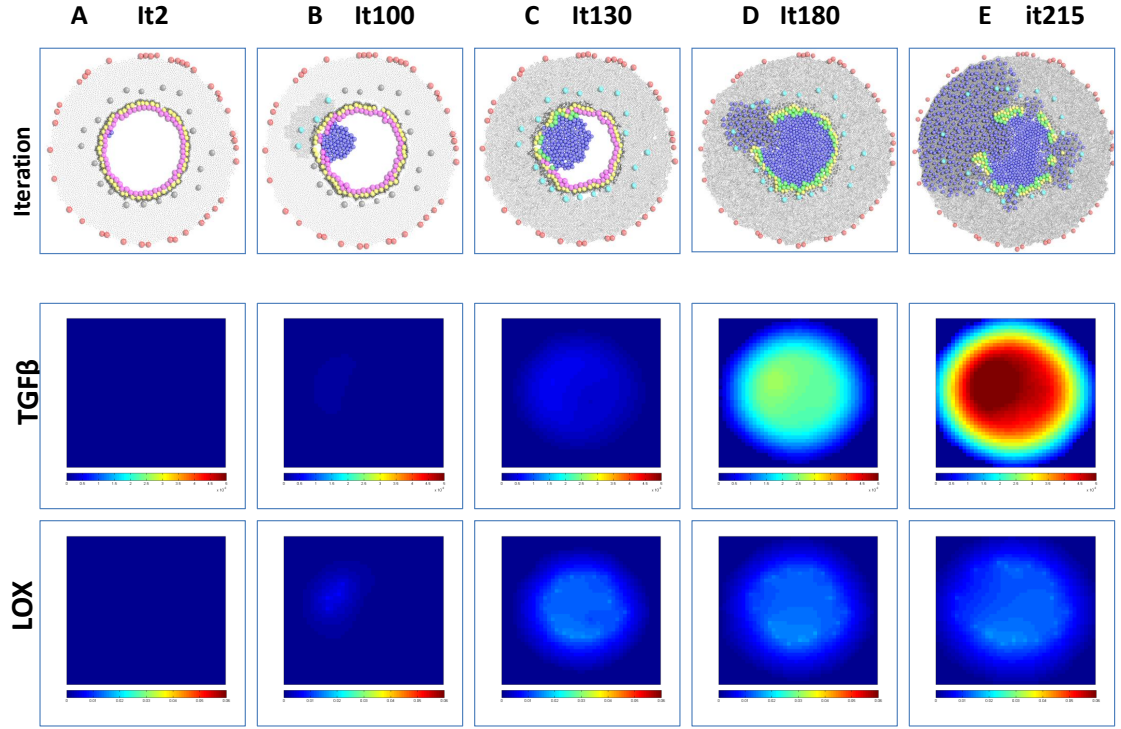


Figure 2.11. Spatial distribution of TGF- β and LOX as the simulation progresses.

active TGF- β triggers the differentiation of fibroblast cells into myofibroblasts in iterations 130. Subsequently, LOX is secreted by myofibroblasts and diffuses into the stroma, cross-linking and thereby stiffening the ECM. The model indicates that, TGF- β and LOX work to modulate the microenvironment in a way that promotes the early stages of metastasis. Disrupting the cross talk between TGF- β and LOX may offer a target to slow or prevent the DCIS to IDC transition.

Figure 2.12 illustrates TGF- β and LOX concentration at different locations around the duct (see Figure 2.8). The distribution of TGF- β is nearly uniform throughout the stroma due to its high diffusibility. LOX on the other hand has low diffusibility and is mostly locally concentrated around the recently differentiated myofibroblasts. The reduction in LOX around the breach point following the breach event is due to the ECM being displaced

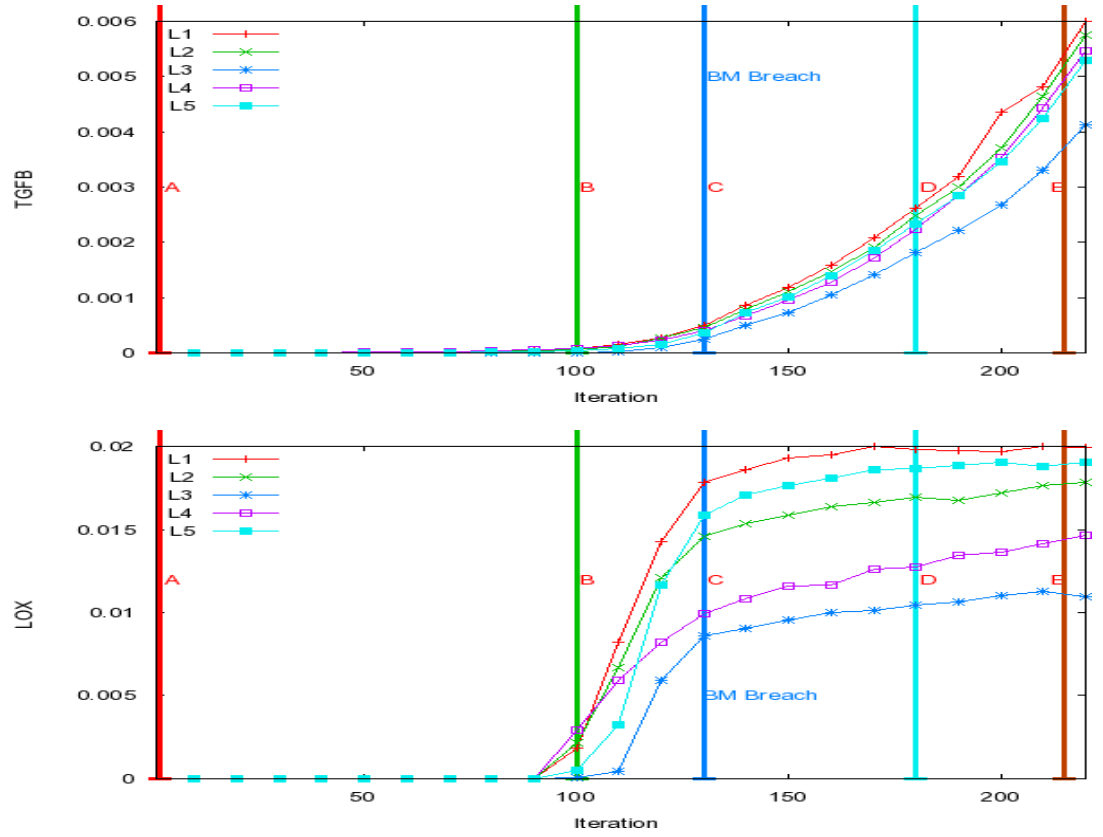


Figure 2.12. TGF- β and LOX concentrations as a function of iteration in different locations in the duct.

by the invading tumor cells.

2.5.4 Cell Population Dynamics

The number of TCs, myofibroblasts, and TCs were monitored over the course of the simulation to understand cell population dynamics in the transition from DCIS to IDC. The upper panel of Figure 2.13 shows the number of tumor cells over the course of the simulation. It illustrates that the number of tumor cells increases exponentially during the initial stages when the cells are confined to the duct. However, as the duct fills and the cells become invasive, the growth rate slows due to increasing stromal pressure. The differentiation of fibroblasts into myofibroblasts takes place relatively quickly and is completed when the duct

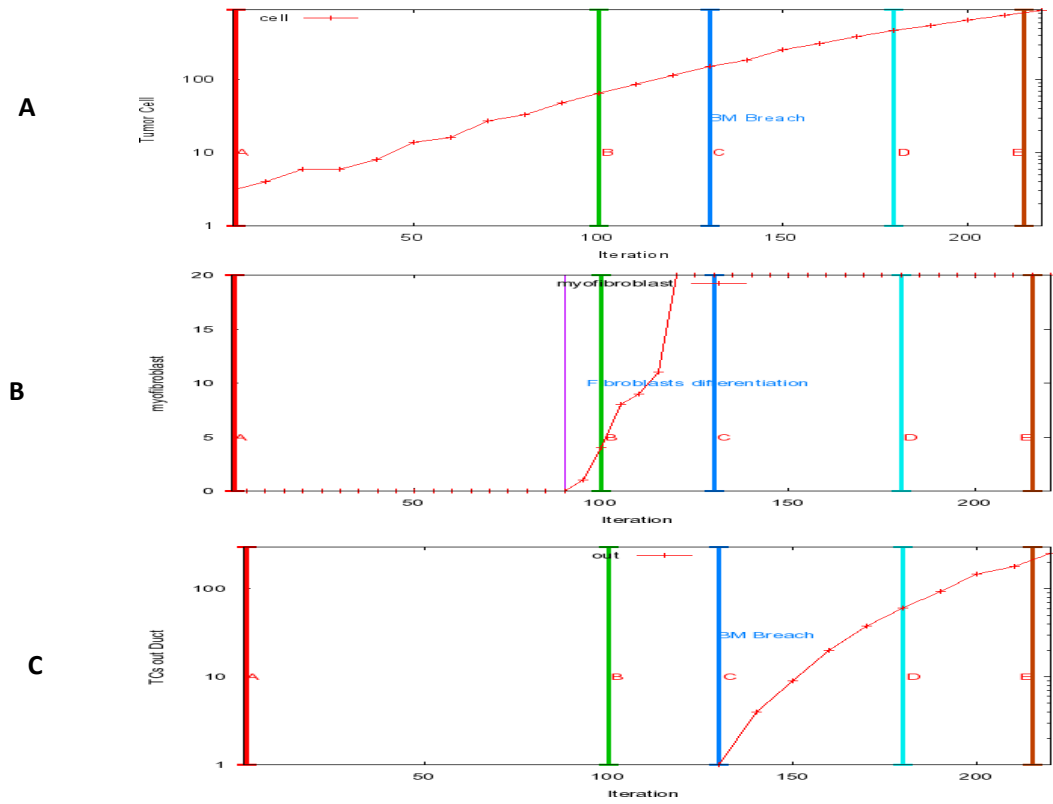


Figure 2.13. The number of TCs, myofibroblasts, and TCs outside the duct as a function of iteration.

is filled with TCs.

2.5.5 Fidelity of the tumor growth model

We compared the model simulation of the normal non-cancerous breast duct with a micrograph of normal duct, and did a similar comparison at the transition to IDC during ductal breach with an image of this stage *in vivo*. Figure 2.14 a micrograph of a normal duct with the corresponding initial state of the model. The normal breast duct shown in the micrograph and at the initial stage of the model are very similar.

Figure 2.15 shows the early stage of IDC as the basement membrane is being breached in a mammary duct and as simulated in the model. Once again, at this level of observation,

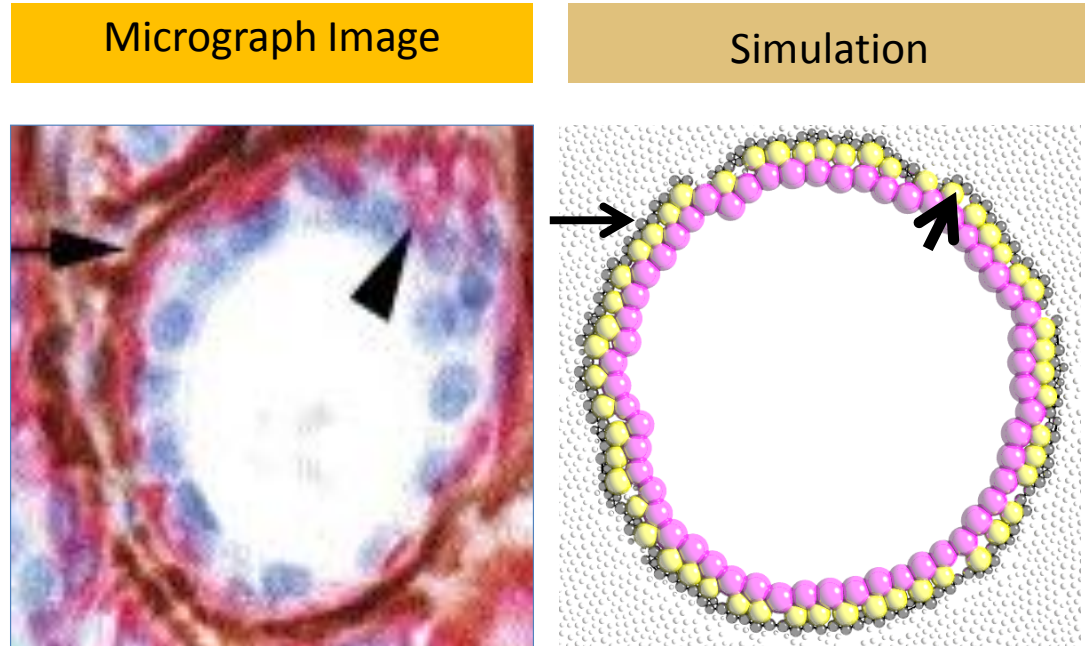


Figure 2.14. The architectural relationship of the basement membrane, myoepithelial cells, and epithelial cells of ducts in a normal human mammary gland. The left one is micrograph image where the arrow identifies the basement membrane (brown), the arrowhead designates a ME cell (red) [5]. The right one is simulation image where the bold arrow identifies the basement membrane (black) and the thin arrow designates myoepithelial cell (yellow).

the agreement is good between the model and the actual progressing cancer in the mammary duct.

2.6 Conclusions

In summary, we developed a 2D agent-based model of the development of ductal carcinoma in situ and its progression to invasive ductal carcinoma. This model is different from the majority of computational models of breast cancer in its explicit consideration of biomechanical forces in addition to the activities of biochemical agents.

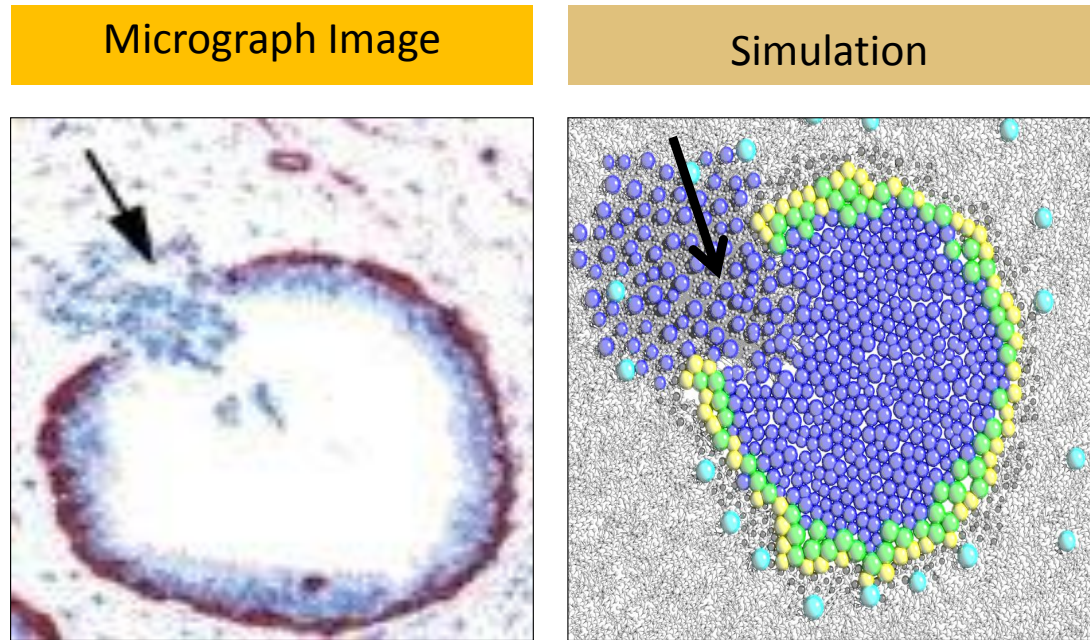


Figure 2.15. Disruption of the myoepithelial cells layer and breach of the basement membrane are prerequisites for invasion. The myoepithelial cell layer and basement membrane in one duct is locally disrupted and the epithelial cells are in direct contact with the stroma (an arrow) [5].

The model supports the idea that the interaction between tumor cells in the duct and the surrounding stroma plays a critical role in tumor growth and invasion of tissues outside the duct. Many mechanical and chemical factors work together to allow invasion. This work may provide a system with a robust predictive modeling and visualization to aid in the discovery of mechanisms of tumorigenesis and the earliest stages of metastasis, and the rapid testing of candidate therapeutics approaches.

2.7 Appendix

Table 2.1. List of parameters symbol description

Symbol	Description
M_{mc}	Biomass of myofibroblasts
M_{fc}	Biomass of fibroblasts
M_{tc}	Biomass of tumor cell
M_e	Biomass of ECM
M_{bc}	Biomass of blood vessels
S_n	Nutrients soluble factor
S_m	MMP soluble factor
S_{tg}	TGF- β soluble factor
S_l	LOX soluble factor
S_e	ECM soluble factor
D_{Se}	ECM proteins solute diffusion coefficient
D_{Sm}	MMP soluble factor diffusion coefficient
D_{Sl}	LOX soluble factor diffusion coefficient
D_{Sn}	Nutrients soluble factor diffusion coefficient
D_{Stg}	TGF- β soluble factor diffusion coefficient
μ_{Sem}	Maximum specific rate for ECM secretion by myofibroblast
μ_{Sef}	Maximum specific rate for ECM secretion by fibroblasts
μ_{Sm}	Maximum specific rate for MMP secretion reaction
μ_{Sl}	Maximum specific rate for LOX secretion reaction
μ_{Me}	Maximum specific rate for ECM degradation reaction
μ_{Sn}	Maximum specific rate for nutrients secretion reaction
μ_{Stg}	Maximum specific rate for TGF- β secretion reaction
μ_{Mtc}	Maximum specific rate for tumor cell growth reaction
K_S	half-maximum concentrations parameter where S denoted soluble factor/biomass type

Table 2.2. List of Equations number per cell type

Cell \ ECM Type	Equations number
Tumor Cell	2.6 , 2.5
MyoFibroblast	2.8 , 2.9
Fibroblasts	2.9
Blood Vessel	2.4
ECM	2.10 , 2.7

Table 2.3. List of soluble factor per cell type

Secreted soluble Factor	Variables
MMP	S_m
LOX	S_l
Continuous ECM protin	S_e
Nutrients	S_n
TGF- β	S_{tg}

Table 2.4. *In Vitro* Parameters for DCIS Model

Parameter	Explanation	Value	Refs.
Epithelial cell radius	0.5	[63]	
Myoepithelial cell radius	0.25	[63]	
Tumor Cell Radius	9.953 μm	[65]	
Production rate of TGF- β from TCs	$1.72 \times 10^{-9} s^{-1}$	[88]	
TGF- β Diffusion Coefficient	$1.8 \times 10^{-7} cm^2 s^{-1}$	[89]	
Oxygen Diffusion Coefficient	$1.55 \times 10^{-4} m^2 day^{-1}$	[64]	
MMP Diffusion Coefficient	$1 \times 10^{-6} cm^2 s^{-1}$	[64]	

CHAPTER 3

DEVELOPING AN *IN SILICO* MODEL TO STUDY THE EFFECT OF RETINAL PIGMENT EPITHELIAL CELL PATCH SIZE ON VEGF PRODUCTION

3.1 Abstract

The spatial organization and growth of retinal pigment epithelial (RPE) cells is a vital process in the progress of age-related macular degeneration (AMD). While *in vitro* experiments provide models for replicating disease states associated with the deterioration of retinal tissue during AMD, the progression and behaviors of RPE cells in AMD and the stimuli leading to the enhanced secretion of the central driver of AMD progression, vascular endothelial growth factor (VEGF) from RPE cells are not fully understood. In addition, *in vitro* culture methods are generally expensive and time-consuming. In this study, an *in silico* model was developed to provide a framework used for understanding the underlying mechanism of VEGF production, predicting the VEGF produced by each cellin colonies (patches) of different sizes, and analyzing the effect of a VEGF agonist. We also present experimental validation of the simulated results and predict the spatial distribution of VEGF produced by cells in different sized patches. This model may provide a system with robust predictive modeling and visualization that could enable discovery of the molecular mechanisms involved in AMD progression and provide routers to the development of effective treatments.

⁰The coauthors for this chapter are: Qanita Bani Baker, Gregory J. Podgorski, Elizabeth Vargis, and Nicholas S. Flann

3.2 Introduction

Age-related macular degeneration (AMD) is a leading cause of irreversible blindness, particularly among adults over age 50 [44,45,90]. Degeneration of retinal pigment epithelial (RPE) cells severely damages the visual function of retina photoreceptors. In AMD, new blood vessels from the underlying choriocapillaris disruptively invades the retina [91]. Vascular Endothelial Growth Factor (VEGF) is the primary growth factor in angiogenesis [92] and an important biomarker of AMD [93]. In the retina, VEGF is secreted in the RPE and is mainly responsible for retinal vasculature development [94,95]. *In vitro* models that allow controlling the spatial organization and growth of RPE cells can provide important tools for understanding cell behavior in AMD processes. Monitoring the expression of VEGF within the controlled environments of these model systems can lead to new insights that improve our understanding of how AMD is initiated and developed over time.

In the cell culture model of AMD that is the focus of this work, micropatterning techniques are used to restrict the location and shape of the substrate regions on which cells attach [96–98]. The impact of micropatterning on cellular functions and morphologies has been investigated with many types of cells including fibroblasts [99], neuronal cells [100], retinal pigment epithelial cells [1,101–104], stem cells [105], epithelial cells [106], and cancer cells [107]. Vargis et al. [1] used micropatterned surfaces to control the spatial organization of RPE cells in Figure 3.1 to explore how atrophy, loss-of-function, or tissue damage within the retina affect VEGF production. While cell culture provides a model for replicating disease states associated with the deterioration of retinal tissue during AMD, the stimuli leading to enhanced VEGF secreted from RPE cells and the subsequent neovascularization processes in the choroid are still not fully understood [48,49], and little is known about the VEGF regulation in the eye [95]. In addition, little is known about the drugs’ mechanisms of action, how and why several diseases such as AMD become resistant to the treatment, or the types of patients that can benefit most from these drugs [108]. Computational approaches combined with *in vitro* experimental studies can shed light on these issues by providing a framework for generating and testing hypotheses related to VEGF regulation and transport

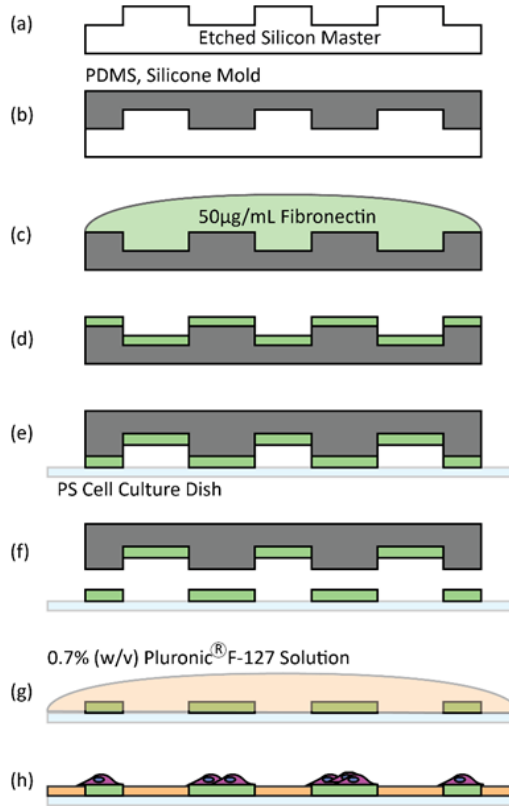


Figure 3.1. Micropatterning method used in [1]. Substrate functionalization and cell seeding are accomplished by molding a PDMS stamp from an etched silicon master as in steps (a, and b). Then, the stamp is inked using a fibronectin solution, allowed to dry and then placed in contact with a polystyrene or glass culture dish as in steps(c-f). After that, the surface is blocked with Pluornic prior to seeding RPE cells onto the fibronectin-patterned substrate as in steps (g, and h).

in the tissue retina [109].

Developing an *in silico* framework for the *in vitro* cell patterning model provides a system that could be extremely useful in evaluating the temporal-spatial effects of VEGF transport and expression within these controlled environments, and in replicating the disease state to gain new insights on disease progression and outcomes. It also can be used to study internal and external regulatory mechanisms influenced by feedback from the evolving cellular environment. Developing this predictive model is essential to improve understanding and generate new hypotheses that may be used in the development of pharmaceutical agents.

The goal of this study was to develop an *in silico* model to replicate and extend cell microprinting model for AMD reported in [1]. Using this model, we studied the growth of RPE cells in discrete patches and measure the effect of patch size on VEGF expression. The VEGF level in each patch is studied as a function of cell number and patch area over time. To study the hypothesis that VEGF expression is linked to global VEGF concentration in culture, VEGF expression from various size patches was quantified following VEGF agonist administration. This study complements experiments performed *in vitro* and provides a framework that can be used to study the influence of cell patterning on the secretion of VEGF by the RPE tissue, and opens a path towards mimicking the effects of tissue damage or atrophy in tissue engineering. This model is applied to extend the study of Vargis et al [1] and to make new predictions. The *in silico* model may be used to examine the effects of anti-VEGF agents that potentially can aid in the optimization of anti-angiogenic therapeutics.

3.3 Materials and Methods

3.3.1 *In vitro* methods

The bioengineered micropatterning techniques are used to create a regular arrangement of circular colonies, called patches, populated with RPE cells surrounded by a empty substrate as shown in [1]. Creation of this micropatterns involves multiple sequential steps as shown in Figure 3.1. The non-populated regions imitate necrotic regions in the retina that result from repeated exposure to reactive oxidative species, triggering death of the retinal pigment epithelium followed by death of the overlying photoreceptors and neovascularization, leading exudative AMD [50,51]. Recreating these regular spatially-organized cellular configurations helps to isolate the impact that local cell-cell and cell-environment interactions have on VEGF expression.

In the experimental study, described in [1], stamps with patches of 100 μm , 200 μm , 300 μm , and 400 μm were employed to vary the mix of cell-cell and cell-environment in each experiment. Each patch was seeded with retinal pigment epithelial cells and grown in

a cellular culture. VEGF per cell was measured at regular intervals: 4, 24, 30 48, 54, and 72 h after cells seeding and reported in pg/ml. To measure the VEGF per cell, the total VEGF contained within the cell culture was determined using enzyme-linked immunosorbent assay (human VEGF ELISA kit), and the number of cells per patch was determined using image analysis proceeded by staining. Figure 4.1(a) (taken from [1]) illustrates the stained patches at 72 h. The experiments were repeated at least ten times and averaged. The final spatial-temporal data obtained are illustrated in Figure 4.1(b). The final spatial-temporal data obtained after adding the VEGF agonist are illustrated in Figure 4.1(c)

A VEGF agonist was also added to the patterned surfaces at a concentration of 5 ng/mL after 20 h in culture, in order to determine if the higher levels of VEGF expression observed in cells grown in small patches was the result of cells responding to lower initial overall levels of VEGF in the RPE microenvironment. VEGF expression was also measured before the addition of the VEGF agonist (at 4 h) and after the addition at (24, 30 48, 54, and 72 h). The final spatial-temporal data produced are illustrated in Figure 4.1(c).

3.3.2 Hybrid Agent-Based Model Framework

In silico computer-based modeling has proved its effectiveness in several biological research studies [110]. *In silico* models, especially agent-cell-based models, can bridge *in vitro* and *in vivo* experiments since they can integrate measurements from several *in vitro* experiments, reconstruct certain aspects of *in vivo* environments, and provide the capabilities for a systematic analysis of the influence of individual as well as combined factors on full-scale biological system behavior [111]. To simulate the RPE cell growth in several patch sizes, we extend the agent-based modeling framework developed by the Kreft group at University of Birmingham, called iDynoMiCs [55].

In this framework, we have two main components: particles and soluble products, integrated within a reaction diffusion system. Particles represent individual cells that mechanically interact, secrete, consume or react to soluble products. They are positioned in space and occupy the volume of a single cell. Soluble product distributions make up the continuous component of the system and are determined by a diffusion solver which resolves

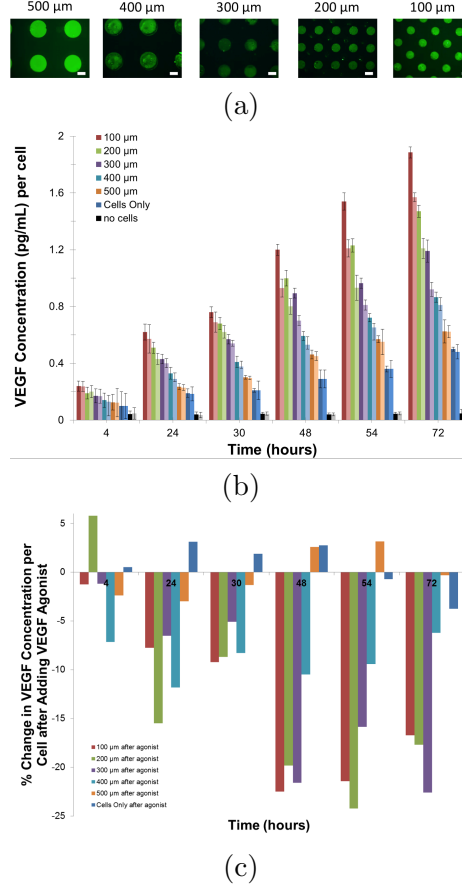


Figure 3.2. The result as shown in the experiments performed by Vargis et al. in [1] (a) Patches of stained RPE cells at 72 h for each patch size. [1]. (b) Time course of VEGF expression per cell measured at 4, 24, 30, 48, and 72 h as in [1]. (c) Time course of VEGF expression per cell measured before the addition of the VEGF agonist(at 4 h) and after (24, 30, 48, 54, 72 h) [1].

all the local changes in concentration induced by the particle and long range diffusion. In the simulation, it is assumed that the soluble product fields are in steady-state with respect to cell mechanisms since solute reaction and diffusion occur on the order of seconds, while cell mechanisms occur on the order of hours to days.

Reactions drive growth to increase the biomass of a particle. As the biomass increases so does the particle radius, based on the cubic root of the volume. When the radius equals or exceeds a maximum state-specific particle size parameter called the split radius R_{sp} in

units μm , the particle is divided into two particles along a random cleavage plane, such that the sum of the volumes of the new particles approximately equals the specified maximum volume. The two smaller particles are positioned without mutual overlap in the place of the parent particle. Any overlap with neighboring cells is ignored during placement and resolved during force relaxation. Particle size can be reduced through biochemical reactions that cause biomass consumption, decay, particle apoptosis, or necrosis. When the radius equals or falls below the minimum particle size parameter, called the death radius R_d in units μm , the particle is removed from the domain. This framework is explained in more detail in the Supporting Information section.

In this model, it is assumed that the boundary conditions are cyclic for the sides of the 2D domain. Cyclic boundaries allow simulation of larger domains by assuming that the computation domain region is replicated indefinitely. The two connected boundaries are specified together when creating cyclic boundary conditions. Solute concentrations are kept constant across cyclic boundaries, and any agent crossing one of the cyclic boundaries will be instantly moved to the connected boundary.

3.3.3 *In silico* model for RPE growth in several *in vitro* patch sizes

The bioengineered experiments are simulated using the hybrid agent-based approach. The setup of the simulations replicates the same experimental conditions and units as in the *in vitro* experiments. The domain size of each simulation is $2400 \mu m$, initial cell size is set to $80 \mu m^2$, and 36 h is the doubling time due to growth. Each simulation begins with multiple RPE cells distributed at the reported patterning efficiency (cell density) in several patches arranged in the specific experimental pattern. The simulation replicates the first 72 h of the *in vitro* experiments. The initial conditions for different patches are shown in Figure 3.3. Illustrations of the simulated experiments, after 72 h, are shown in Figure 4.2.

The autoregulation of VEGF secretion as a function of biomass M and local VEGF concentration V is described using Equation 4.1. The diffusion coefficient of VEGF D_V is set to $5.8 \times 10^{-11} m^2 s^{-1}$, taken from microfluidic experiments described in [112]. As shown from this Equation 4.1, VEGF expression is auto-regulated by negative feedback inhibition

Table 3.1. Initial Number of Cells in Each Patch based on [1]

PatchSize	Initial Number of Cells.
Patch 100	15 Cells
Patch 200	74 Cells
Patch 300	189 Cells
Patch 400	351 Cells
Patch 500	612 Cells

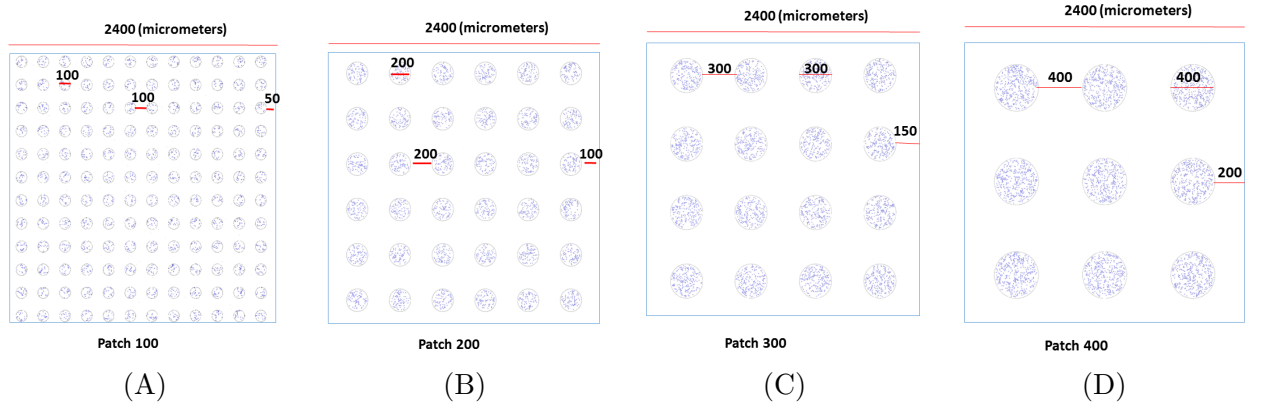


Figure 3.3. Patch arrangement in the simulation. (A) Patch 100 μm , 12 patches in each side. (B) Patch 200 μm , 6 patches in each side. (C) Patch 300 μm , 4 patches in each side. (D) Patch 400 μm , 3 patches in each side.

loop via the amount of VEGF in the surrounding domain.

$$\frac{\partial V}{\partial t} = D_V \nabla^2 V + \alpha_V \frac{K}{\beta V + K} M \quad (3.1)$$

The equation after adding VEGF agonist will be as in Equation 3.2. This equation assumed that the receptor singling for VEGF is the same for VRGF agonist. This suggest that the cell may function to maintain a consistent level of VEGF and VEGF agonist within their local environment.

$$\frac{\partial V}{\partial t} = D_{(V+Va)} \nabla^2 V + \alpha_V \frac{K}{\beta(V + Va) + K} M \quad (3.2)$$

Over time, the RPE cells grow based on a doubling time of 36 h [113], which determines the growth rate parameter μ_M . Since nutrient is unlimited and cell crowding is not an issue within the 72 hour time line, we applied first order kinetics reaction for cell growth as shown in Equation 4.2.

$$\frac{\partial M}{\partial t} = \mu_M M \quad (3.3)$$

Table 3.2 summarizes the description of the parameters used in the equations above and identifies the known parameters and those that need to be determined by the method developed in Chapter 4.

Table 3.2. Model's parameter descriptions

Parameter	Value	Description	Ref
D_V	$5.8 \times 10^{-11} m^2 s^{-1}$	Diffusion coefficient	[112]
μ_M	1.0194 hour^{-1}	Max. growth rate for RPE cells	[113]
K	0.13	Auto regulation rate	Chapter 4
μ_V	0.09	Secretion rate	Chapter 4
β	0.850	Binding affinity	Chapter 4
R_{sp}	$6.2996 \mu m$	Cell Division Radius	[1]

3.4 Results

In this study, we utilized the hybrid agent-based framework to model RPE cell growth within different patches size setups. The *in silico* model was executed from the initial condition, shown in Figure 3.3, and assessed the simulated changes from the first hour to the end of the experiments at hour 72. In this section, using the developed *in silico* model, the VEGF concentration per cell was measured at various time intervals and after adding a VEGF agonist to the patterned surfaces with several sizes. The visualization of VEGF distribution in different patch sizes was also reported. This framework was also applied to study a more realistic model of retinal degeneration when open areas with no living cells develop in the retinal endothelium. Additionally, we used this model to study the effect of VEGF agonist concentration on the final VEGF concentration per cell. Here, the concentration of VEGF per cell was measured after adding several VEGF agonist concentrations

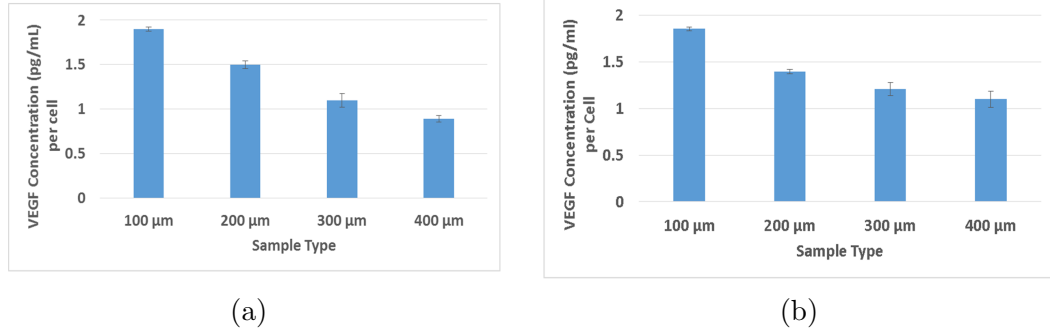


Figure 3.4. Comparing VEGF concentration per cell *in vitro* and in simulation. (a) The left graph represents the data obtained *in vitro* from [1]. (b) The right graph represents the data obtained from the simulation.

at the same time intervals as previous experiments.

VEGF concentration per cell

The total VEGF expression in the simulation was first calculated for each domain after 72 h and was reported as VEGF concentration per cell as shown in Figure 3.4 (b). In these studies, the VEGF concentration per cell is inversely proportional to the patch size, i.e. RPE cells in the smaller patches express higher levels of VEGF per cell. To validate the *in silico* model, we compared the simulation results with the *in vitro* data from [1]. In both, 3.4 (a) and 3.4 (b), it is noted that the RPE cells in small patches express higher levels of VEGF per cell. This indicates that these cells are auto-regulated VEGF to maintain a consistent level of VEGF within their local microenvironment. Cells in smaller patches respond by expressing higher amounts of VEGF to maintain basal VEGF levels, while RPE cells in larger patches maintain the same basal levels of VEGF by expressing smaller amounts of VEGF per cell.

To show how the concentration of VEGF changes over time in the simulation, VEGF expression levels were also calculated at various time intervals (4, 24, 30, 48, 54, and 72 h) and reported as VEGF concentration per cell. As shown in Figure 3.5 (b), the level of VEGF increased over time. At hour 4, VEGF concentration per cell was approximately

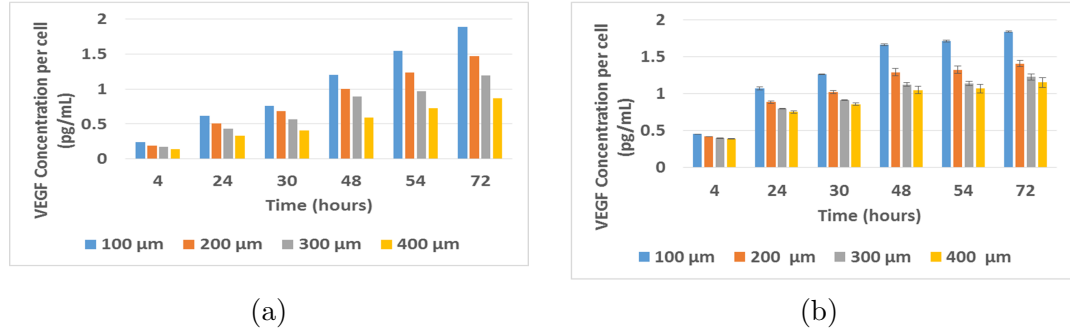


Figure 3.5. Comparing the time course of VEGF expression per cell measured at 4, 24, 30, 48, and 72 h, different patch sizes (100 μm , 200 μm , 300 μm , and 400 μm), *in vitro* and in simulation. (a) The left graph represents the data obtained *in vitro* from [1]. (b) The right graph represents the data obtained from the simulation.

the same for all patch sizes. However, significant differences were observed after hour 48, where smaller patches produced a higher amount of VEGF than larger patches. In both 3.4 (a) and 3.4 (B), it is noted that the RPE cells in small patches expressed higher levels of VEGF per cell than the larger patches. This confirms that cells growing in small patches may experience different local concentrations of VEGF compared to cells in larger patches.

VEGF concentration per cell with VEGF agonist

To determine if the higher levels of VEGF expression observed in cells grown in small patches are the result of cells responding to lower initial overall levels of VEGF in the RPE cells microenvironment, the VEGF agonist was added to the patches 20 h after the initial cell seeding, at a concentration of 5 ng/ml based in both *in vitro* experiments and *in silico* simulations. In the *in silico* VEGF agonist V_a is auto-regulated based on Equation 3.2. Then the concentration of VEGF per cell after the addition of the VEGF agonist was calculated at the same intervals as previous experiments and reported as the change in VEGF expression per cell for each patch size.

In both the *in vitro* and *in silico*, as shown in 3.6 (a) and 3.6 (b), respectively, adding the VEGF agonist effectively increased the amount of VEGF detected by the cultured cells in each sample. In both the *in vitro* culture and the simulation, the VEGF levels per cell

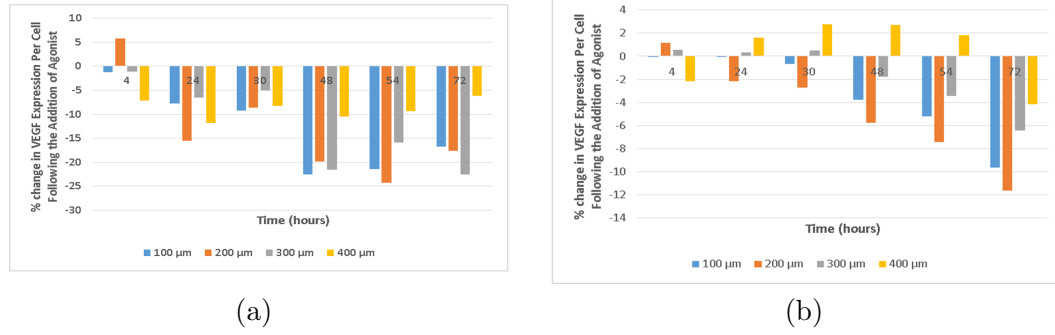


Figure 3.6. *In vitro* and simulated effects of the VEGF agonist addition on VEGF expression. The agonist was added after 20 h of culture. (a) Data obtained *in vitro*. (b) Results of the simulation.

obtained from smaller patch sizes (100, 200, 300 μm) decreased after the VEGF agonist was added. This confirms the hypothesis that cells within these smaller patches reduce VEGF expression levels because of the increased levels of VEGF detected within their local environment. The patches of larger sizes (400 μm) were already exposed to higher levels of VEGF; hence they showed small changes in expression levels after the addition the VEGF agonist.

VEGF Distribution

Using the *in silico* model, we monitored the spatial distribution of VEGF in the different patches. Simultaneous VEGF concentration profile is evolved using the *in silico* models. Figure 3.7 shows the VEGF distribution profile in 2400 μm X 2400 μm area for different patch sizes 100 μm , 200 μm , 300 μm , and 400 μm). This insight gained by the model observations, cannot be made experimentally either through *in vitro* or *in vivo* models.

The results indicate that VEGF distribution in tissues increased gradually over a specific period. This also suggest that patterning efficiency and detailed quantitative distribution of VEGF could be another factors that are worth to study their effects in the disease progression.

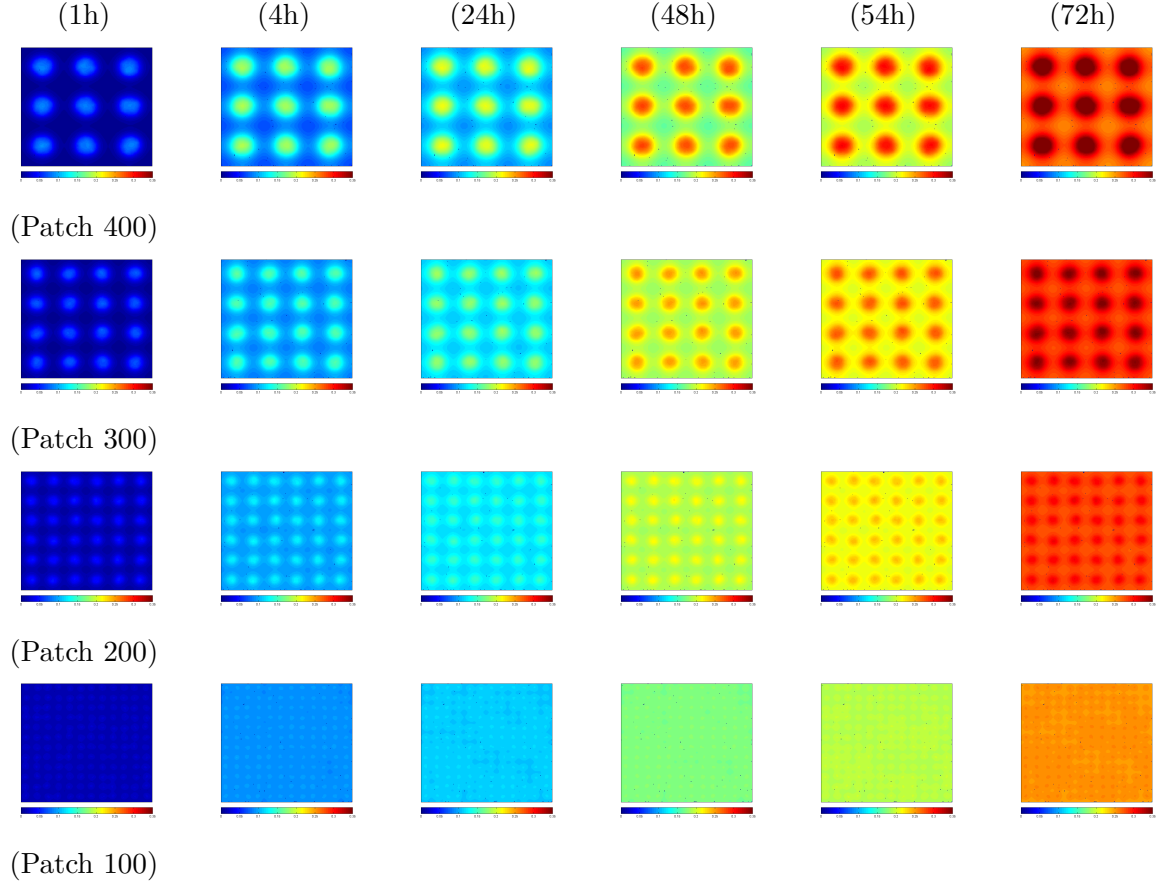


Figure 3.7. Simultaneous evolution of the VEGF distribution profile in 2400 micrometers area for different patches size.

Prediction

The ultimate goal of any modeling effort is to provide actionable predictions [34]. Ideally, important experiments that could not be performed *in vitro* could instead be done using the developed *in silico* approach. For instance, a more realistic model of retinal degeneration is one in which open areas with no living cells develop in the retinal endothelium. This can be modeled using a similar arrangement of patches, but where the cells are applied to the areas outside of the disks, which are left empty. The inverse distributions of the cells (where cells is located outside the patches and all patches are empty) were modeled and the effects of different sizes patches were simulated and studied through the developed

framework.

To show how the concentration of VEGF changes over time in the simulation with inverse distributions setup, VEGF expression levels were also calculated at various time intervals (4, 24, 30, 48, 54, and 72 h) and reported as VEGF concentration per cell as shown in Figure 3.10. The results got from this experiments suggest that this inverse setup is not so informative, since the several patches' sizes do not play a critical role in such distribution.

3.5 Discussion

This study offers an *in silico* model that utilized a hybrid agent based framework to model bioengineering *in vitro* experiments. The coupling between *in silico* models and bioengineering laboratory works provide an effective strategy for mechanistic understanding of mechanisms and interaction using spatial-temporal data. This coupling could help in identifying key regulating parameters of the laboratory process and predicting the early information in order to assess the systems' and processes' behaviors. We argue that using a hybrid agent based framework for such system is adequate, since this framework is implicitly include the spatiotemporal locality effects within the cell, or cell-cell interactions.

In vitro experiments provide a model for replicating disease states associated with the deterioration of retinal tissue during age-related macular degeneration (AMD). To quantitatively interpret such experimental results, an *in silico* model can be beneficial and predictive. In this study, *in silico* model was developed in order to replicate the *in vitro* experiments in [1]. The setups of the *in silico* model imitate the same experimental conditions and units as described in the *in vitro* works and predict the VEGF concentrations per cell in several spatiotemporal conditions. The results obtained from the *in silico* model confirm that the RPE cells in small patches expressed higher levels of VEGF per cell. This suggests that these cells may function to maintain a consistent level of VEGF within their local microenvironment. Additionally, cells in smaller patches respond by expressing higher amounts of VEGF to maintain VEGF levels. RPE cells in larger patches can maintain the same levels of VEGF by expressing smaller amounts of VEGF per cell.

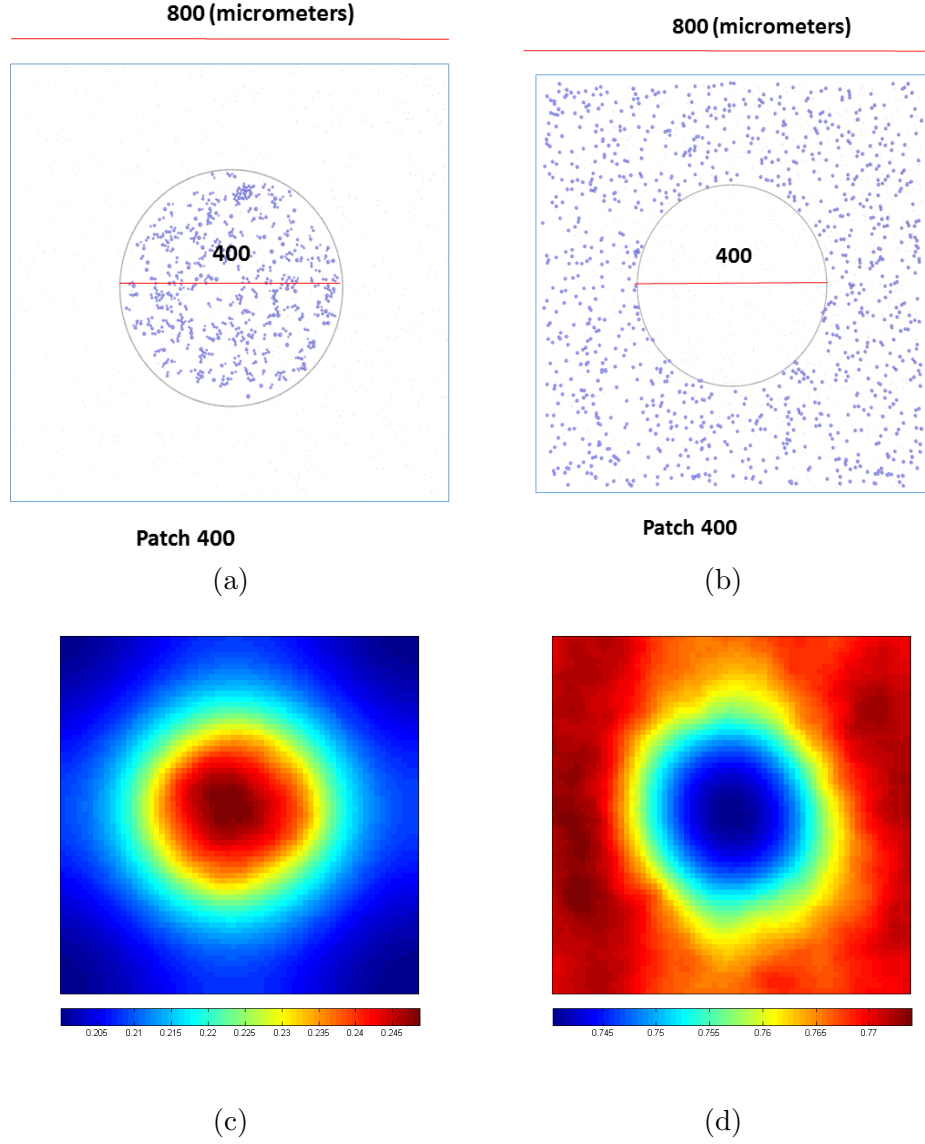


Figure 3.8. (a) Closeup of initial condition of a 400 μm patch (b) Experiment with 400 μm , 3 patches in each side. (c) Closeup of the VEGF distribution after 72 h, (d) VEGF distribution over whole domain after 72 h.

The developed *in silico* model is quantitatively validated based on the available experimental data. The model can provide quantitative interpretation of the *in vitro* data and may be used in predicating the effects of further spatial cells distribution conditions. In future work, we suggest to use a searching approach to find the patches organization

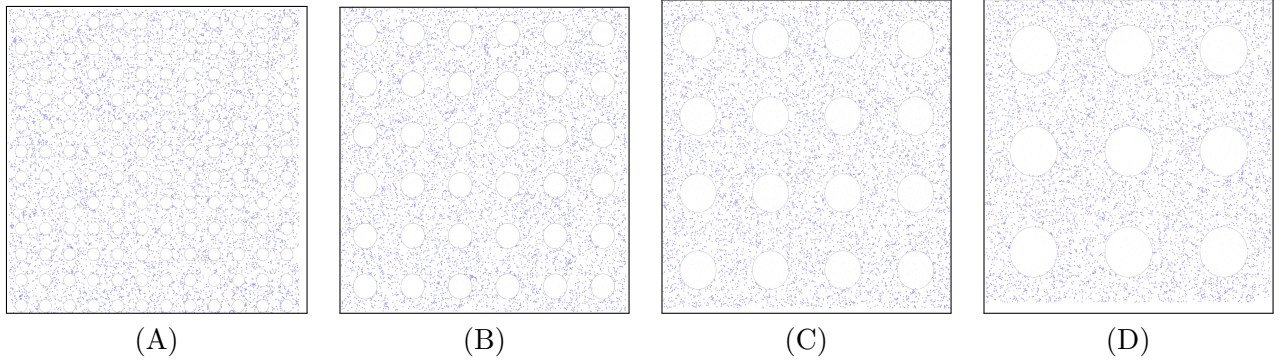


Figure 3.9. Patch arrangement in the simulation. (A) Patch $100\ \mu\text{m}$, 12 patch in each side. (B) Patch $200\ \mu\text{m}$, 6 patches in each side. (C) Patch $300\ \mu\text{m}$, 4 patches in each side. (D) Patch $400\ \mu\text{m}$, 3 patches in each side.

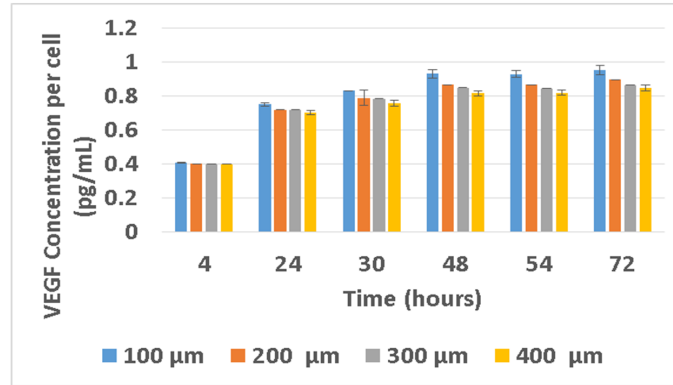


Figure 3.10. VEGF expression per cell measured at 4, 24, 30, 48, and 72 h from the simulation in inverse distributions of the cells as shown in Figure 3.9.

that identify the most informative configuration. This search will identify several spatial cell organizations that may effectively mimic the effect of atrophy and loss-of-function that occurs in the retina during degenerative diseases. The model can be utilized to guide the laboratory towards the most informative experiments.

CHAPTER 4

BRIDGING THE MULTISCALE GAP: IDENTIFYING CELLULAR PARAMETERS FROM MULTICELLULAR DATA

4.1 Abstract

Multiscale models that link sub-cellular, cellular and multicellular components offer powerful insights in disease development. Such models need a realistic set of parameters to represent the physical and chemical mechanisms at the sub-cellular and cellular levels to produce high fidelity multicellular outcomes. However, determining correct values for some of the parameters is often difficult and expensive using high-throughput microfluidic approaches. This work presents an alternative approach that estimates cellular parameters from spatiotemporal data produced from bioengineered multicellular *in vitro* experiments. Specifically, we apply a search technique to an integrated cellular and multicellular model of retinal pigment epithelial (RPE) cells to estimate the binding rate and auto-regulation rate of vascular endothelial growth factor (VEGF). Understanding VEGF regulation is critical in treating age-related macular degeneration and many other diseases. The method successfully identifies realistic values for autoregulatory cellular parameters that reproduce the spatiotemporal *in vitro* experimental data.

⁰The coauthors for this chapter are: Qanita Bani Baker, Gregory J. Podgorski, Christopher D. Johnson, Elizabeth Vargis, and Nicholas S. Flann

4.2 Introduction

An important aspect of computational systems biology is the investigation of dynamic biological processes that operate across multiple temporal and spatial scales by constructing and running multiscale models [2], [10], [15], [114], [115]. These models incorporate a set of parameters that represent the physical and chemical properties of the biological system [116]. The parameters are used to define the components of the models that when simulated reproduce the behavior of the biological system. Often the correct values of these parameters are unknown or difficult to obtain [117], [118].

Recently, there has been an increase in the number of model-fitting methods proposed to estimate model parameters' values [119], [120], [121] from experimental data. Without accurate estimations of parameters, predictions from simulation studies will most likely be erroneous and provide little scientific insight and guidance in disease treatment [122]. This scenario can be ameliorated by fitting the model to experimental *in vitro* / *in vivo* data [123] [124]. Finding the best-fit values for the unknown parameters enhances the possibility of performing accurate quantitative predictions.

Vascular endothelial growth factor (VEGF) is a key promoter of angiogenesis and vascular development and is the target in numerous anti-angiogenic therapies [125]. Angiogenesis is the growth of blood vessels from the preexisting vasculature, a process involved in the physiological functions of several diseases, such as cancer and age-related macular degeneration (AMD). Moreover, in spite of substantial basic science and translational research to develop anti-angiogenic therapies, many questions remain about the mechanisms of action of angiogenic drugs, how and why several diseases such as AMD become resistant to the treatment, or the patient conditions that can benefit most from these drugs [108]. For these reasons, computational models of angiogenesis have been developed to simulate the process and provide a framework for generating and testing hypotheses of VEGF-driven processes [109, 126, 127]. Models have aided in the development of novel and effective anti-angiogenic therapeutics that target VEGF regulation and receptors [116], [128, 129]. Advancing these computational approaches combined with progress in *in vitro* experimental

studies will shed light on these issues by providing an effective framework for generating and testing hypotheses related to VEGF regulation and transport in the tissue [109].

An essential mechanism for understanding VEGF’s role in disease development is its auto-regulation. The rate of VEGF secretion is controlled through an auto-inhibitory regulatory mechanism where the VEGF concentration of a cell’s microenvironment down-regulates the secretion of VEGF. This control loop enables a community of cells to maintain a stable background concentration of VEGF [130]. Disruption of the loop is implicated in multiple disease states.

This paper presents a method for accurately characterizing this auto-regulation, not from microfluidic assays that interrogate individual or mixed cell populations but from spatially organized multicellular experimental data sampled over time. As will be explained later, spatiotemporal data provides unique insights because auto-regulation is inherently a mechanism that is manifested over space and time. The rest of the paper is structured as follows: First the experimental setup and computational model is described, along with the specific autoregulatory parameters that are known and those to be estimated. Second, the search method for finding the values for the parameters is described in detail. Next the method is evaluated by validating the identified parameter values. Finally, a summary of the method’s effectiveness and suggestions for future work are given.

4.3 Multicellular Experiment and Model

The experiment from which the unknown parameter values are derived employs bio-engineered micropatterning techniques. The micropatterns form a regular arrangement of circular 2D patches populated with cells surrounded by an exposed substrate. The exposed regions emulate necrotic areas of the retinal tissue that result from repeated exposure to reactive oxidative species, triggering neovascularization and exudative AMD [50]. Recreating these regular spatially organized cellular configurations is essential to understanding the impact of local cell-cell and cell-environment interactions on VEGF autoregulation.

In the experimental study, described in [1], the bioengineered circular micro patterns were employed to control the extent of cell-cell interactions, which occur within the patch,

and cell-environment interactions, which occur at the perimeter. Several patch sizes were used in this study (100 μm , 200 μm , 300 μm , and 400 μm) to sample the proportion of cell-cell and cell-environment interactions in each experiment. Such sampling constrains the possible parameter values. Each patch was seeded with retinal pigment epithelial (RPE) cells and grown in a cellular culture. As the cells grew, the VEGF per cell was measured at regular intervals: 4, 24, 30 48, 54, 72 h. To measure the VEGF per cell, enzyme-linked immunosorbent assay (ELISA) was used to determine the total VEGF contained within the cell culture, and the number of cells per patch was determined by image analysis proceeded by staining. Figure 4.1(a) (taken from [1]) illustrates the stained patches at 72 hours. Experiments were repeated ten times and averaged. The final spatiotemporal data produced is illustrated in Figure 4.1(b) and forms the target prediction for the computational model simulation.

The bioengineered experiments were simulated using a hybrid agent-based approach, which is an extension of *iDynoMiCs* framework developed by the Kreft group at University of Birmingham [55]. This model was selected because of its extensibility and easy of use. All inputs to the model such as parameter values and initial condition are easily specified using an XML document called the protocol file. Hybrid models integrate discrete components to represent the cells and continuous equations to represent biochemical reactions and diffusion. Each cell is a spherical particle that grows by consuming nutrient and accumulating biomass volume; when the volume exceeds twice the initial volume, cell division is simulated by splitting the particle into two. Particles can secrete and uptake soluble biochemicals (such as VEGF) which diffuse through the domain; regulatory reactions that model interactions among intracellular and inter-cellular proteins become PDEs. The simulation interlaces cellular growth and movement (implemented by relaxing forces between particles) with biochemical redistribution (implemented by solving the PDEs). Random noise disrupts cellular movement and the division volume to represent the inherent stochasticity of the biological processes.

The setup of the simulations replicate the experimental conditions and units of the

in vitro experiments. The 2D domain size of each simulation is $2400\mu m$ by $2400\mu m$, initial cell size is set to $80\mu m^2$ and the doubling time due to growth is set at 36 hours. Each simulation begins with multiple RPE cells distributed randomly at the same density and with the patch pattern. The simulation replicates the first 72 hours of the *in vitro* experiments. Illustrations of the simulated experiments are shown in Figure 4.2.

This framework is inherently multiscale in that the parameters that control the low-level mechanisms at the cellular level, e.g., growth, the VEGF secretion rate and autoregulation, determine the cell population and VEGF concentration over the complete multicellular domain. Figure 4.2 illustrate the VEGF distributions in the domain. To compute the VEGF concentration per cell, the total VEGF is computed over the whole domain, while the number of cells is directly determined by the simulator. This approach intrinsically includes the quantitative spatiotemporal control effects as the cells grow, secret VEGF which diffuses over the domain. Moreover, the simulations provide insight into the spatial VEGF gradients within and between patches, unavailable in *in vitro* studies.

The autoregulation of VEGF secretion is described in Equation 4.1 as a function of biomass M and local VEGF concentration V . The diffusion coefficient of VEGF, D_V , is set to $5.8 \times 10^{-11} m^2 s^{-1}$ given in microfluidic experiments from [112].

$$\frac{\partial V}{\partial t} = D_V \nabla^2 V + \mu_V \frac{K}{\beta V + K} M \quad (4.1)$$

Over time, the RPE cells grow based on a doubling time of 36 hours [113], which determines the growth rate parameter μ_M . Since nutrient is unlimited and cell crowding is not an issue within the 72 hour time line, we applied first order kinetics for cell growth as shown in Equation 4.2.

$$\frac{\partial M}{\partial t} = \mu_M M \quad (4.2)$$

Table 4.1 summarizes the description of the parameters used in the equations above

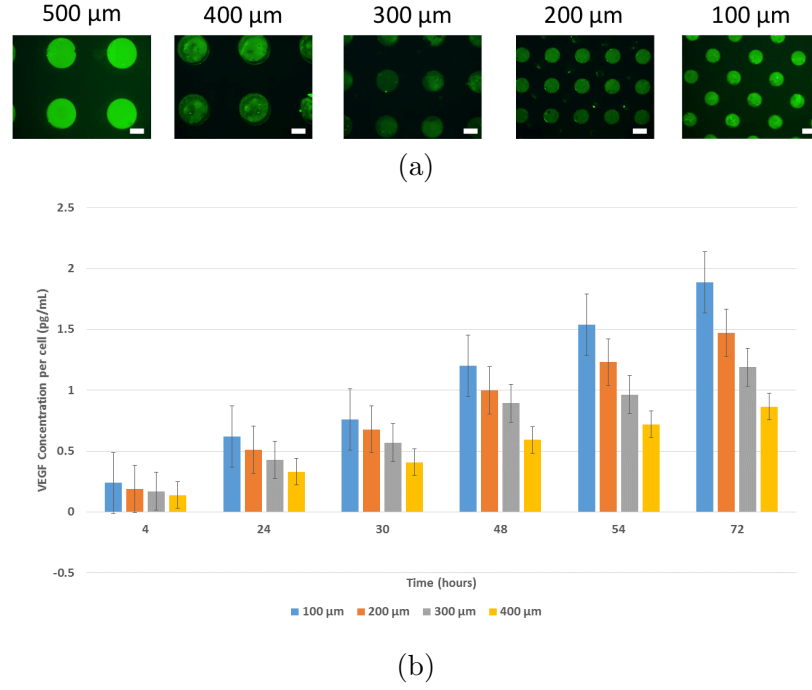


Figure 4.1. (a) Patches of stained RPE cells at 72 h for each patch size [1]. (b) Time course of VEGF expression per cell measured at 4, 24, 30, 48, and 72 h (data for each time from the *in vitro* [1]).

and identifies the known parameters and those that need to be determined by the method introduced in this paper.

Table 4.1. Known and unknown parameter descriptions

Parameter	Value	Description
D_V	$5.8 \times 10^{-11} m^2 s^{-1}$	Diffusion coefficient
μ_M	1.0194 hour^{-1}	Max. growth rate for RPE cells
K	<i>Unknown</i>	Auto regulation rate
μ_V	<i>Unknown</i>	Secretion rate
β	<i>Unknown</i>	Binding affinity

4.4 Method

In this work, we apply a parameter fitting technique to validate a hybrid agent-based model with available *in vitro* experimental data in order to explore the best-fit values for the unknown parameters given in Table 4.1. The three unknown parameters are termed

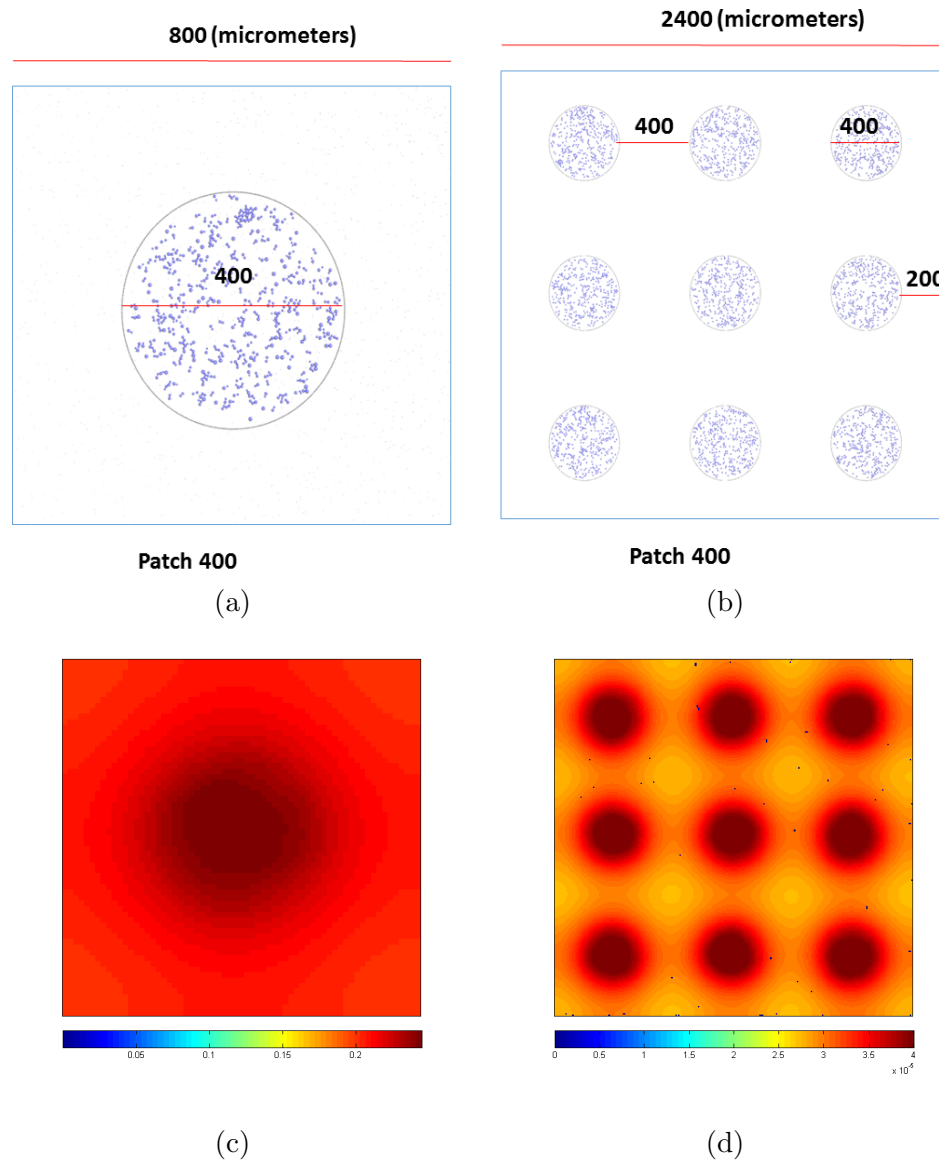


Figure 4.2. (a) Closeup of initial condition of a $400 \mu m$ patch (b) Experiment with $400 \mu m$, 3 patches in each side. (c) Closeup of the VEGF distribution after 72 h, (d) VEGF distribution over whole domain after 72 h.

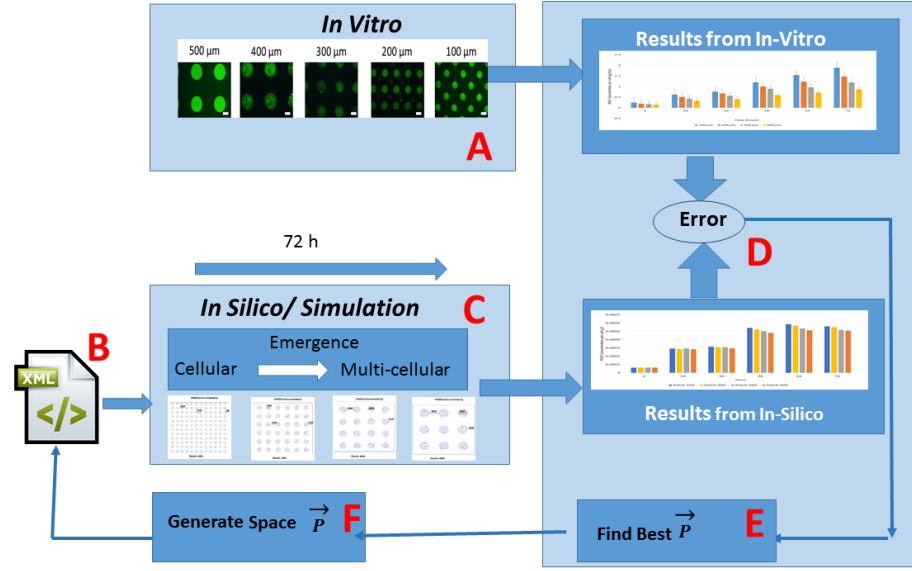


Figure 4.3. An overview for the error-minimization multicellular search-based approach. In (A), RPE cells are cultured using micropatterning techniques. In (B), the parameters are initialized in the XML protocol file. In (C), a simulation is performed and the results are calculated. In (D), the error is calculated based on the difference in VEGF concentration per cell between the experimental results and simulation outputs as in Equation 4.3. Based on the change in error, new parameter values are selected for another simulation run (E and F). This process(B-F) will be repeated until an exit condition is met where the error improvement is below a threshold value or the search time runs out.

the free parameters and together they define the vector $\bar{P} = \langle K, \mu_V, \beta \rangle$. We use an error-minimization search approach that explores the space of free parameters and returns the vector \bar{P} that yields the simulation results best fitting the experimental data [1]. The fitting process is summarized as follows:

Given: *Model free parameters, simulation outputs, and experimental in vitro data.*

Find: *Best-fit values for the free parameters (best \bar{P})*

Such: *The error between the simulation and experimental in vitro data is minimized.*

The search for the correct \bar{P} (described in Algorithm 1 and Figure 4.3) starts by sweeping over an initial range of values for each free parameter being fitted. A single sweep consists of running simulations for the space of \bar{P} (all combinations of free parameter values

based on their ranges). The range is defined by a minimum value, a maximum value, and a step value. In a sweep, each parameter starts from its minimum value and incrementally increases to its maximum value by its step value. An error is calculated for each parameter vector by comparing the time-series outputs of the simulation with experimental *in vitro* data (see Figure 4.3D). The vector \bar{P} of parameter values with the minimum error is selected and becomes the midpoint for the parameter ranges in the next sweep (see Figure 4.3E and F). The process continues until an exit condition is met where the reduction in error is below a threshold or the preset search time runs out. The parameter values (both free and known parameters) for a simulation are specified via the protocol file. (see Figure 4.3B).

In this model, the error was calculated using Equation 4.3. $V_s(i, t)$ and $V_e(i, t)$ are the VEGF concentrations per cell in the simulation and *in vitro*, respectively; i is the patch size, $i \in \{100, 200, 300, 400\mu m\}$ and t is the time in hours, $t \in \{4, 24, 30, 48, 54, 72 \text{ hours}\}$. The model error (εm) is the sum of the errors over the four patch sizes and six time points. The error was calculated for each parameter vector \bar{P} . Additionally, since the simulation process is stochastic, each simulation was repeated 10 times, starting from different random seeds, and the results averaged for all presented data. Here it is important to note that this approach could be used to fit other models using different parameters, experimental results, and error functions.

$$\varepsilon m = \sum_i \sum_t (V_e(i, t) - V_s(i, t))^2 \quad |\bar{P} = \langle K, \mu_V, \beta \rangle \quad (4.3)$$

4.5 Results

Initially the method was applied to a single parameter, K . Figure 4.4 shows the error values for five sweep iterations over K . In each iteration, a parameter sweep for each patch size was performed. In this run, the values of VEGF secretion rate μ_V and VEGF binding rate β were set to 0.09 pg/ml and 1.0, respectively. In iteration 1 (*It1*) the parameters were swept from 0.1 to 0.9, then the best value was chosen to determine the sweeping range for iteration 2 (*It2*). Over repeated sweeps the range of possible valid values for K was greatly

Algorithm 1 Algorithm for the Error-Minimization Search-Based approach using parameter sweeps which identifies a parameters vector \bar{P} that is locally optimal

- 1: **Input:** List of Free-Parameters P , XML Protocol Files P_{files} , and realistic parameter ranges Rs .
 - 2: For each parameter p_k in P , initialize max_k , min_k , $step_k$ randomly within Rs .
 - 3: **while** *time-out is not reached and error_{change} > error_{threshold}* **do**
 - 4: $SWEEP(P_{files}, 1, max_1, min_1, step_1, \{\}, 10)$ \triangleright Recursive parameter sweeping algorithm. Started with the first parameter. See Algorithm 2
 - 5: For each simulation result from the space of \bar{P} s, calculate the VEGF concentration per cell for each patch size i and time t \triangleright There are 10 repeats for each simulation using different random seeds
 - 6: Calculate the *average_{VEGF}* concentration
 - 7: Find the *error* based on equation 4.3
 - 8: $error_{change} = error_{previous} - error$
 - 9: **if** $error < error_{lowest}$ **then**
 - 10: $error_{lowest} = error$ \triangleright Keep track of the lowest error found so far and the change in error from the last sweep
 - 11: Change max_k , min_k , $step_k$ based on parameter values associated with *error*
 - 12: **end if**
 - 13: **end while**
 - 14: Return the parameters values \bar{P} associated with $error_{lowest}$ \triangleright this will return the best value(s) found
-

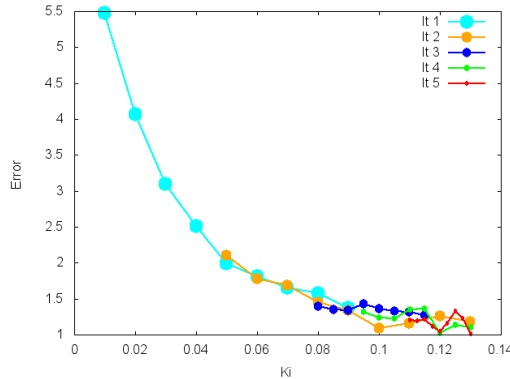


Figure 4.4. Error based on different K values with iteration number It

reduced. After five iterations of sweep processes, the best K value obtained was 0.13 and the associated error was 1.01. This search considered many potential solutions and all but one were rejected as sub-optimal.

Algorithm 2 The parameter sweep algorithm that performs a simulation for all \bar{P} (a combination of free parameters). P_{files} are the XML protocol files that define the model input and initial condition, K is the parameter count, k is a counter that ranges from 1 to K , max_k is the maximum value for parameter k , min_k is the minimum value for the k th parameter, and $step_k$ is the value by which parameter k is incremented, \bar{P} holds a single combination of parameter values for which a simulation will be performed, P is a matrix of size $K \times j$ where j is the number of values in the range of some parameter (which changes as the algorithm progresses) and $P[k][j]$ holds the j th value of the k th parameter, and Run_N is the number of repeated runs, each using different random seeds

```

procedure SWEEP( $P_{files}, k, max_k, min_k, step_k, \bar{P}, Run_N$ )
2:   if  $k = K$  then
      Generate XML Protocol Files  $G_{P_{files}}$  with the same setup as in  $P_{files}$  with the
      parameter values  $\bar{P}$ 
4:      $Run(G_{P_{files}}, P_{set}, Run_N)$  ▷ random seeds runs
       $\bar{P}.Empty$ 
6:   else
       $j = 1$ 
8:      $P[k][j] = min_k - step_k$ 
      while  $P[k][j] < max_k$  do
10:       $P[k][j] = P[k][j] + step_k$ 
       $\bar{P}.Add(P[k][j])$ 
12:       $j = j + 1$ 
       $k = k + 1$ 
14:       $SWEEP(G_{P_{files}}, k, max_k,$ 
       $min_k, step_k, \bar{P}, 10)$ 
16:    end while
      end if
18: end procedure

```

Figure 4.5 shows the error heat map of the first sweep iteration (*It1*) over two parameters (K and β). For this run, the VEGF secretion rate μ_V was set to 0.078 pg/ml/hour. As shown, the error is lowest when the VEGF binding rate (β) is less than 0.3 and the K value is greater than 0.03. Figure 4.6 shows the second sweep (*It2*), which has adjusted sweeping ranges for K and β . Successive iterations refine the parameter values, as shown through reduced error in Figure 4.7, which shows the third sweep (*It3*). The same sweeping processes was also performed between (μ_V and K) and (μ_V and β) (data not shown).

To show how the concentration of VEGF changes over time in the simulation, VEGF expression levels were calculated at various time intervals (4, 24, 30, 48, 54, 72 h). Figure

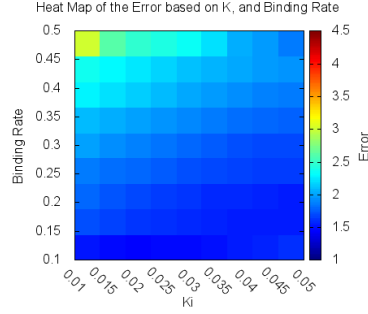


Figure 4.5. The heat map of error between K and VEGF binding coefficient/rate (β) determined from the first round sweep.

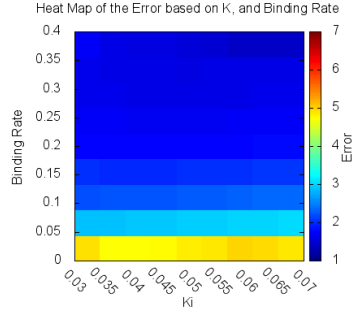


Figure 4.6. The heat map of error between K and VEGF binding coefficient/rate (β) determined from the second round sweep.

4.9(a) shows the data from *in vitro* and Figure 4.9(b) the *in silico* model, K , μ_V , and β are set to 0.13, 0.09 and 0.85, respectively, which were determined from a near-optimal solution discovered by the search method. The error associated with these results is 0.925. As shown in figure 4.9(a) and 4.9(b), in both *in silico* and *in vitro*, RPE cells in the smaller patches expressed higher levels of VEGF per cell. This indicates that these cells function to maintain a consistent level of VEGF within their local microenvironment. Cells in smaller patches respond by expressing higher amounts of VEGF because the VEGF expression levels are dominated by cell-environment interactions. In contrast, larger patches maintain

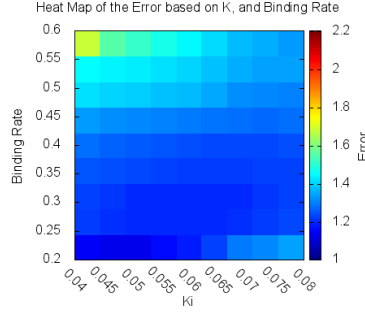


Figure 4.7. The heat map of error between K and VEGF binding coefficient/rate (β) from the third round sweep.

lower basal levels of VEGF because cell-cell auto-inhibitory regulation dominates.

Now the parameters K , μ_V and β have been determined, we replace the variables with their values in Equation 4.1 and set the mass M to that of a single cell ($M = 25.95pg$) resulting in the VEGF autoregulatory function for RPE cells being:

$$\frac{dV}{dt} = 0.09 \times \frac{0.13}{0.85V + 0.13} \times 25.95 \quad (4.4)$$

This function is plotted in Figure 4.8.

4.6 Conclusions

One of the main challenges in the computational modeling of biological systems is the determination of the models' parameters. This problem is particularly acute with multiscale models that are gaining in popularity due to their realism. In this work, we identified the parameter values of a cellular regulatory mechanism using spatiotemporal multicellular data. While the problem of finding parameter values that describe the VEGF autoregulatory mechanism of RPE cells is simple, this problem domain serves as a proof-of-concept for the overall method. Most importantly, the method demonstrates that it is possible to utilize data at one scale to determine parameter values at a different scale.

In the work presented here, thousands of simulations were performed as the search

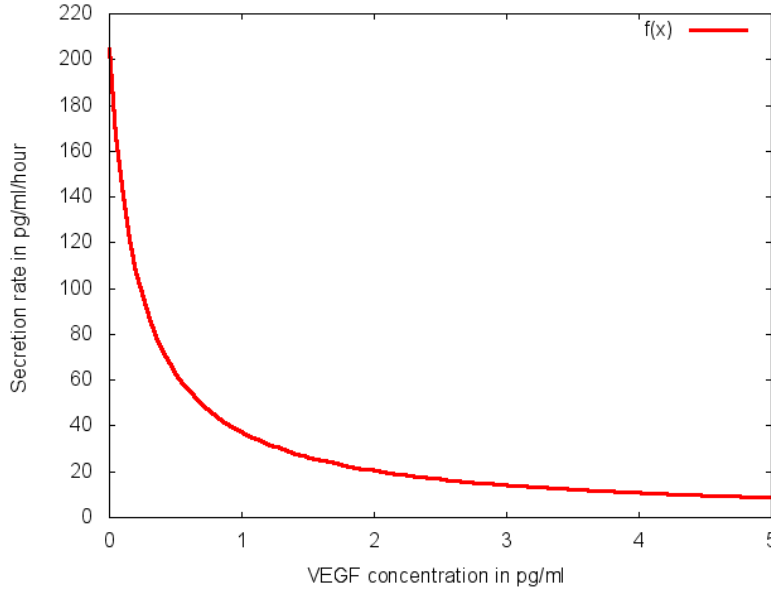
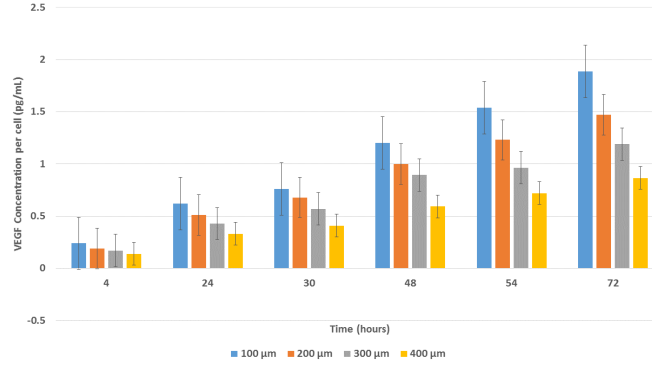


Figure 4.8. The VEGF autoregulatory function of RPE cells showing how the secretion rate of VEGF is down regulated as a function of the VEGF in the microenvironment.

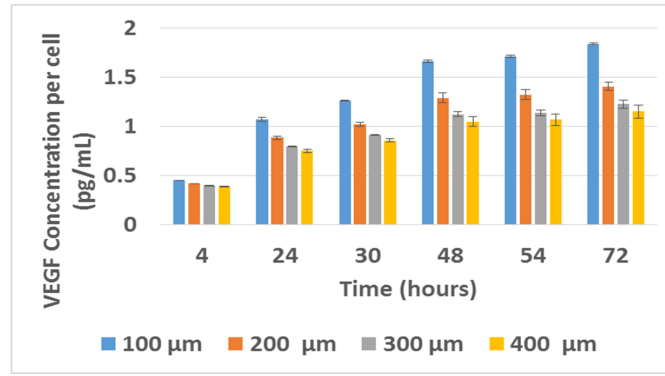
method explored the parameter space. For each potential solution, multiple simulations were needed over each experimental case (different patch sizes) and because of the need for repeats due to model stochasticity. For the simple 2D RPE model, each simulation took less than a minute and so the process could be completed quickly. In general, the method can rapidly become infeasible as the number of unknown parameters grows, domains become larger and more complex, and the number of specific experimental cases grows.

A recently developed hybrid simulation system called Biocellion [114] could be used instead of the iDynamics to speedup the rate of simulations. Biocellion can utilize thousands of processing nodes and rapidly simulate complex models of billions of cells. The search method utilized in this paper was chosen for its simplicity and insights on the local error surfaces provided by the sweeping process. However, the fitting method is independent of the method employed to search the parameter space. Alternative methods of combinatorial optimization may improve performance.

One problem all fitting methods must deal with is under or over fitting the model. There is a possibility that the fitting problem may be under-constrained for lack of data.



(a)



(b)

Figure 4.9. (a) Time course of VEGF expression per cell measured at 4, 24, 30, 48, and 72 h (data from the *in vitro* work [1]). (b) Time course of VEGF expression per cell measured at 4, 24, 30, 48, and 72 h (data from the *in silico* model after optimization).

This problem will be explored in the RPE domain by expanding the data set to include additional studies with VEGF agonists and alternative pattern arrangements.

To extend the method to other domains, alternative error functions can be employed that measure discrepancies over a diversity of spatiotemporal features which quantify both the experimental observations and simulator outcomes. For instance, in [131] image processing is applied to bright field time-lapse images of growing yeast colonies to extract trajectories of many visual features including volume, roughness, dominant frequency etc. The same features could be extracted from the morphologies of simulated colonies and used to fit parameters of the yeast model.

CHAPTER 5

CONCLUSIONS

Computational biology is an integrative and holistic rather than reductionist approach to understanding and controlling biological complexity [132]. It permits the development of predictive and actionable models of multiscale biological systems that are vital to making strides against the constellation of diseases that affect the world. These diseases are defined by their mechanistic complexity and nonlinearity, which spans several spatiotemporal scales. The ability of agent-based modeling to encompass multiple spatiotemporal scales of biological processes, suggests that this modeling framework is well suited for studying these complex systems.

In this research, a multicellular hybrid agent-based modeling approach is utilized in order to study disease development and progression, particularly in two applications: breast cancer and bioengineered experiments. The models outlined were used to study *in vitro* experimental work and *in vivo* development to gain new insights and integrate experimental data to validate simulations.

In the first study, we developed a 2D agent-based model that attempted to emulate the *in vivo* structure of breast cancer. The model was used to describe the transition from DCIS into DCI. We concluded that the interaction between tumor cells and the surrounding stroma in the duct plays a critical role in tumor growth and metastasis. This interaction depends on many mechanical and chemical factors that work with each other to produce tumor invasion of the surrounding tissue. In the second study, an *in silico* model was proposed and applied to understanding the underlying mechanism of VEGF auto-regulation in REP and emulate the *in vitro* experiments as part of bioengineering research. In the third and final study, an innovative approach was presented that estimates cellular parameters from spatiotemporal data produced from bioengineered multicellular *in vitro* experiments.

We applied a search method to an integrated cellular and multicellular model of retinal pigment epithelial cells to estimate the auto-regulation parameters of VEGF. This searching method can be extended to other domains and alternative error functions, which can be employed to measure discrepancies over a diversity of spatiotemporal features to quantify both the experimental *in vitro in vivo* observations and simulator outcomes

From the studies performed in this research, we learned that models are more useful if they can be predictive and the predictions are in a form that can be directly measured in laboratory and clinical experiments. These predictive models can be utilized to guide the laboratory towards the most informative experiments. To obtain such predictive models, parameters estimation and models validation are essential. We have found that as granularity of model becomes more complex, the amount of data needed for validation becomes greater than what can be generated by typical laboratory experiments, and so is often difficult to obtain. Finding the right model size is a challenge. The opportunities for the future is to better understand how to take the large model, such as breast cancer it down to a level where the parameters can be estimated robustly from experimental data, as illustrated in the bioengineered application.

Future prospects for such modeling approaches include the development of patient-calibrated models by specialization of cell physiology obtained from clinical histopathology data. These also include the creation of patient-specific digitized cell lines, which can then be read by a collection of appropriate simulators to search, visualize, compare, predict, and help guide the patient's treatment options. Attaining this future will require considerable cooperation among *in vitro* research, clinical data, and computational biology work. Another developed hybrid simulation system called Biocellion [114] could be used instead of the iDynamics to speed up the simulations. Biocellion has the ability to utilize thousands of processing nodes and rapidly simulate complex models of billions of cells. Using the Biocellion framework, the models developed in this dissertation can be extends to large-scale in order to support of high-throughput experiments and the discovery and evaluation of therapies.

REFERENCES

- [1] E. Vargis, C. B. Peterson, J. L. Morrell-Falvey, S. T. Retterer, and C. Patrick, "The effect of retinal pigment epithelial cell patch size on growth factor expression." *Biomaterials*, vol. 35, no. 13, pp. 3999–4004, Apr. 2014. [Online]. Available: <http://dx.doi.org/10.1016/j.biomaterials.2014.01.016>
- [2] F. Castiglione, F. Pappalardo, C. Bianca, G. Russo, and S. Motta, "Modeling biology spanning different scales: an open challenge," *BioMed Research International*, vol. 2014, pp. 1–9, 2014. [Online]. Available: <http://dx.doi.org/10.1155/2014/902545>
- [3] M. Meier-Schellersheim, I. D. Fraser, and F. Klauschen, "Multiscale modeling for biologists." *Wiley Interdisciplinary Reviews. Systems Biology and Medicine*, vol. 1, no. 1, pp. 4–14, Jul. 2009. [Online]. Available: <http://dx.doi.org/10.1002/wsbm.33>
- [4] D. T. Butcher, T. Alliston, and V. M. Weaver, "A tense situation: forcing tumour progression," *Nature Reviews Cancer*, vol. 9, no. 2, pp. 108–122, Feb. 2009. [Online]. Available: <http://dx.doi.org/10.1038/nrc2544>
- [5] Y.-G. G. Man and Q.-X. Amy, "The significance of focal myoepithelial cell layer disruptions in human breast tumor invasion: a paradigm shift from the "protease-centered" hypothesis." *Experimental cell research*, vol. 301, no. 2, pp. 103–118, Dec. 2004. [Online]. Available: <http://dx.doi.org/10.1016/j.yexcr.2004.08.037>
- [6] J. Southern, J. Pitt-Francis, J. Whiteley, D. Stokeley, H. Kobashi, R. Nobes, Y. Kadooka, and D. Gavaghan, "Multi-scale computational modelling in biology and physiology." *Progress in Biophysics and Molecular Biology*, vol. 96, no. 1-3, pp. 60–89, Jan. 2008. [Online]. Available: <http://dx.doi.org/10.1016/j.pbiomolbio.2007.07.019>

- [7] A. Gautieri and M. Buehler, “Multi-scale modeling of biomaterials and tissues,” in *Materiomics: Multiscale Mechanics of Biological Materials and Structures*, ser. CISM International Centre for Mechanical Sciences, M. Buehler and R. Ballarini, Eds. Springer Vienna, 2013, vol. 546, pp. 13–55. [Online]. Available: http://dx.doi.org/10.1007/978-3-7091-1574-9_2
- [8] T. Eissing, L. Kuepfer, C. Becker, M. Block, K. Coboecken, T. Gaub, L. Goerlitz, J. Jaeger, R. Loosen, B. Ludewig, M. Meyer, C. Niederaalt, M. Sevestre, H.-U. U. Siegmund, J. Solodenko, K. Thelen, U. Telle, W. Weiss, T. Wendl, S. Willmann, and J. Lippert, “A computational systems biology software platform for multiscale modeling and simulation: integrating whole-body physiology, disease biology, and molecular reaction networks.” *Frontiers in Physiology*, vol. 2, 2011. [Online]. Available: <http://dx.doi.org/10.3389/fphys.2011.00004>
- [9] D. Noble, “Modeling the heart—from genes to cells to the whole organ.” *Science (New York, N.Y.)*, vol. 295, no. 5560, pp. 1678–1682, Mar. 2002. [Online]. Available: <http://dx.doi.org/10.1126/science.1069881>
- [10] W. Materi and D. S. Wishart, “Computational systems biology in drug discovery and development: methods and applications,” *Drug Discovery Today*, vol. 12, no. 7-8, pp. 295–303, Apr. 2007. [Online]. Available: <http://dx.doi.org/10.1016/j.drudis.2007.02.013>
- [11] Z. Qu, A. Garfinkel, J. N. Weiss, and M. Nivala, “Multi-scale modeling in biology: How to bridge the gaps between scales?” *Progress in Biophysics and Molecular Biology*, vol. 107, no. 1, pp. 21–31, Oct. 2011. [Online]. Available: <http://dx.doi.org/10.1016/j.pbiomolbio.2011.06.004>
- [12] E. Weinberg, D. Shahmirzadi, and M. Mofrad, “On the multiscale modeling of heart valve biomechanics in health and disease,” *Biomechanics and Modeling in Mechanobiology*, vol. 9, no. 4, pp. 373–387, Jan. 2010. [Online]. Available: <http://dx.doi.org/10.1007/s10237-009-0181-2>

- [13] M. B. Panzer, K. A. Matthews, A. W. Yu, B. Morrison, D. F. Meaney, and C. R. Bass, “A multiscale approach to blast neurotrauma modeling: part I - development of novel test devices for in vivo and in vitro blast injury models.” *Frontiers in Neurology*, vol. 3, 2012. [Online]. Available: <http://dx.doi.org/10.3389/fneur.2012.00046>
- [14] I. Hosseini and F. Mac Gabhann, “Multi-Scale modeling of HIV infection in vitro and APOBEC3G-based anti-retroviral therapy,” *PLoS Comput Biol*, vol. 8, no. 2, pp. e1002371+, Feb. 2012. [Online]. Available: <http://dx.doi.org/10.1371/journal.pcbi.1002371>
- [15] J. G. Diaz Ochoa, J. Bucher, A. R. Péry, J. M. Zaldivar Comenges, J. Niklas, and K. Mauch, “A multi-scale modeling framework for individualized, spatiotemporal prediction of drug effects and toxicological risk.” *Frontiers in Pharmacology*, vol. 3, 2012. [Online]. Available: <http://dx.doi.org/10.3389/fphar.2012.00204>
- [16] J. Walpole, J. A. Papin, and S. M. Peirce, “Multiscale computational models of complex biological systems.” *Annual Review of Biomedical Engineering*, vol. 15, no. 1, pp. 137–154, 2013. [Online]. Available: <http://dx.doi.org/10.1146/annurev-bioeng-071811-150104>
- [17] C. Talcott, “Pathway logic,” in *Proceedings of the Formal Methods for the Design of Computer, Communication, and Software Systems 8th International Conference on Formal Methods for Computational Systems Biology*, ser. SFM’08. Berlin, Heidelberg: Springer-Verlag, 2008, pp. 21–53. [Online]. Available: <http://portal.acm.org/citation.cfm?id=1786701>
- [18] J. B. Bassingthwaighe, H. Jay, and L. E. Atlas, “Strategies and tactics in multiscale modeling of cell-to-organ systems.” *Proceedings of the IEEE. Institute of Electrical and Electronics Engineers*, vol. 94, no. 4, pp. 819–830, Apr. 2006. [Online]. Available: <http://view.ncbi.nlm.nih.gov/pubmed/20463841>

- [19] J. O. Dada and P. Mendes, “Multi-scale modelling and simulation in systems biology,” *Integrative Biology*, vol. 3, no. 2, pp. 86–96, 2011. [Online]. Available: <http://dx.doi.org/10.1039/c0ib00075b>
- [20] S. Ballereau, E. Glaab, A. Kolodkin, A. Chaiboonchoe, M. Biryukov, N. Vlassis, H. Ahmed, J. Pellet, N. Baliga, L. Hood, R. Schneider, R. Balling, and C. Auffray, “Functional Genomics, Proteomics, Metabolomics and Bioinformatics for Systems Biology,” in *Systems Biology*, A. Prokop and B. Csukás, Eds. Springer Netherlands, 2013, pp. 3–41. [Online]. Available: http://dx.doi.org/10.1007/978-94-007-6803-1_1
- [21] F. J. Bruggeman and H. V. Westerhoff, “The nature of systems biology,” *Trends in Microbiology*, vol. 15, no. 1, pp. 45–50, Jan. 2007. [Online]. Available: <http://dx.doi.org/10.1016/j.tim.2006.11.003>
- [22] E. C. Butcher, E. L. Berg, and E. J. Kunkel, “Systems biology in drug discovery,” *Nature Biotechnology*, vol. 22, no. 10, pp. 1253–1259, Oct. 2004. [Online]. Available: <http://dx.doi.org/10.1038/nbt1017>
- [23] S. Hildebrandt, D. Raden, L. Petzold, A. Skaja, and F. J. Doyle, “A top-down approach to mechanistic biological modeling: application to the single-chain antibody folding pathway.” *Biophysical Journal*, vol. 95, no. 8, pp. 3535–3558, Oct. 2008. [Online]. Available: <http://view.ncbi.nlm.nih.gov/pubmed/18641066>
- [24] C. E. Hagemeyer, C. von Zur Muhlen, D. von Elverfeldt, and K. Peter, “Single-chain antibodies as diagnostic tools and therapeutic agents.” *Thrombosis and Haemostasis*, vol. 101, no. 6, pp. 1012–1019, Jun. 2009. [Online]. Available: <http://view.ncbi.nlm.nih.gov/pubmed/19492141>
- [25] N. E. Weissner and J. C. Hall, “Applications of single-chain variable fragment antibodies in therapeutics and diagnostics,” *Biotechnology Advances*, vol. 27, no. 4, pp. 502–520, Jul. 2009. [Online]. Available: <http://dx.doi.org/10.1016/j.biotechadv.2009.04.004>

- [26] T. Ideker and D. Lauffenburger, “Building with a scaffold: emerging strategies for high- to low-level cellular modeling.” *Trends in Biotechnology*, vol. 21, no. 6, pp. 255–262, Jun. 2003. [Online]. Available: <http://view.ncbi.nlm.nih.gov/pubmed/12788545>
- [27] J. I. Allen and E. A. Fulton, “Top-down, bottom-up or middle-out? Avoiding extraneous detail and over-generality in marine ecosystem models,” *Progress in Oceanography*, vol. 84, no. 1-2, pp. 129–133, Jan. 2010. [Online]. Available: <http://dx.doi.org/10.1016/j.pocean.2009.09.016>
- [28] R. L. Hester, R. Iliescu, R. Summers, and T. G. Coleman, “Systems biology and integrative physiological modelling.” *The Journal of Physiology*, vol. 589, no. Pt 5, pp. 1053–1060, Mar. 2011. [Online]. Available: <http://dx.doi.org/10.1113/jphysiol.2010.201558>
- [29] M. Hwang, M. Garbey, S. A. Berceli, and R. Tran-Son-Tay, “Rule-Based Simulation of Multi-Cellular Biological SystemsA Review of Modeling Techniques,” *Cellular and Molecular Bioengineering*, vol. 2, no. 3, pp. 285–294, Sep. 2009. [Online]. Available: <http://dx.doi.org/10.1007/s12195-009-0078-2>
- [30] T. S. Deisboeck, Z. Wang, P. Macklin, and V. Cristini, “Multiscale Cancer Modeling,” *Annual Review of Biomedical Engineering*, vol. 13, no. 1, pp. 127–155, Aug. 2011. [Online]. Available: <http://dx.doi.org/10.1146/annurev-bioeng-071910-124729>
- [31] Z. Wang and T. Deisboeck, “Computational modeling of brain tumors: discrete, continuum or hybrid?” *Scientific Modeling and Simulation*, vol. 15, no. 1-3, pp. 381–393, Apr. 2008. [Online]. Available: <http://dx.doi.org/10.1007/s10820-008-9094-0>
- [32] D. S. Wishart, R. Yang, D. Arndt, P. Tang, and J. Cruz, “Dynamic cellular automata: an alternative approach to cellular simulation.” *In Silico Biology*, vol. 5, no. 2, pp. 139–161, 2005. [Online]. Available: <http://view.ncbi.nlm.nih.gov/pubmed/15972011>
- [33] M. Alber, M. Kiskowski, J. Glazier, and Y. Jiang, “On cellular automaton approaches to modeling biological cells,” in *Mathematical Systems Theory in Biology*,

- Communications, Computation, and Finance*, ser. The IMA Volumes in Mathematics and its Applications, J. Rosenthal and D. Gilliam, Eds. Springer New York, 2003, vol. 134, pp. 1–39. [Online]. Available: http://dx.doi.org/10.1007/978-0-387-21696-6_1
- [34] G. An, Q. Mi, J. Dutta-Moscato, and Y. Vodovotz, “Agent-based models in translational systems biology,” *Wiley Interdisciplinary Reviews. Systems Biology and Medicine*, vol. 1, no. 2, pp. 159–171, Sep. 2009. [Online]. Available: <http://dx.doi.org/10.1002/wsbm.45>
- [35] L. Zhang, Z. Wang, J. A. Sagotsky, and T. S. Deisboeck, “Multiscale agent-based cancer modeling,” *Journal of Mathematical Biology*, vol. 58, no. 4-5, pp. 545–559, Apr. 2009. [Online]. Available: <http://dx.doi.org/10.1007/s00285-008-0211-1>
- [36] S. C. Banks, “Agent-based modeling: a revolution?” *Proceedings of the National Academy of Sciences of the United States of America*, vol. 99 Suppl 3, no. Suppl 3, pp. 7199–7200, May 2002. [Online]. Available: <http://dx.doi.org/10.1073/pnas.072081299>
- [37] Z. Wang, J. D. Butner, R. Kerketta, V. Cristini, and T. S. Deisboeck, “Simulating cancer growth with multiscale agent-based modeling,” *Seminars in Cancer Biology*, vol. 30, pp. 70–78, Feb. 2015. [Online]. Available: <http://view.ncbi.nlm.nih.gov/pubmed/24793698>
- [38] A. R. A. Anderson, “A hybrid mathematical model of solid tumour invasion: the importance of cell adhesion,” *Mathematical Medicine and Biology*, vol. 22, no. 2, pp. 163–186, Jun. 2005. [Online]. Available: <http://dx.doi.org/10.1093/imammb/dqi005>
- [39] K. A. Rejniak and A. R. A. Anderson, “Hybrid models of tumor growth,” *Wiley Interdisciplinary Reviews: Systems Biology and Medicine*, vol. 3, no. 1, pp. 115–125, Jan. 2011. [Online]. Available: <http://dx.doi.org/10.1002/wsbm.102>
- [40] Y. Kim, M. A. Stolarska, H. G. Othmer, Y. Kim, M. A. Stolarska, and H. G. Othmer, “A hybrid model for tumor spheroid growth in vitro

- i: Theoretical development and early results,” 2007. [Online]. Available: <http://citeseerx.ist.psu.edu/viewdoc/summary?doi=10.1.1.131.391>
- [41] C. A. Chung, T.-H. H. Lin, S.-D. D. Chen, and H.-I. I. Huang, “Hybrid cellular automaton modeling of nutrient modulated cell growth in tissue engineering constructs.” *Journal of Theoretical Biology*, vol. 262, no. 2, pp. 267–278, Jan. 2010. [Online]. Available: <http://view.ncbi.nlm.nih.gov/pubmed/19808041>
- [42] L. C. Collins, R. M. Tamimi, H. J. Baer, J. L. Connolly, G. A. Colditz, and S. J. Schnitt, “Outcome of patients with ductal carcinoma in situ untreated after diagnostic biopsy,” *Cancer*, vol. 103, no. 9, pp. 1778–1784, May 2005. [Online]. Available: <http://dx.doi.org/10.1002/cncr.20979>
- [43] B. Erbas, E. Provenzano, J. Armes, and D. Gertig, “The natural history of ductal carcinoma in situ of the breast: a review,” *Breast Cancer Research and Treatment*, vol. 97, no. 2, pp. 135–144, May 2006. [Online]. Available: <http://dx.doi.org/10.1007/s10549-005-9101-z>
- [44] B. E. Klein, R. Klein, and K. E. Lee, “Incidence of age-related cataract over a 10-year interval: The Beaver Dam Eye Study.” *Ophthalmology*, vol. 109, no. 11, pp. 2052–2057, Nov. 2002. [Online]. Available: <http://view.ncbi.nlm.nih.gov/pubmed/12414414>
- [45] J.-D. Ding, L. V. Johnson, R. Herrmann, S. Farsiu, S. G. Smith, M. Groelle, B. E. Mace, P. Sullivan, J. A. Jamison, U. Kelly, O. Harrabi, S. S. Bollini, J. Dilley, D. Kobayashi, B. Kuang, W. Li, J. Pons, J. C. Lin, and C. B. Rickman, “Anti-amyloid therapy protects against retinal pigmented epithelium damage and vision loss in a model of age-related macular degeneration,” *Proceedings of the National Academy of Sciences*, vol. 108, no. 28, pp. E279–E287, Jul. 2011. [Online]. Available: <http://dx.doi.org/10.1073/pnas.1100901108>
- [46] E. A. Rossi, P. Rangel-Fonseca, K. Parkins, W. Fischer, L. R. Latchney, M. A. Folwell, D. R. Williams, A. Dubra, and M. M. Chung, “In vivo

- imaging of retinal pigment epithelium cells in age related macular degeneration.” *Biomedical Optics Express*, vol. 4, no. 11, pp. 2527–2539, 2013. [Online]. Available: <http://dx.doi.org/10.1364/boe.4.002527>
- [47] A. P. Adamis, D. T. Shima, K. T. Yeo, T. K. Yeo, L. F. Brown, B. Berse, P. A. Damore, and J. Folkman, “Synthesis and Secretion of Vascular Permeability Factor/Vascular Endothelial Growth Factor by Human Retinal Pigment Epithelial Cells,” *Biochemical and Biophysical Research Communications*, vol. 193, no. 2, pp. 631–638, Jun. 1993. [Online]. Available: <http://dx.doi.org/10.1006/bbrc.1993.1671>
- [48] A. Pollreisz, T. Afonyushkin, O. V. Oskolkova, F. Gruber, V. N. Bochkov, and U. Schmidt-Erfurth, “Retinal pigment epithelium cells produce VEGF in response to oxidized phospholipids through mechanisms involving ATF4 and protein kinase CK2,” *Experimental Eye Research*, vol. 116, pp. 177–184, Nov. 2013. [Online]. Available: <http://dx.doi.org/10.1016/j.exer.2013.08.021>
- [49] P. T. de Jong, “Age-Related Macular Degeneration,” *N Engl J Med*, vol. 355, no. 14, pp. 1474–1485, Oct. 2006. [Online]. Available: <http://dx.doi.org/10.1056/nejmra062326>
- [50] A. Chopdar, U. Chakravarthy, and D. Verma, “Age related macular degeneration,” *BMJ*, vol. 326, no. 7387, pp. 485–488, Mar. 2003. [Online]. Available: <http://dx.doi.org/10.1136/bmj.326.7387.485>
- [51] A. King, E. Gottlieb, D. G. Brooks, M. P. Murphy, and J. L. Dunaief, “Mitochondria-derived reactive oxygen species mediate blue light-induced death of retinal pigment epithelial cells.” *Photochemistry and Photobiology*, vol. 79, no. 5, pp. 470–475, May 2004. [Online]. Available: <http://view.ncbi.nlm.nih.gov/pubmed/15191057>
- [52] E. Duh and L. P. Aiello, “Vascular endothelial growth factor and diabetes: the agonist versus antagonist paradox.” *Diabetes*, vol. 48, no. 10, pp. 1899–1906, Oct. 1999. [Online]. Available: <http://view.ncbi.nlm.nih.gov/pubmed/10512352>

- [53] A. Amoroso, F. Del Porto, C. Di Monaco, P. Manfredini, and A. Afeltra, “Vascular endothelial growth factor: a key mediator of neoangiogenesis. A review.” *European Review for Medical and Pharmacological Sciences*, vol. 1, no. 1-3, pp. 17–25, 1997. [Online]. Available: <http://view.ncbi.nlm.nih.gov/pubmed/9444794>
- [54] M. R. Kudelka, H. E. Grossniklaus, and K. J. Mandell, “Emergence of dual VEGF and PDGF antagonists in the treatment of exudative age-related macular degeneration,” *Expert Review of Ophthalmology*, vol. 8, no. 5, pp. 475–484, Oct. 2013. [Online]. Available: <http://dx.doi.org/10.1586/17469899.2013.840095>
- [55] L. A. Lardon, B. V. Merkey, S. Martins, A. Dötsch, C. Picioreanu, J.-U. Kreft, and B. F. Smets, “iDynoMiCS: next-generation individual-based modelling of biofilms,” *Environmental Microbiology*, vol. 13, no. 9, pp. 2416–2434, Sep. 2011. [Online]. Available: <http://dx.doi.org/10.1111/j.1462-2920.2011.02414.x>
- [56] P. A. Kenny, G. Y. Lee, C. A. Myers, R. M. Neve, J. R. Semeiks, P. T. Spellman, K. Lorenz, E. H. Lee, M. Helen, O. W. Petersen, J. W. Gray, and M. J. Bissell, “The morphologies of breast cancer cell lines in three-dimensional assays correlate with their profiles of gene expression,” *Molecular Oncology*, vol. 1, no. 1, pp. 84–96, Jun. 2007. [Online]. Available: <http://dx.doi.org/10.1016/j.molonc.2007.02.004>
- [57] S. J. Schnitt, “Classification and prognosis of invasive breast cancer: from morphology to molecular taxonomy.” *Modern Pathology: An Official Journal of the United States and Canadian Academy of Pathology, Inc*, vol. 23 Suppl 2, May 2010. [Online]. Available: <http://view.ncbi.nlm.nih.gov/pubmed/20436504>
- [58] S. J. Franks, H. M. Byrne, J. R. King, J. C. E. Underwood, and C. E. Lewis, “Modelling the early growth of ductal carcinoma in situ of the breast,” *Journal of Mathematical Biology*, vol. 47, no. 5, pp. 424–452, Nov. 2003. [Online]. Available: <http://dx.doi.org/10.1007/s00285-003-0214-x>
- [59] S. J. Franks, H. M. Byrne, J. C. Underwood, and C. E. Lewis, “Biological inferences from a mathematical model of comedo ductal carcinoma in situ of the breast,”

- Journal of Theoretical Biology*, vol. 232, no. 4, pp. 523–543, Feb. 2005. [Online]. Available: <http://dx.doi.org/10.1016/j.jtbi.2004.08.032>
- [60] L. Sontag and D. E. Axelrod, “Evaluation of pathways for progression of heterogeneous breast tumors,” *Journal of Theoretical Biology*, vol. 232, no. 2, pp. 179–189, Jan. 2005. [Online]. Available: <http://dx.doi.org/10.1016/j.jtbi.2004.08.002>
- [61] K. A. Rejniak and R. H. Dillon, “A single cell-based model of the ductal tumour microarchitecture,” *Computational and Mathematical Methods in Medicine*, vol. 8, no. 1, pp. 51–69, Mar. 2007. [Online]. Available: <http://dx.doi.org/10.1080/17486700701303143>
- [62] G. Figueredo, P. O. Siebers, and U. Aickelin, “Investigating mathematical models of immuno-interactions with early-stage cancer under an agent-based modelling perspective,” *BMC Bioinformatics*, vol. 14, no. Suppl 6, pp. S6+, 2013. [Online]. Available: <http://dx.doi.org/10.1186/1471-2105-14-s6-s6>
- [63] K.-A. Norton, M. Wininger, G. Bhanot, S. Ganesan, N. Barnard, and T. Shinbrot, “A 2D mechanistic model of breast ductal carcinoma in situ (DCIS) morphology and progression,” *Journal of Theoretical Biology*, vol. 263, no. 4, pp. 393–406, Apr. 2010. [Online]. Available: <http://dx.doi.org/10.1016/j.jtbi.2009.11.024>
- [64] Y. Kim, M. A. Stolarska, and H. G. Othmer, “The role of the microenvironment in tumor growth and invasion,” *Progress in Biophysics and Molecular Biology*, vol. 106, no. 2, pp. 353–379, Aug. 2011. [Online]. Available: <http://dx.doi.org/10.1016/j.pbiomolbio.2011.06.006>
- [65] P. Macklin, M. E. Edgerton, A. M. Thompson, and V. Cristini, “Patient-calibrated agent-based modelling of ductal carcinoma in situ (DCIS): From microscopic measurements to macroscopic predictions of clinical progression,” *Journal of Theoretical Biology*, vol. 301, pp. 122–140, May 2012. [Online]. Available: <http://dx.doi.org/10.1016/j.jtbi.2012.02.002>

- [66] G. D'Antonio, P. Macklin, and L. Preziosi, "An agent-based model for elasto-plastic mechanical interactions between cells, basement membrane and extracellular matrix." *Mathematical Biosciences and Engineering*, vol. 10, no. 1, pp. 75–101, Feb. 2013. [Online]. Available: <http://view.ncbi.nlm.nih.gov/pubmed/23311363>
- [67] K. Polyak, "Breast cancer: origins and evolution." *The Journal of Clinical Investigation*, vol. 117, no. 11, pp. 3155–3163, Nov. 2007. [Online]. Available: <http://dx.doi.org/10.1172/jci33295>
- [68] R. Derynck, R. J. Akhurst, and A. Balmain, "TGF-[beta] signaling in tumor suppression and cancer progression," *Nature Genetics*, vol. 29, no. 2, pp. 117–129, Oct. 2001. [Online]. Available: <http://dx.doi.org/10.1038/ng1001-117>
- [69] Q. Yu, Q. Yu, I. Stamenkovic, and I. Stamenkovic, "Transforming growth factor-beta facilitates breast carcinoma metastasis by promoting tumor cell survival." *Clinical & experimental metastasis*, vol. 21, no. 3, pp. 235–242, 2004. [Online]. Available: <http://view.ncbi.nlm.nih.gov/pubmed/15387373>
- [70] A. L. Bauer, C. A. A. Beauchemin, and A. S. Perelson, "Agent-based modeling of hostpathogen systems: The successes and challenges," *Information Sciences*, vol. 179, no. 10, pp. 1379–1389, Apr. 2009. [Online]. Available: <http://dx.doi.org/10.1016/j.ins.2008.11.012>
- [71] S. Suresh, "Biomechanics and biophysics of cancer cells." *Acta Biomaterialia*, vol. 3, no. 4, pp. 413–438, Jul. 2007. [Online]. Available: <http://dx.doi.org/10.1016/j.actbio.2007.04.002>
- [72] S. L. Payne, M. J. Hendrix, and D. A. Kirschmann, "Paradoxical roles for lysyl oxidases in cancerA prospect," *Journal of Cellular Biochemistry*, vol. 101, no. 6, pp. 1338–1354, Aug. 2007. [Online]. Available: <http://dx.doi.org/10.1002/jcb.21371>

- [73] C. Rodríguez, A. Rodríguez-Sinovas, and J. Martínez-González, “Lysyl oxidase as a potential therapeutic target.” *Drug News & Perspectives*, vol. 21, no. 4, pp. 218–224, May 2008. [Online]. Available: <http://dx.doi.org/10.1358/dnp.2008.21.4.1213351>
- [74] J.-L. L. Liu, J.-L. L. Liu, W. Wei, W. Wei, W. Tang, W. Tang, Y. Jiang, Y. Jiang, H.-W. W. Yang, H.-W. W. Yang, J.-T. T. Li, J.-T. T. Li, X. Zhou, and X. Zhou, “Silencing of lysyl oxidase gene expression by RNA interference suppresses metastasis of breast cancer.” *Asian Pacific Journal of Cancer Prevention*, vol. 13, no. 7, pp. 3507–3511, 2012. [Online]. Available: <http://view.ncbi.nlm.nih.gov/pubmed/22994786>
- [75] L.-C. C. Chen, S.-H. H. Tu, C.-S. S. Huang, C.-S. S. Chen, C.-T. T. Ho, H.-W. W. Lin, C.-H. H. Lee, H.-W. W. Chang, C.-H. H. Chang, C.-H. H. Wu, W.-S. S. Lee, and Y.-S. S. Ho, “Human breast cancer cell metastasis is attenuated by lysyl oxidase inhibitors through down-regulation of focal adhesion kinase and the paxillin-signaling pathway,” *Breast Cancer Research and Treatment*, vol. 134, no. 3, pp. 989–1004, Aug. 2012. [Online]. Available: <http://dx.doi.org/10.1007/s10549-012-1986-8>
- [76] N. Patani, W. Jiang, R. Newbold, and K. Mokbel, “Prognostic implications of carboxyl-terminus of Hsc70 interacting protein and lysyl-oxidase expression in human breast cancer.” *Journal of Carcinogenesis*, vol. 9, 2010. [Online]. Available: <http://dx.doi.org/10.4103/1477-3163.72505>
- [77] A. Y. Strongin, “Mislocalization and unconventional functions of cellular MMPs in cancer,” *Cancer Metastasis Reviews*, vol. 25, no. 1, pp. 87–98, Mar. 2006. [Online]. Available: <http://dx.doi.org/10.1007/s10555-006-7892-y>
- [78] S. Jodele, L. Blavier, J. M. Yoon, and Y. A. DeClerck, “Modifying the soil to affect the seed: role of stromal-derived matrix metalloproteinases in cancer progression,” *Cancer Metastasis Reviews*, vol. 25, no. 1, pp. 35–43, Mar. 2006. [Online]. Available: <http://dx.doi.org/10.1007/s10555-006-7887-8>

- [79] G. Akiri, E. Sabo, H. Dafni, Z. Vadasz, Y. Kartvelishvily, N. Gan, O. Kessler, T. Cohen, M. Resnick, M. Neeman, and G. Neufeld, “Lysyl oxidase-related protein-1 promotes tumor fibrosis and tumor progression in vivo.” *Cancer Research*, vol. 63, no. 7, pp. 1657–1666, Apr. 2003. [Online]. Available: <http://view.ncbi.nlm.nih.gov/pubmed/12670920>
- [80] M. Decitre, C. Gleyzal, M. Raccurt, S. Peyrol, E. Aubert-Foucher, K. Csiszar, and P. Sommer, “Lysyl oxidase-like protein localizes to sites of de novo fibrinogenesis in fibrosis and in the early stromal reaction of ductal breast carcinomas.” *Laboratory Investigation; A Journal of Technical Methods and Pathology*, vol. 78, no. 2, pp. 143–151, Feb. 1998. [Online]. Available: <http://view.ncbi.nlm.nih.gov/pubmed/9484712>
- [81] T. J. Newman, “Modeling multicellular systems using subcellular elements.” *Mathematical Biosciences and Engineering*, vol. 2, no. 3, pp. 613–624, Jul. 2005. [Online]. Available: <http://view.ncbi.nlm.nih.gov/pubmed/20369943>
- [82] E. Alpkvist, C. Picioreanu, M. C. van Loosdrecht, and A. Heyden, “Three-dimensional biofilm model with individual cells and continuum EPS matrix,” *Biotechnology and Bioengineering*, vol. 94, no. 5, pp. 961–979, Aug. 2006. [Online]. Available: <http://dx.doi.org/10.1002/bit.20917>
- [83] J. Dockery and I. Klapper, “Finger formation in biofilm layers,” in *Society for Industrial and Applied Mathematics*, 2001, pp. 853–869. [Online]. Available: <http://citeseerx.ist.psu.edu/viewdoc/summary?doi=10.1.1.71.1967>
- [84] S. M. Mumenthaler, G. D’Antonio, L. Preziosi, and P. Macklin, “The Need for Integrative Computational Oncology: An Illustrated Example through MMP-Mediated Tissue Degradation,” *Frontiers in Oncology*, vol. 3, 2013. [Online]. Available: <http://dx.doi.org/10.3389/fonc.2013.00194>
- [85] J. Massagué, “TGF in cancer,” *Cell*, vol. 134, no. 2, pp. 215–230, Jul. 2008. [Online]. Available: <http://dx.doi.org/10.1016/j.cell.2008.07.001>

- [86] F. Klingberg, B. Hinz, and E. S. White, “The myofibroblast matrix: implications for tissue repair and fibrosis,” *The Journal of Pathology*, vol. 229, no. 2, pp. 298–309, Jan. 2013. [Online]. Available: <http://dx.doi.org/10.1002/path.4104>
- [87] M. Perepelyuk, M. Terajima, A. Y. Wang, P. C. Georges, P. A. Janmey, M. Yamauchi, and R. G. Wells, “Hepatic stellate cells and portal fibroblasts are the major cellular sources of collagens and lysyl oxidases in normal liver and early after injury.” *American Journal of Physiology. Gastrointestinal and Liver Physiology*, vol. 304, no. 6, Mar. 2013. [Online]. Available: <http://view.ncbi.nlm.nih.gov/pubmed/23328207>
- [88] Y. Kim, J. Wallace, F. Li, M. Ostrowski, and A. Friedman, “Transformed epithelial cells and fibroblasts/myofibroblasts interaction in breast tumor: a mathematical model and experiments,” *Journal of Mathematical Biology*, vol. 61, no. 3, pp. 401–421, Sep. 2010. [Online]. Available: <http://dx.doi.org/10.1007/s00285-009-0307-2>
- [89] Y. Kim and A. Friedman, “Interaction of Tumor with Its Micro-environment: A Mathematical Model,” *Bulletin of Mathematical Biology*, vol. 72, no. 5, pp. 1029–1068, Jul. 2010. [Online]. Available: <http://dx.doi.org/10.1007/s11538-009-9481-z>
- [90] A. C. Bird, N. M. Bressler, S. B. Bressler, I. H. Chisholm, G. Coscas, M. D. Davis, P. T. V. M. de Jong, C. C. W. Klaver, B. E. K. Klein, R. Klein, P. Mitchell, J. P. Sarks, S. H. Sarks, G. Soubrane, H. R. Taylor, and J. R. Vingerling, “An international classification and grading system for age-related maculopathy and age-related macular degeneration,” *Survey of Ophthalmology*, vol. 39, no. 5, pp. 367–374, Mar. 1995. [Online]. Available: [http://dx.doi.org/10.1016/s0039-6257\(05\)80092-x](http://dx.doi.org/10.1016/s0039-6257(05)80092-x)
- [91] J. Ambati and B. J. Fowler, “Mechanisms of age-related macular degeneration.” *Neuron*, vol. 75, no. 1, pp. 26–39, Jul. 2012. [Online]. Available: <http://dx.doi.org/10.1016/j.neuron.2012.06.018>
- [92] N. Ferrara, K. Carver-Moore, H. Chen, M. Dowd, L. Lu, K. S. O’Shea, L. Powell-Braxton, K. J. Hillan, and M. W. Moore, “Heterozygous embryonic lethality induced

- by targeted inactivation of the VEGF gene.” *Nature*, vol. 380, no. 6573, pp. 439–442, Apr. 1996. [Online]. Available: <http://view.ncbi.nlm.nih.gov/pubmed/8602242>
- [93] R. J. Ross, V. Verma, K. I. Rosenberg, C.-C. C. Chan, and J. Tuo, “Genetic markers and biomarkers for age-related macular degeneration,” *Expert Review of Ophthalmology*, vol. 2, no. 3, pp. 443–457, Jun. 2007. [Online]. Available: <http://dx.doi.org/10.1586/17469899.2.3.443>
- [94] J. Stone, A. Itin, T. Alon, J. Pe’er, H. Gnessin, T. Chan-Ling, and E. Keshet, “Development of retinal vasculature is mediated by hypoxia-induced vascular endothelial growth factor (VEGF) expression by neuroglia.” *The Journal of Neuroscience*, vol. 15, no. 7 Pt 1, pp. 4738–4747, Jul. 1995. [Online]. Available: <http://view.ncbi.nlm.nih.gov/pubmed/7623107>
- [95] A. Klettner, D. Westhues, J. Lassen, S. Bartsch, and J. Roeder, “Regulation of constitutive vascular endothelial growth factor secretion in retinal pigment epithelium/choroid organ cultures: p38, nuclear factor B, and the vascular endothelial growth factor receptor-2/phosphatidylinositol 3 kinase pathway.” *Molecular Vision*, vol. 19, pp. 281–291, 2013. [Online]. Available: <http://view.ncbi.nlm.nih.gov/pubmed/23401656>
- [96] M. Théry, “Micropatterning as a tool to decipher cell morphogenesis and functions,” *Journal of Cell Science*, vol. 123, no. 24, pp. 4201–4213, Dec. 2010. [Online]. Available: <http://dx.doi.org/10.1242/jcs.075150>
- [97] R. Singhvi, A. Kumar, G. P. Lopez, G. N. Stephanopoulos, D. I. Wang, G. M. Whitesides, and D. E. Ingber, “Engineering cell shape and function,” *Science*, vol. 264, no. 5159, pp. 696–698, Apr. 1994. [Online]. Available: <http://dx.doi.org/10.1126/science.8171320>
- [98] W.-W. Liu, Z.-L. Chen, and X.-Y. Jiang, “Methods for Cell Micropatterning on Two-Dimensional Surfaces and Their Applications in Biology,” *Chinese Journal of*

- Analytical Chemistry*, vol. 37, no. 7, pp. 943–949, Jul. 2009. [Online]. Available: [http://dx.doi.org/10.1016/s1872-2040\(08\)60113-9](http://dx.doi.org/10.1016/s1872-2040(08)60113-9)
- [99] I.-K. K. Kang, G. Ja, O. Hyeong, and Y. Ito, “Co-culture of hepatocytes and fibroblasts by micropatterned immobilization of beta-galactose derivatives.” *Biomaterials*, vol. 25, no. 18, pp. 4225–4232, Aug. 2004. [Online]. Available: <http://view.ncbi.nlm.nih.gov/pubmed/15046912>
- [100] D. R. Reyes, E. M. Perruccio, P. P. Becerra, L. E. Locascio, and M. Gaitan, “Micropatterning neuronal cells on polyelectrolyte multilayers.” *Langmuir: The ACS Journal of Surfaces and Colloids*, vol. 20, no. 20, pp. 8805–8811, Sep. 2004. [Online]. Available: <http://view.ncbi.nlm.nih.gov/pubmed/15379510>
- [101] L. Lu, L. Kam, M. Hasenbein, K. Nyalakonda, R. Bizios, A. Göpferich, J. F. Young, and A. G. Mikos, “Retinal pigment epithelial cell function on substrates with chemically micropatterned surfaces.” *Biomaterials*, vol. 20, no. 23-24, pp. 2351–2361, Dec. 1999. [Online]. Available: <http://view.ncbi.nlm.nih.gov/pubmed/10614941>
- [102] L. Lu, K. Nyalakonda, L. Kam, R. Bizios, A. Göpferich, and A. G. Mikos, “Retinal pigment epithelial cell adhesion on novel micropatterned surfaces fabricated from synthetic biodegradable polymers.” *Biomaterials*, vol. 22, no. 3, pp. 291–297, Feb. 2001. [Online]. Available: <http://view.ncbi.nlm.nih.gov/pubmed/11197504>
- [103] J.-M. Lim, S. Byun, S. Chung, T. H. Park, J.-M. Seo, C.-K. Joo, H. Chung, and D.-i. Cho, “Retinal Pigment Epithelial Cell Behavior is Modulated by Alterations in Focal CellSubstrate Contacts,” *Investigative Ophthalmology & Visual Science*, vol. 45, no. 11, pp. 4210–4216, Nov. 2004. [Online]. Available: <http://dx.doi.org/10.1167/iovs.03-1036>
- [104] J. Fink, M. Théry, A. Azioune, R. Dupont, F. Chatelain, M. Bornens, and M. Piel, “Comparative study and improvement of current cell micro-patterning techniques.” *Lab on a Chip*, vol. 7, no. 6, pp. 672–680, Jun. 2007. [Online]. Available: <http://view.ncbi.nlm.nih.gov/pubmed/17538708>

- [105] C. L. Bauwens, R. Peerani, S. Niebruegge, K. A. Woodhouse, E. Kumacheva, M. Husain, and P. W. Zandstra, “Control of human embryonic stem cell colony and aggregate size heterogeneity influences differentiation trajectories,” *STEM CELLS*, vol. 26, no. 9, pp. 2300–2310, Sep. 2008. [Online]. Available: <http://dx.doi.org/10.1634/stemcells.2008-0183>
- [106] J.-P. Frimat, H. Menne, A. Michels, S. Kittel, R. Kettler, S. Borgmann, J. Franzke, and J. West, “Plasma stencilling methods for cell patterning,” *Analytical and Bioanalytical Chemistry*, vol. 395, no. 3, pp. 601–609, 2009. [Online]. Available: <http://dx.doi.org/10.1007/s00216-009-2824-7>
- [107] C. Smulovitz, L. E. Dickinson, and S. Gerecht, “Micropatterned surfaces for the study of cancer and endothelial cell interactions with hyaluronic acid,” *Israel Journal of Chemistry*, vol. 53, no. 9-10, pp. 710–718, Oct. 2013. [Online]. Available: <http://dx.doi.org/10.1002/ijch.201300058>
- [108] G. Bergers and D. Hanahan, “Modes of resistance to anti-angiogenic therapy,” *Nature Reviews Cancer*, vol. 8, no. 8, pp. 592–603, Aug. 2008. [Online]. Available: <http://dx.doi.org/10.1038/nrc2442>
- [109] M. O. Stefanini, F. T. Wu, F. M. Gabhann, and A. S. Popel, “A compartment model of VEGF distribution in blood, healthy and diseased tissues,” *BMC Systems Biology*, vol. 2, no. 1, pp. 77+, Aug. 2008. [Online]. Available: <http://dx.doi.org/10.1186/1752-0509-2-77>
- [110] J. A. Lerman, D. R. Hyduke, H. Latif, V. A. Portnoy, N. E. Lewis, J. D. Orth, A. C. Schrimpe-Rutledge, R. D. Smith, J. N. Adkins, K. Zengler, and B. O. Palsson, “In silico method for modelling metabolism and gene product expression at genome scale,” *Nature Communications*, vol. 3, pp. 929+, Jul. 2012. [Online]. Available: <http://dx.doi.org/10.1038/ncomms1928>
- [111] Y. Kam, K. A. Rejniak, and A. R. Anderson, “Cellular modeling of cancer invasion: integration of in silico and in vitro approaches.” *Journal of Cellular*

- Physiology*, vol. 227, no. 2, pp. 431–438, Feb. 2012. [Online]. Available: <http://view.ncbi.nlm.nih.gov/pubmed/21465465>
- [112] Y. Shin, S. Han, J. S. Jeon, K. Yamamoto, I. K. Zervantonakis, R. Sudo, R. D. Kamm, and S. Chung, “Microfluidic assay for simultaneous culture of multiple cell types on surfaces or within hydrogels,” *Nature Protocols*, vol. 7, no. 7, pp. 1247–1259, Jul. 2012. [Online]. Available: <http://dx.doi.org/10.1038/nprot.2012.051>
- [113] M. Bryckaert, X. Guillonnet, C. Hecquet, P. Perani, Y. Courtois, and F. Mascarelli, “Regulation of proliferation-survival decisions is controlled by FGF1 secretion in retinal pigmented epithelial cells.” *Oncogene*, vol. 19, no. 42, pp. 4917–4929, Oct. 2000. [Online]. Available: <http://view.ncbi.nlm.nih.gov/pubmed/11039909>
- [114] S. Kang, S. Kahan, J. McDermott, N. Flann, and I. Shmulevich, “Biocellion: accelerating computer simulation of multicellular biological system models,” *Bioinformatics*, vol. 30, no. 21, pp. 3101–3108, Nov. 2014. [Online]. Available: <http://dx.doi.org/10.1093/bioinformatics/btu498>
- [115] P. Vicini, “Multiscale modeling in drug discovery and development: future opportunities and present challenges.” *Clinical Pharmacology and Therapeutics*, vol. 88, no. 1, pp. 126–129, Jul. 2010. [Online]. Available: <http://view.ncbi.nlm.nih.gov/pubmed/20520608>
- [116] A. W. Mahoney, G. J. Podgorski, and N. S. Flann, “Multiobjective Optimization Based-Approach for Discovering Novel Cancer Therapies,” *IEEE/ACM Transactions on Computational Biology and Bioinformatics*, vol. 9, no. 1, pp. 169–184, Jan. 2012. [Online]. Available: <http://dx.doi.org/10.1109/tcbb.2010.39>
- [117] E. Walker and C. Guiang, “Challenges in executing large parameter sweep studies across widely distributed computing environments,” in *Proceedings of the 5th IEEE Workshop on Challenges of Large Applications in Distributed Environments*, ser. CLADE '07. New York, NY, USA: ACM, 2007, pp. 11–18. [Online]. Available: <http://dx.doi.org/10.1145/1273404.1273411>

- [118] M. K. Transtrum, B. B. Machta, and J. P. Sethna, “Why are nonlinear fits so challenging?” *Physical Review Letters*, vol. 104, no. 6, pp. 060 201+, Dec. 2009. [Online]. Available: <http://dx.doi.org/10.1103/physrevlett.104.060201>
- [119] M. Rodriguez-Fernandez, J. A. Egea, and J. R. Banga, “Novel metaheuristic for parameter estimation in nonlinear dynamic biological systems.” *BMC Bioinformatics*, vol. 7, pp. 483+, Nov. 2006. [Online]. Available: <http://dx.doi.org/10.1186/1471-2105-7-483>
- [120] I.-C. Chou and E. O. Voit, “Recent developments in parameter estimation and structure identification of biochemical and genomic systems,” *Mathematical Biosciences*, vol. 219, no. 2, pp. 57–83, Jun. 2009. [Online]. Available: <http://dx.doi.org/10.1016/j.mbs.2009.03.002>
- [121] J. Sun, J. M. Garibaldi, and C. Hodgman, “Parameter Estimation Using Metaheuristics in Systems Biology: A Comprehensive Review,” *Computational Biology and Bioinformatics, IEEE/ACM Transactions on*, vol. 9, no. 1, pp. 185–202, Jan. 2012. [Online]. Available: <http://dx.doi.org/10.1109/tcbb.2011.63>
- [122] J. R. Banga, “Optimization in computational systems biology,” *BMC Systems Biology*, vol. 2, no. 1, pp. 47+, May 2008. [Online]. Available: <http://dx.doi.org/10.1186/1752-0509-2-47>
- [123] E. Balsa-Canto, M. Peifer, J. R. Banga, J. Timmer, and C. Fleck, “Hybrid optimization method with general switching strategy for parameter estimation,” *BMC Systems Biology*, vol. 2, no. 1, pp. 26+, Mar. 2008. [Online]. Available: <http://dx.doi.org/10.1186/1752-0509-2-26>
- [124] G. Lillacci and M. Khammash, “Parameter estimation and model selection in computational biology,” *PLoS Computational Biology*, vol. 6, no. 3, pp. e1 000 696+, Mar. 2010. [Online]. Available: <http://dx.doi.org/10.1371/journal.pcbi.1000696>

- [125] P. Carmeliet and R. K. Jain, “Angiogenesis in cancer and other diseases,” *Nature*, vol. 407, no. 6801, pp. 249–257, Sep. 2000. [Online]. Available: <http://dx.doi.org/10.1038/35025220>
- [126] F. Mac Gabhann, J. W. Ji, and A. S. Popel, “Computational Model of Vascular Endothelial Growth Factor Spatial Distribution in Muscle and Pro-Angiogenic Cell Therapy,” *PLoS Computational Biology*, vol. 2, no. 9, pp. e127+, Sep. 2006. [Online]. Available: <http://dx.doi.org/10.1371/journal.pcbi.0020127>
- [127] F. Gabhann, M. Stefanini, and A. Popel, “Simulating therapeutics using multiscale models of the VEGF receptor system in cancer,” in *Modeling Tumor Vasculature*, T. L. Jackson, Ed. Springer New York, 2012, pp. 37–53. [Online]. Available: http://dx.doi.org/10.1007/978-1-4614-0052-3_2
- [128] S. D. Finley, M. Dhar, and A. S. Popel, “Compartment model predicts VEGF secretion and investigates the effects of VEGF trap in tumor-bearing mice.” *Frontiers in Oncology*, vol. 3, 2013. [Online]. Available: <http://view.ncbi.nlm.nih.gov/pubmed/23908970>
- [129] P. Yen, S. D. Finley, M. O. Engel-Stefanini, and A. S. Popel, “A two-compartment model of VEGF distribution in the mouse,” *PloS ONE*, vol. 6, no. 11, pp. e27514+, Nov. 2011. [Online]. Available: <http://dx.doi.org/10.1371/journal.pone.0027514>
- [130] H. Takahashi and M. Shibuya, “The vascular endothelial growth factor (VEGF)/VEGF receptor system and its role under physiological and pathological conditions.” *Clinical science (London, England : 1979)*, vol. 109, no. 3, pp. 227–241, Sep. 2005. [Online]. Available: <http://dx.doi.org/10.1042/cs20040370>
- [131] P. Ruusuvuori, J. Lin, A. C. Scott, Z. Tan, S. Sorsa, A. Kallio, M. Nykter, O. Yli-Harja, I. Shmulevich, and A. M. Dudley, “Quantitative analysis of colony morphology in yeast.” *BioTechniques*, vol. 56, no. 1, pp. 18–27, Jan. 2014. [Online]. Available: <http://dx.doi.org/10.2144/000114123>

- [132] E. A. Logsdon, S. D. Finley, A. S. Popel, and F. M. Gabhann, “A systems biology view of blood vessel growth and remodelling,” *Journal of Cellular and Molecular Medicine*, vol. 18, no. 8, pp. 1491–1508, Aug. 2014. [Online]. Available: <http://dx.doi.org/10.1111/jcmm.12164>

APPENDICES

6/2/2015

Aggiemail Mail - To coauthor Ahmadreza Ghaffarizadeh



Qanita Bani Baker <qanita@aggiemail.usu.edu>

To coauthor Ahmadreza Ghaffarizadeh

Farzin Ghaffarizadeh <farzin.ghaffarizadeh@cammlab.org>

Wed, May 27, 2015 at 11:22 AM

To: Qanita Bani Baker <qanita@aggiemail.usu.edu>

Cc: nicholas flann <nick.flann@gmail.com>

Hi Qanita.

Here is the permission:

I hereby give permission to Qanita Bani Baker to reprint the article in her dissertation.

Ahmadreza (Farzin) Ghaffarizadeh

On Wed, May 27, 2015 at 11:02 AM, Qanita Bani Baker <qanita@aggiemail.usu.edu> wrote:

Date May,27,2015

Name: Qanita Bani Baker

Dear Ahmadreza Ghaffarizadeh:

I am in the process of preparing my dissertation in the Computer Science department at Utah State University. I hope to complete my degree program in Computer Science.

The article: Interactions of Stroma and Tumor Cells in Ductal Carcinoma in Situ to Invasion: An Agent-Based Modeling Approach, of which I am the first author, and which you are the coauthor in this article. I am requesting your permission to include this article as chapter in my dissertation. Please indicate your approval of this request by reply for this email.

You can use the following format to send me the permission:

I hereby give permission to Qanita Bani Baker to reprint the article in her dissertation.

--

Best,

Qanita Bani Baker

PhD Candidate

Department of Computer Science.

Utah State University, Logan, UT-84322-3900.

6/2/2015

Aggiemail Mail - To coauthor Soonjo Kwon



Qanita Bani Baker <qanita@aggiemail.usu.edu>

To coauthor Soonjo Kwon

Soonjo Kwon <soonjo@gmail.com>
 To: Qanita Bani Baker <qanita@aggiemail.usu.edu>

Wed, May 27, 2015 at 6:49 PM

Hi, Qanita

I hereby give permission to Qanita Bani Baker to reprint the following article her dissertation.

The article: Interactions of Stroma and Tumor Cells in Ductal Carcinoma in Situ to Invasion: An Agent-Based Modeling Approach.

Was this article published in 'Computational and Mathematical methods in Medicine'? If this was published, please send me the final copy of the paper.^

Sincerely,

Soonjo

Soonjo Kwon, Ph.D.
 Professor and Chair of Biological Engineering
 Director of Integrated Tissue Engineering Laboratory (ITEL)
 Vice-Dean of International Affairs
 INHA University, Incheon, Korea
 (Office) +82-32-860-9176
 (Fax) +82-32-872-4046
 (Mobile) +82-10-8266-1238
 (email) soonjo@gmail.com

On Thu, May 28, 2015 at 3:01 AM, Qanita Bani Baker <qanita@aggiemail.usu.edu> wrote:

Date May,27,2015

Name: Qanita Bani Baker

Dear Soonjo Kwon:

I am in the process of preparing my dissertation in the Computer Science department at Utah State University. I hope to complete my degree program in Computer Science.

The article: Interactions of Stroma and Tumor Cells in Ductal Carcinoma in Situ to Invasion:

An Agent-Based Modeling Approach, of which I am the first author, and which you are the coauthor in this article

I am requesting your permission to include this article as chapter in my dissertation. Please indicate your approval of this request by reply for this email.

You can use the following format to send me the permission:

I hereby give permission to Qanita Bani Baker to reprint the article her dissertation.

6/2/2015

Aggiemail Mail - To coauthor Christopher D. Johnson



Qanita Bani Baker <qanita@aggiemail.usu.edu>

To coauthor Christopher D. Johnson

Chris Johnson <christopher.d.johnson@aggiemail.usu.edu>
To: Qanita Bani Baker <qanita@aggiemail.usu.edu>

Wed, May 27, 2015 at 10:54 AM

I hereby give permission to Qanita Bani Baker to reprint the article her dissertation.

-Christopher Johnson

On Wed, May 27, 2015 at 11:50 AM, Qanita Bani Baker <qanita@aggiemail.usu.edu> wrote:

Date May,27,2015

Name: Qanita Bani Baker

Dear Christopher D. Johnson:

I am in the process of preparing my dissertation in the Computer Science department at Utah State University. I hope to complete my degree program in Computer Science.

The article Bridging the Multiscale Gap: Identifying Cellular Parameters from Multicellular Data, of which I am the first author, and which you are the coauthor in this article

I am requesting your permission to include this article as chapter in my dissertation. Please indicate your approval of this request by reply for this email.

You can use the following format to send me the permission:

I hereby give permission to Qanita Bani Baker to reprint the article her dissertation.

--

Best,

Qanita Bani Baker

PhD Candidate

Department of Computer Science.

Utah State University, Logan, UT-84322-3900.

CURRICULUM VITAE

Qanita Bani Baker

EDUCATION

- Ph.D., Computer Science. Utah State University, Logan, UT. 2015.
- M.S., Computer Science. Jordan University of Science and Technology, Irbid, Jordan. 2007.
- B.S., Computer Science. Jordan University of Science and Technology, Irbid, Jordan. 2004.

RESEARCH INTERESTS

- Bioinformatics (Multi-scale modeling).
- Sensor technology.

PUBLICATION

THESIS

- Developing Middleware Mechanisms to Support Energy-Efficient Wireless Sensor Networks. By Qanita BaniBaker, Dr. Ayad Salhie. Thesis submitted in partial fulfillment of the requirements for the degree of M.Sc. in Computer Science .At The Faculty of Graduate Studies Jordan University of Science and Technology. May 2007.

PUBLICATIONS IN CONFERENCE

- Qanita BaniBaker, Soonjo Kwon, Ahmadreza Ghaffarizadeh, Gregory J.Podgorski, Nicholas S. Flann, An Agent-based Model of Ductal Carcinoma in situ (DCIS) and its Validation in a Tissue-engineered . IBE Annual Conference. Raleigh. North Carolina. (March. 6-8, 2013)
- Qanita BaniBaker, Gregory J.Podgorski, Nicholas S. Flann, Interaction Stroma and Tumor Growth in Ductal Carcinoma in Situ Metastasis: 2D and 3D Agent-Based Modeling .Utah state university tenth annual celebration of faculty and student research at Utah State University. Logan. USA (Apr. 4-11, 2014).

- Agentbased model for breast tissue culture development in vitro. Qanita Bani Baker, Nicholas S. Flann, Soonjo Kwon, Gregory J. Podgorski, and Ahmadreza Ghaffarizadeh, Utah State University. IBe 2014
- A 3D agentbased model of the transition from ductal carcinoma in situ to invasion. Qanita Bani Baker, Nicholas S. Flann, Soonjo Kwon, Gregory J. Podgorski, Ahmadreza Ghaffarizadeh, IBe 2014
- Qanita Bani Baker, Gregory J. Podgorski, Christopher D. Johnson, Elizabeth Vargis, Nicholas S. Flann, Bridging the Multiscale gap: Identifying Cellular Parameters from Multicellular Data. IEEE, 2015

PUBLICATIONS IN JOURNALS

- Qanita Bani Baker, Ahmadreza Ghaffarizadeh, Soonjo Kwon, Gregory J. Podgorski and Nicholas S. Flann. Interaction of Stroma and Tumor Growth in Ductal Carcinoma in Situ Metastasis: An Agent-Based Modeling Approach. 2015(under review)
- Qanita Bani Baker, Gregory J. Podgorski, and Elizabeth Vargis , Nicholas S. Flann. Developing in Silico Model to Study the Effect of Retinal Pigment Epithelial Cell Patch Size.2015(under review)

POSTER

- Qanita Bani Baker, Ahmadreza Ghaffarizadeh, Soonjo Kwon, Gregory J. Podgorski and Nicholas S. Flann. Interaction of Stroma and Tumor Growth in Ductal Carcinoma in Situ Metastasis. An agent based model. Short Course. USC. Los Anglos. USA. (Oct.21 2013)
- Qanita Bani Baker, Ahmadreza Ghaffarizadeh, Soonjo Kwon, Gregory J. Podgorski and Nicholas S. Flann. Interaction of Stroma and Tumor Growth in Ductal Carcinoma in Situ Metastasis. Utah state university tenth annual celebration of faculty and student research at Utah State University. Logan. USA (Apr. 4-11, 2014).
- Interaction of Stroma and Tumor Growth in Ductal Carcinoma in Situ Metastasis: A 2D Agent-Based Modeling. SBI Science and Technology Review Winter Meeting. Utah State University Eccles Conference Center. (Feb.12, 2014)
- Developing in Silico Model to Study The Effect of Retinal Pigment Epithelial Cell Patch Size. USU Jan 6 2015

HONORS AND AWARDS

- Scholarship from Jordan University of Science and Technology to study PhD in computer science at Utah state university. August 2011
- Travel award from USC (university of southern California) to attend the Short Course and participate in poster session. October 2013

- Wining poster award among the graduated students in Utah State University CS department. Fall 2013.
- Wining poster award among the graduated students in Utah State University CS department. Spring 2014.
- USU Pinnacle Honor Society.
- USU Golden Key Society.

TEACHING EXPERIENCE

- Graduated Student/Teaching Assistant , Department of Computer Science, Utah State University (Sep 2011- now)
- Full Time Instructor, Computer Science Department Jordan University of Science and Technology (May2008 - July 2011): Teaching C++, visual basic, Vb.Net, introduction to information technology. Web design courses, computer skills, and working as supervisor for graduated project.
- Part Time Instructor, Computer Science Department Jordan University of Science and Technology (July 2007 - May 2008): Teaching web design courses, computer skills, and different programming language courses (C++,Java,Vb,and Vb.Net).
- Graduated Student/Research Assistant Department Jordan University of Science and Technology (Feb 2005 - May 2007)

TRAINING AND WORKSHOP

- International Teacher Assistance workshop nov-2011(USU,UT,USA)
- INTERNATIONAL VISITOR LEADER SHIP PROGRAM. UNITED STATE DEPARTMENT OF STATE .BUREAU OF EDUCATIONAL AND CULTURAL AFFAIRS.
- Attendance in the 23rd Annual Conference on Distance Teaching And Learning ACADEMY FOR EDUCATIONAL DEVELOPMENT. August, 2007 .Monona Terrace Convention Center. Madison, Wisconsin, U.S.A.
- International Computer Driving License certification/issued by the UNESCO Cairo office.
- Three (3) months in JUST computer center to learn Oracle.2003.
- World-links certificate/worlds linked organization (160 hours).
- Computer maintenance courses and certification/Al- shark center (84 hours).
- English conservation Certification / from oxford center (32 hours).
- online training courses/ HKJ -Ministry Of Education and ESP(100 hours).
- Teaching methods / HKJ -Ministry Of Education(60 hours).

KEY SKILLS

- 2D/3D Modeling , Multi-scale Modeling
- Programming Language :(C++(under window or linux), VISUAL BASIC.NET, C, Java, AspectJ).
- Web Programming (XHTML, HTML, XPath, XQuery, XML)
- Database Management System: (SQL, Oracle, Advanced Access)
- Web Page Application (ASP.NET)
- Multimedia Software/Visualizations: POV-Ray, ImageJ, Parview.
- Parallel Computing: MPI under Linux-C++.
- Image Processing Language MATLAB.

PERSONAL SKILLS AND COMPETENCES

- Communication skills, Team work and Ability to work under pressure for long hours. Have the potential of learning new programming languages and technologies. Have the spirit of proficiency and creativity. Fast learner, enthusiastic, dedicated, organized, clear and logical thinker, motivated, reliable. Ability to work as programming Languages Instructor and applications trainer.
- LANGUAGES: Arabic (Fluent), English (Excellent) 99 in TOEFL-IBT